CONFORMATIONAL ENTROPY IN PEPCK CATALYSIS: DYNAMIC MOTIONS CRITICAL TO FUNCTION.

BY

Troy A. Johnson

Submitted to the graduate degree program in Biochemistry and Molecular Biology and the Graduate Faculty of the University of Kansas in partial fulfillment of the requirements for the degree of Doctor of Philosophy.

Committee:

_____
Dr. Todd Holyoak,
Mentor

_____
Dr. Aron Fenton,
Chairperson

_____
Dr. Gerald Carlson

_____
Dr. Mark Fisher

_____
Dr. Joe Lutkenhaus

Date Defended: _____

The Dissertation Committee for Troy A. Johnson

certifies that this is the approved version of the following dissertation:

CONFORMATIONAL ENTROPY IN PEPCK CATALYSIS: DYNAMIC MOTIONS CRITICAL TO FUNCTION.

_____

Chairperson

Date approved:_____

Abstract

Enzymes increase the rate at which chemical reactions occur. How they achieve this rate increase has been an area of intense research for many years. Multiple studies have shown that dynamic motions of individual protein segments can play a role in enzyme function. Our enzyme of interest, phosphoenolpyruvate carboxykinase (PEPCK), has multiple dynamic motions that work in concert during the catalytic cycle. One of these mobile elements, termed the Ω-loop due to its architecture, acts like a lid that closes over the active site and has been hypothesized to serve multiple functions during the catalytic cycle. Furthermore, the act of opening and closing the lid domain is thought to be a delicate free energy balance, meaning the lid pays an energetic penalty to close, which is offset by the energetic contribution from substrate binding. To investigate the role of the loop, specifically the open/closed transition, and to probe for unappreciated roles, multiple mutant enzymes were created. In the first set of mutations the lid region was removed to investigate other potential roles for the Ω-loop. In the second set two different amino acid residues (Ala-467 and Glu-89) were mutated to either increase the energetic penalty of lid closure or decrease the energetic contribution from substrate binding. The resultant mutants were characterized via structure/function experiments. The data revealed two new roles for the Ω-loop lid, confirmed the delicate free energy balance, and shed light on the energetic pathway between the active site and the lid. Taking into account the data from the WT and all seven mutant PEPCK enzymes, a revised model for the role of the Ω-loop lid during catalysis is proposed: The role of the lid during the catalytic cycle is to correctly position the substrates in the active site, stabilize the R-loop and N/C-terminal lobe closure, and sequester and protect the reaction intermediate.

Acknowledgments

First and foremost, I want to thank my wife and best friend Erin. You have given me more love and support over the past 5 years than any other individual. I can never thank you enough for your encouragement, ability to adjust to my hectic schedule, and patience with the graduate school process. I love you and Logan with all my heart. Next, I would like to thank my parents David and Roseann Johnson for their love and support through all of the years of schooling I have chosen to undertake. Obviously, a project of this magnitude would not have been possible without the guidance and mentoring of Dr. Todd Holyoak. You allowed me to develop the project and make it my own, while teaching me various techniques and how to apply them to other projects. I would also like to thank Dr. Aron Fenton for your countless hours of guidance with the fluorescence quenching experiments and your valuable insight during lab meetings as the project developed. Further, I would like to thank my other committee members Drs. Gerald Carlson, Mark Fisher, and Joe Lutkenhaus, for critically evaluating the project every semester and offering advice on how I should proceed. I want to thank the entire faculty of the Department of Biochemistry and Molecular Biology for creating an atmosphere of higher learning in which I could succeed. Lastly, I want to thank all of the members of the Holyoak group that came through during my tenure here: Josh Wheatley who helped in countless ways over the years, Sarah Holyoak, Will Lotosky, Marc Balan, and Laura Draxler. This work would not have been possible without the support of everyone listed here and more; I thank all of you from the bottom of my heart.

Table of Contents

List of Tables

List of Figures

List of Equations

List of Abbreviations

ADP	adenosine-5'-diphosphate
ASU	asymmetric unit
ATP	adenosine-5'-triphosphate
βSP	3-sulfopyruvate
cPEPCK	cytosolic phosphoenolpyruvate carboxykinase
cmPEPCK	chicken mitochondrial phosphoenolpyruvate carboxykinase
DTT	1,4-dithiothreitol
GDP	guanosine-5'-diphosphate
GTP	guanosine-5'-triphosphate
HEPES	4-(2-hydroxyethyl)-1-piperazineethanesulfonic acid
IDP	inosine-5'-diphosphate
IPTG	isopropyl β-D-1-thiogalactopyranoside
ITP	inosine-5'-triphosphate
mPEPCK	mitochondrial phosphoenolpyruvate carboxykinase
OAA	oxaloacetic acid
PDB	protein data bank (http://www.rcsb.org/pdb/home/home.do)
PEG	polyethylene glycol
PEP	phosphoenolpyruvate
PEPCK	phosphoenolpyruvate carboxykinase
PGA	2-phosphoglycolate
rcPEPCK	rat cytosolic phosphoenolpyruvate carboxykinase
RMSD	root-mean-square-deviation
TCA	tricarboxylic acid cycle (aka citric acid cycle and/or Krebs cycle)
TCEP	tris-2-carboxyethyl-phosphine
TIM	triosephosphate isomerase
TLS	translation/libration/screw

Chapter 1 . Introduction to phosphoenolpyruvate carboxykinase and enzyme dynamics

Phosphoenolpyruvate carboxykinase, hereafter referred to as PEPCK, catalyzes the decarboxylation of oxaloacetate (OAA) with subsequent phosphorylation to form phosphoenolpyruvate (PEP), utilizing a triphosphate nucleotide as the phosphoryl donor. Drs. Merton Utter and Kiyoshi Kurahashi discovered PEPCK in 1954 while they were investigating CO_2 fixation in heterotrophic bacteria (*1*). Since that time the enzyme has been isolated and studied from a multitude of species, including yeast, *Escherichia coli* (*E. coli*), plants, rodents, and humans.

Isozymes of PEPCK

From the first characterization by Utter and Kurahashi it was realized that PEPCK requires a nucleotide (ATP or GTP) for enzymatic activity (*1*). The ATP-dependent PEPCK is found in *E. coli*, yeast, C4 plants, and other bacteria, while GTP-dependent PEPCK is found in all higher eukaryotes, e.g. rodents, birds, mammals (*2, 3*). The GTP-dependent class of PEPCK can further be divided into two isoforms, cytosolic PEPCK (cPEPCK) and mitochondrial PEPCK (mPEPCK), so named for their final intracellular locations (*1, 4*). The percent of activity of each isoform, specifically in the liver, is variable and species-dependent: humans have a 50-50 split of the two isoforms, rats and mice have 90-95% cytosolic, and chickens have 100% mitochondrial (Table 1-1) (*2, 3*). A comparison of the ATP and GTP classes of PEPCK reveals that, despite sharing very little sequence homology, the overall structural topology is highly similar (backbone RMSD) with all active site residues and architecture conserved (Appendix 1) (*5*).

Table 1-1. Ratio of cytosolic vs. mitochondrial PEPCK isoforms.

The relative distribution of each isoform in the liver of various animals was determined by assaying the enzyme activity in both the cytosol and the mitochondria in the livers of the species listed below. It is assumed that this distribution will be found in the other tissues that express PEPCK (a select few tissues have been tested and this assumption holds true). Adapted from Croniger, et al. (*6*).

Species	cPEPCK	mPEPCK
	% total activity in the liver	
Human	50	50
Sheep	40	60
Cow	40	60
Pig	50	50
Dog	50	50
Rat	90	10
Mouse	85	15
Hamster	90	10
Rabbit	10	90
Pigeon	0	100
Chicken (Liver)	0	100
Chicken (Kidney)	50	50

The Gene

The genes for the cPEPCK and mPEPCK isoforms in humans are located on two different chromosomes, #14 and #20 respectively, with each gene containing ten exons and nine introns (*7, 8*). The two genes differ in the size of their introns, which results in the mitochondrial gene being 9000 base pairs while the cytosolic gene is only 5500 base pairs (*9*). Although mPEPCK is synthesized as a 640 amino acid protein, upon translocation into the mitochondrial matrix the 32 amino acid leader sequence is cleaved, resulting in the active form being 608 amino acids. This final size is comparable to cPEPCK at 622 amino acids. In their mature forms they have a sequence identity of 71%.

Expression and Regulation of PEPCK

The current knowledge about the enzyme PEPCK has been largely derived from studies carried out on rodents. For this reason what is known in detail, about the expression and regulation, is limited to the cytosolic isoform of PEPCK (*10*). Cytosolic PEPCK is expressed in liver, the major organ for gluconeogenesis, but it has also been found in other tissues such as the kidney, white/brown adipose tissue, muscle, brain, and mammary gland (*6*). Beginning with early work on PEPCK, it was recognized that diet and hormones very precisely regulate the transcription and translation of the enzyme. Expression of PEPCK is induced by glucagon (via cAMP), glucocorticoids (except adipose tissue), and in the kidney via a pH change (reviewed in (*11*)). PEPCK expression is down regulated by insulin, pH changes (in the kidney), and glucocorticoids (adipose tissue only) (*11*). Recently it was discovered that PEPCK has a post-translational mechanism of regulation via lysine acetylation (*12-14*). As mentioned above, the information on mPEPCK is very limited, but what has been learned is that mPEPCK is constitutively expressed in multiple tissues and has a half-life of 60 hours; this is significantly different from cPEPCK, which is tightly regulated and has a half-life of only eight hours (*6*).

Metabolic Role of PEPCK

The biological role of PEPCK in metabolism has been extensively studied. PEPCK is often broadly defined as a cataplerotic enzyme, meaning it removes TCA cycle anions for usage in downstream pathways. More specifically, it has been shown to play an active role in glucose homeostasis, triglyceride biosynthesis, and serine synthesis (Figure 1-1) (reviewed in (*9*)). PEPCK participates in glucose homeostasis by catalyzing the first committed step of the gluconeogenesis pathway. This role for PEPCK explains its presence in the liver and kidney, the two major gluconeogenic tissues. However, a role in gluconeogenesis does not explain the enzyme's presence in non-gluconeogenic tissues, such as white and brown adipose tissue, muscle, brain, and small intestine (*15*). The presence of PEPCK in white and brown adipose tissue has been investigated, the evidence data suggests PEPCK is active in glyceroneogenesis, which supplies glyceride-glycerol for triglyceride production (*16, 17*). While the role of cPEPCK has been well characterized in liver, kidney, and adipose tissue, the presence of PEPCK in other tissues and the impact of mPEPCK on metabolism is still unclear.

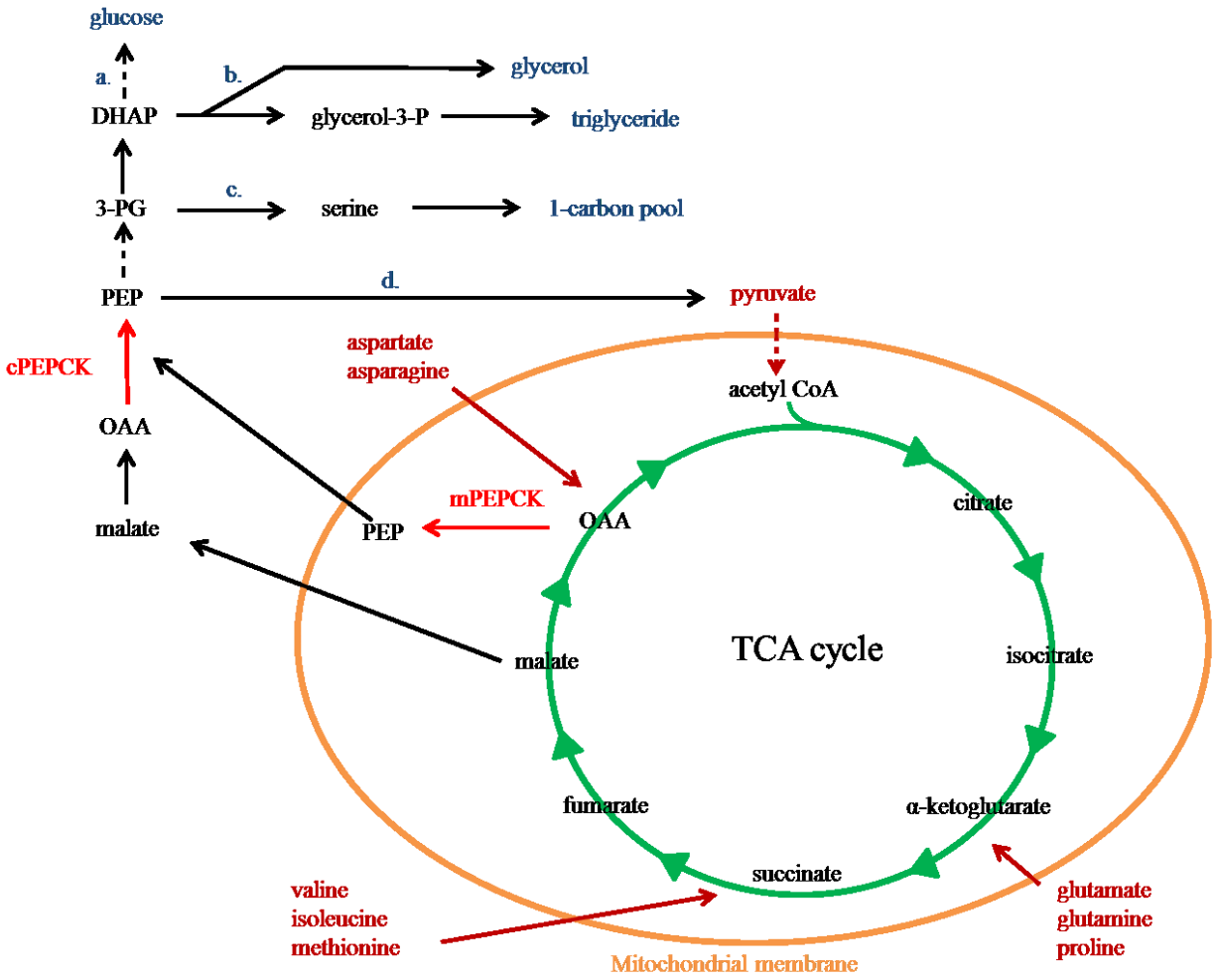

Figure 1-1. Metabolic pathways of PEPCK.

The biosynthetic pathways in which the PEPCK reaction products are utilized are shown in (a) gluconeogenesis, (b) glyceroneogenesis, (c) serine synthesis, and (d) the recycling/oxidation pathway. Adapted from Yang et al. (*9*)

PEPCK Catalysis

GTP-dependent PEPCK (E.C. 4.1.1.32) is a functional monomer that has a molecular mass of ~70 kilo-daltons and an absolute requirement of two divalent cations for activity. Multiple studies have been carried out which determined that Mn^{2+} is the most activating cation for GTP-dependent PEPCKs (*18-20*). Additionally, a second divalent cation is required for reactivity, binding in the active site in the form of a metal-nucleotide substrate complex. The mechanism by which the PEPCK reaction proceeds has been investigated extensively. However, there is still no consensus on the order in which substrates bind to the enzyme. This has led to the conclusion that it has a random binding mechanism (reviewed in (*21*)). There is clear evidence that the chemistry proceeds via a step-wise process in which OAA is decarboxylated, forming an enolate intermediate, followed by the transfer of the γ-phosphate from GTP to the enolate, forming the products PEP, GDP, and CO_2 (Figure 1-2). The PEPCK reaction is freely reversible, but has been shown to proceed only in the OAA to PEP direction *in vivo.* As an exception to this observation, *Ascari Suum,* a parasitic nematode, utilizes PEPCK as an anaplerotic enzyme to refill the TCA cycle by fixing CO_2 and synthesizing OAA from PEP (*22*).

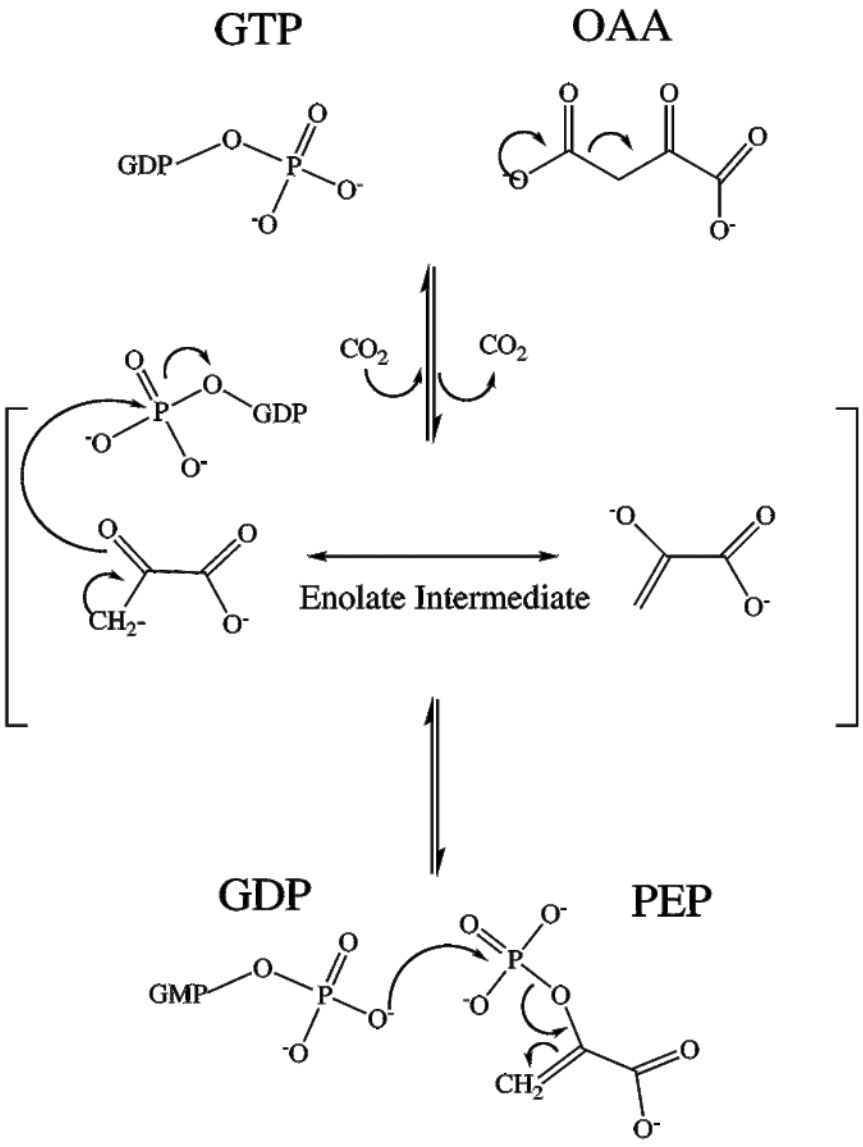

Figure 1-2. Mechanism of PEPCK catalysis

The reaction catalyzed by PEPCK is the decarboxylation of OAA to form the highly reactive enolate intermediate followed by the concomitant transfer of the γ-phosphate from GTP to form PEP, GDP, and CO_2. All structural and biochemical evidence points towards the reaction proceeding through a highly reactive enolate intermediate step.

Structural Characteristics of PEPCK

For the first 40 years of research on PEPCK, all work was carried out utilizing biochemical assays to determine mechanistic properties of the enzyme. In 1996 the first crystal structure was solved of ATP-dependent PEPCK from *E. coli,* allowing the enzyme to be viewed at the molecular level for the first time (*23*). A few years later the structure of both the mitochondrial PEPCK from chicken and the cytosolic PEPCK from rat were solved. These structures revealed extensive details on how the GTP-dependent enzyme catalyzes the conversion of OAA to PEP (*24, 25*). The ATP-PEPCK structural work revealed that PEPCK consists of two globular domains, an N- and C-terminal domain, with the active site in a cleft between the domains (Figure 1-3). One point that must be stressed is that these domains do not fold independently of one another; rather the polypeptide backbone makes multiple passes between the domains. The basic information that is taken from a global look at PEPCK is that the overall fold of the enzyme groups it into the P-loop containing, nucleoside-triphosphate-hydrolase fold and superfamily (*23*).

Nucleotide specificity- As mentioned previously, PEPCK is classified by the nucleotide that it utilizes, ATP or GTP. The structural information revealed a number of features that have evolved to allow nucleotide selectivity (*5*). Recall that the purine ring of guanosine and adenosine differ at the 2- and 6-positions (Figure 1-4). At the C-2 position GTP has an amino group that crystallographic evidence demonstrated interacts with a phenylalanine (PDB ID: 2QEY); ATP lacks this amino group (*25*). This difference is not believed to be the reason for the difference in specificity, due to the fact that GTP-PEPCKs utilize inosine nucleotides (which also lack the C-2 amino group) with similar kinetic efficiency as their guanosine counterparts. The other position on the purine ring that is different between guanosine and adenosine is the C-6 position; in GTP and ITP this is a carbonyl, while ATP has an amino group. The difference at this position on the

purine ring is thought to contribute to the nucleotide specificity, due to the fact that in the PEPCK–Mn^{2+}–Mn^{2+}GTP structure the C-6 carbonyl functions as a hydrogen bond acceptor, interacting with the backbone amide of a phenylalanine and the side chain amide nitrogen of an asparagine (Figure 1-5) (*25*). Obviously, the amino group of ATP does not function as a hydrogen bond acceptor, and therefore, cannot make these interactions. Further studies are needed to completely establish the mechanism of nucleotide specificity.

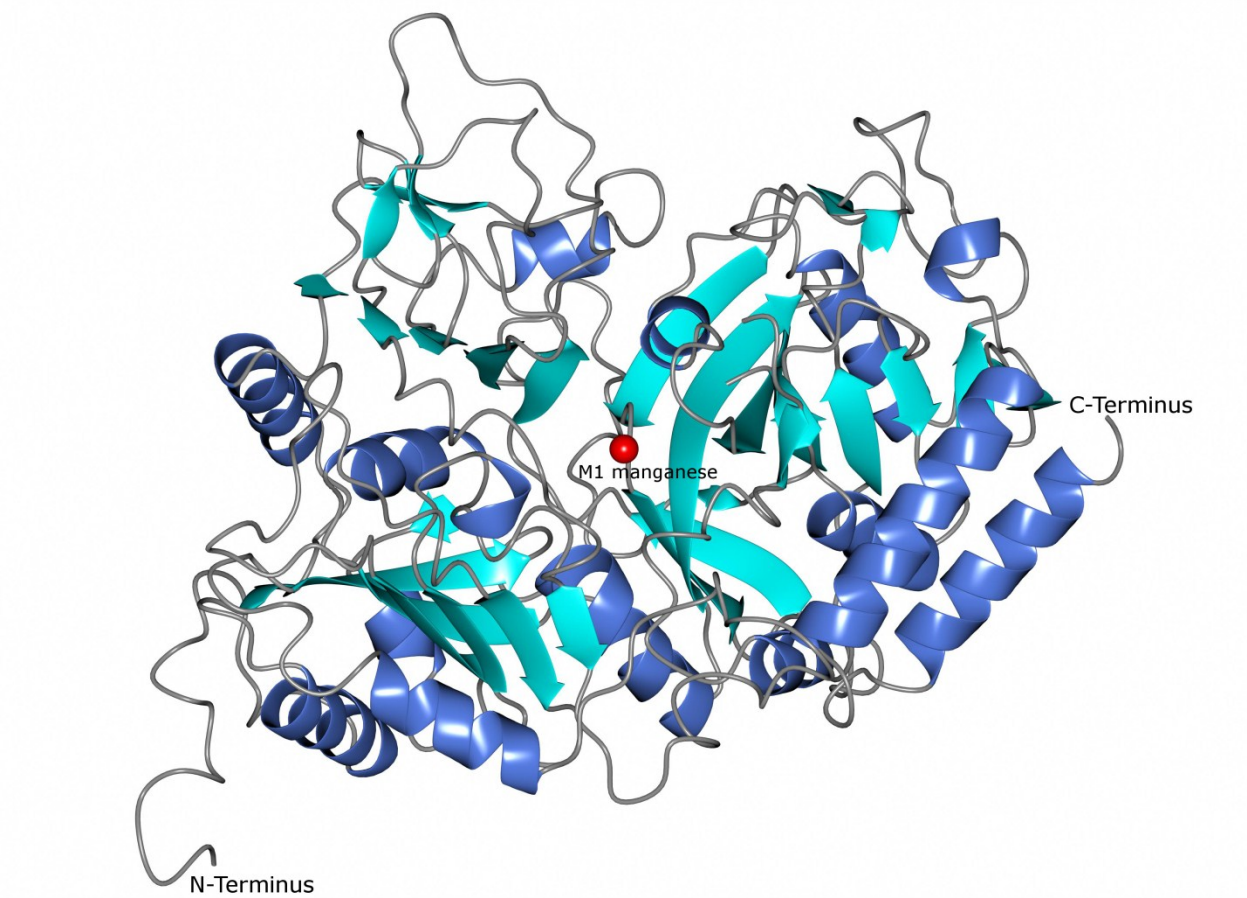

Figure 1-3. Structure of WT PEPCK with Mn^{2+}.

A global view of PEPCK. The M1 manganese atom is shown in red, α-helices in blue, and β-sheets in cyan.

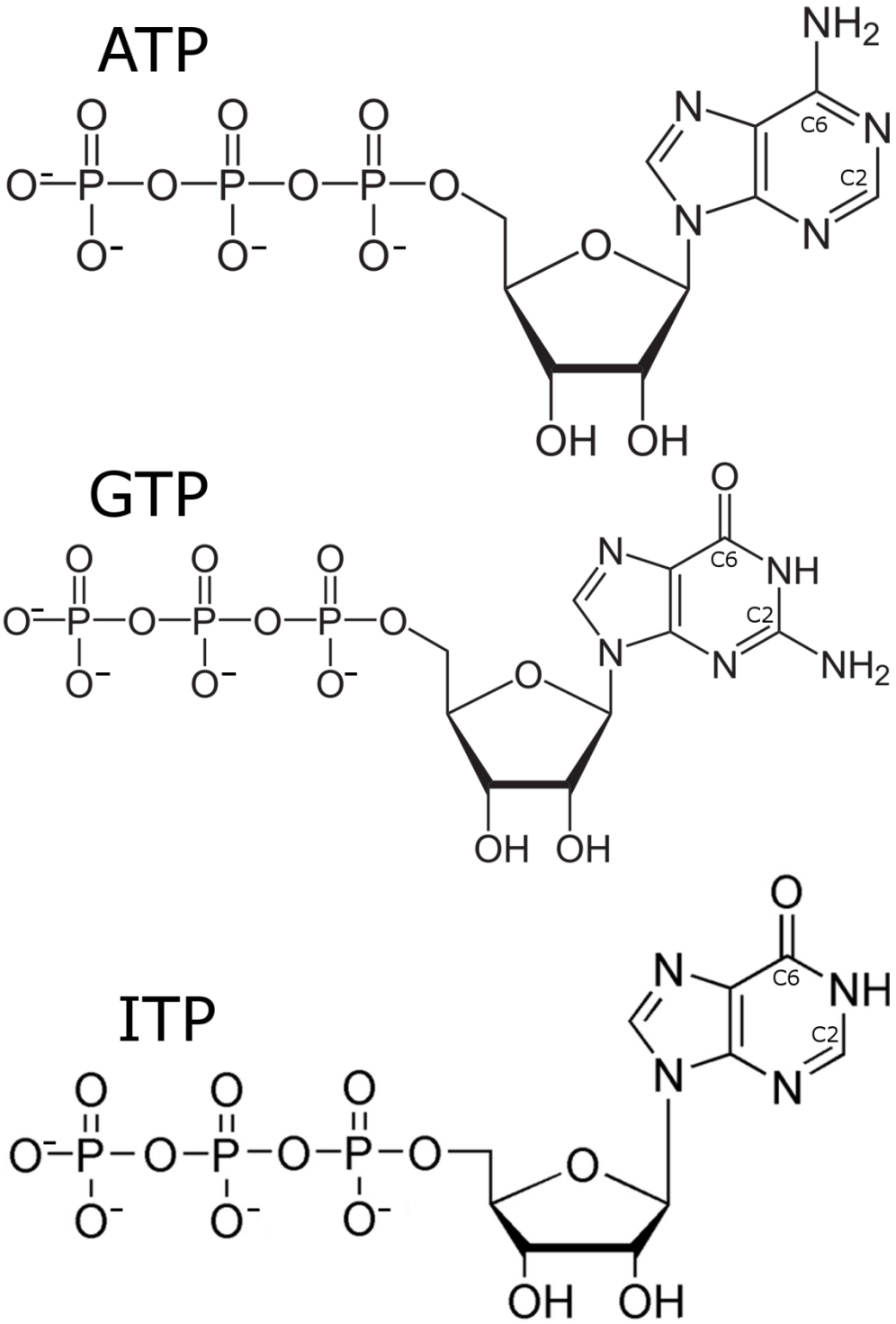

Figure 1-4. Relevant nucleotide triphosphates.

ATP, GTP, and ITP differ at their C2 and C6 positions. Structural studies have revealed that higher eukaryotes utilize GTP and ITP over the ATP nucleotide due to differences at the C6 position of the purine ring.

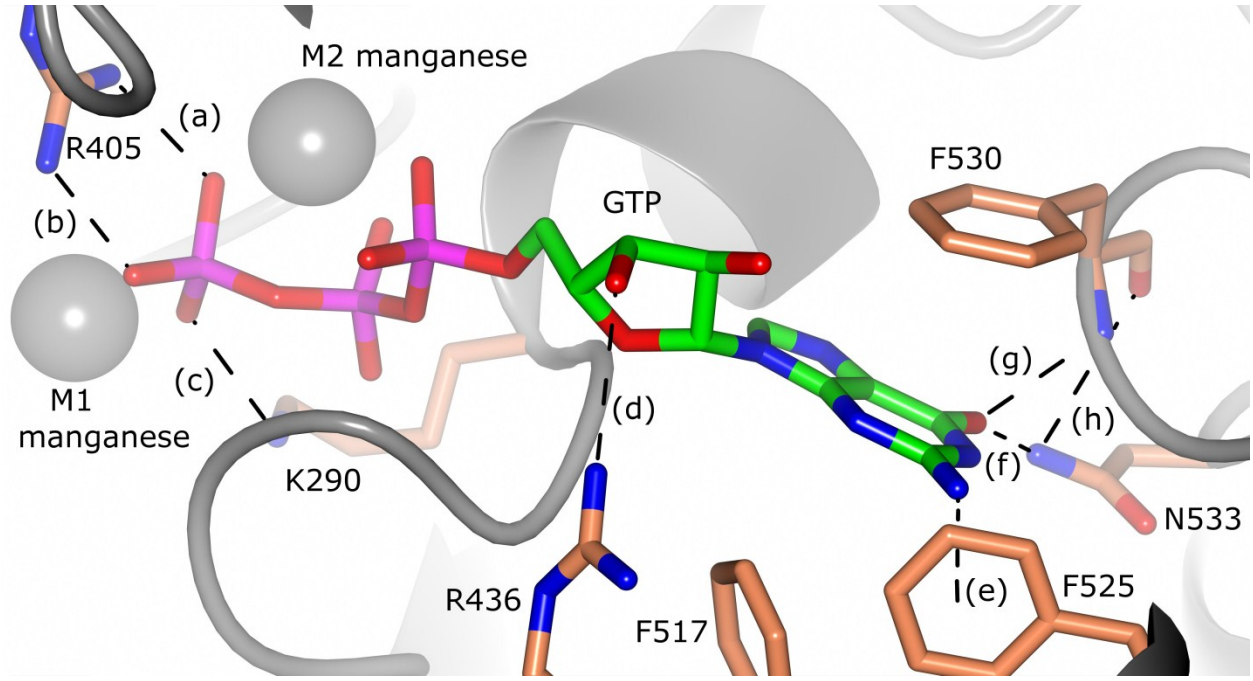

Figure 1-5. GTP binding site

GTP binds to PEPCK through a number of direct interactions that are shown by the dashed lines. The purine ring has pi stacking interactions with the multiple aromatic side chains of phenylalanine, and the γ-phosphate of GTP interacts with the M1 and M2 manganese ions (interactions not shown). The distances of the different interactions are (a) 2.87Å (b) 2.77 Å (c) 2.92 Å (d) 3.37 Å (e) 3.80 Å (f) 2.94 Å (g) 2.78 Å (h) 3.50 Å (PDB ID: 2QEY).

Dynamic Elements- Currently there are over 40 different structures of PEPCK isozymes in the protein data bank (PDB) solved with various small molecules (appendix 2). A number of structures that are deposited were part of a series of experiments designed to map out the reaction coordinate. This was accomplished by crystallizing PEPCK in multiple complexes to analyze structural changes that occur as the enzyme binds the different ligands (*24-27*). A comparison of these structures has identified multiple movements that occur during the catalytic cycle. There are four major loops or regions that display conformational flexibility that need to be highlighted: 1) the 10-residue Ω-loop lid, 2) the P-loop, 3) the R-loop, and 4) the bi-lobal motion of the enzyme (Figure 1-6a). The Ω-loop is a highly mobile region on the protein surface that shifts between an open and closed conformation depending upon the ligands bound in the active site (*27*). The P-loop or kinase-1a motif shows similar mobile behavior, changing its conformation with substrate binding (*25*). The P-loop cradles the nucleotide, aiding in its positioning. In addition, the P-loop contains a reactive cysteine residue whose modification results in inactivation of the enzyme and a lysine residue that aids in the leaving group ability of the γ-phosphate (*28-30*). The R-loop is the third mobile element. This loop contains an arginine residue (R87) that binds directly to the ligand in the OAA/PEP binding site through electrostatic interactions. Unlike the previous two mobile loops, this loop does not have a 0.5 Å or larger movement associated with it. However, crystallographic evidence (compare B-factors in PDB ID: 2QEW, 2QEY and 2RK7) revealed that this loop undergoes an ordered (holo) to disordered (GTP bound) to ordered (oxalate bound) transition, dependent upon the ligand bound. These transitions suggest a role for this loop in allowing or preventing lid closure. The last major motion is imparted by the bi-lobal nature of PEPCK. As previously mentioned, PEPCK folds into two interdependent domains with the active site in a cleft between the two domains or lobes.

When the structures of PEPCK–Mn^{2+} (PDB ID: 2QEW) and PEPCK–Mn^{2+}–Ox–Mn^{2+}GTP (PDB ID: 3DT2) are superposed, the N-terminal lobes overlay precisely while the C-terminal lobes are offset by ~3Å (Figure 1-6b). This led us to hypothesize that as the enzyme progresses through the catalytic cycle, it has a clam-shell type motion that decreases the size of the active site cleft, effectively repositioning the phosphate donor and acceptor to facilitate PEPCK's enzymatic activity.

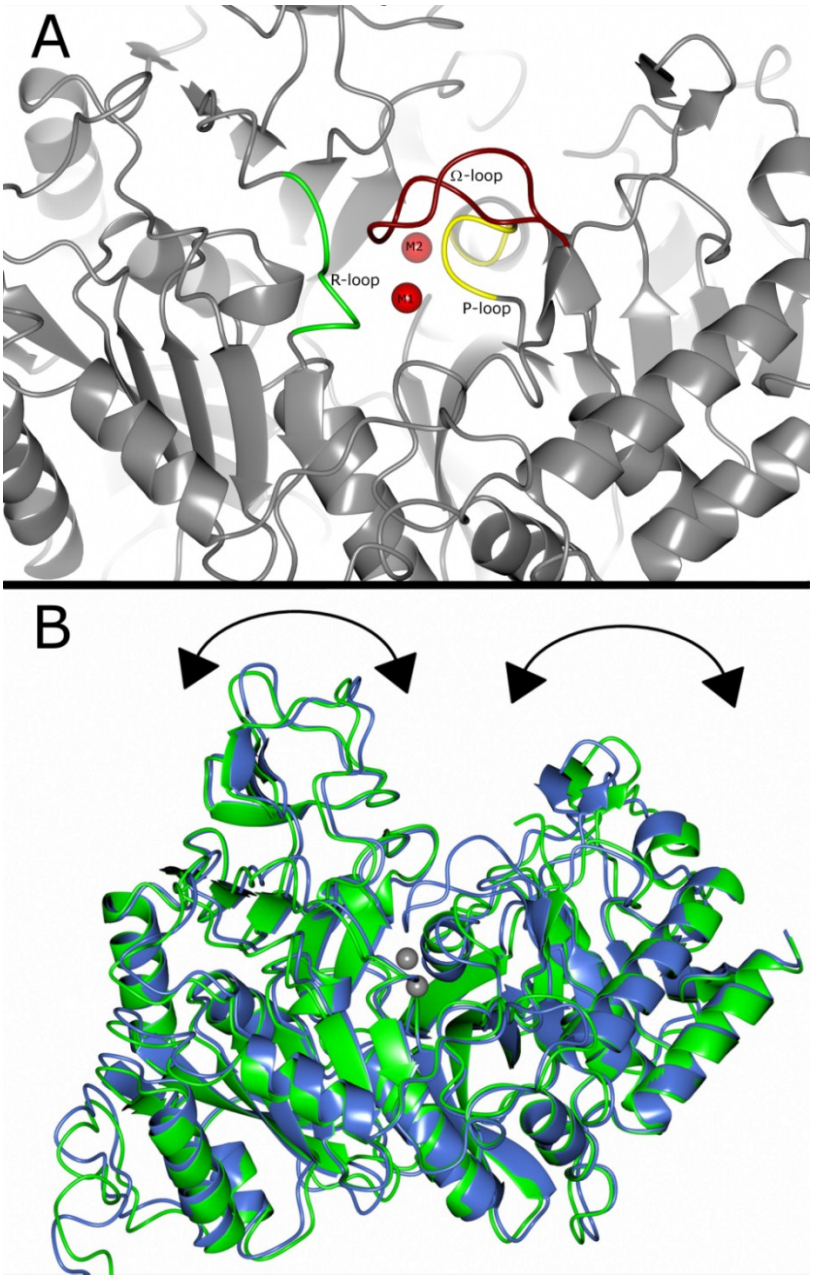

Figure 1-6. Mobile elements of PEPCK.

PEPCK has multiple mobile domains that have been identified via X-ray crystallography. (A) The Ω-loop lid (red) has been shown to change its conformation from open/disordered to closed/ordered upon substrate binding. The P-loop (yellow) cradles the GTP nucleotide shifting it forward by ~0.5Å to correctly position it for phosphoryl transfer. The R-loop (green), which contains arginine 87 (essential for OAA/PEP binding), has been observed in either an ordered or disordered state dependent upon the substrates in the active site. (B) The last motion associated with PEPCK is the bi-lobal motion in which the N and C-terminal lobes transition from open (green: PEPCK–Mn^{2+}) to closed (blue: PEPCK–oxalate–Mn^{2+}–Mn^{2+}GTP) upon substrate binding to constrict access to the active site by bulk solvent.

Enzyme Dynamics

Enzymes have evolved to efficiently catalyze chemical reactions, but understanding how they operate has been an area of extensive research for decades. It is widely accepted that enzymes achieve their significant catalytic power by their unique ability to decrease the free energy or transition state barrier of a chemical reaction (Figure 1-7a). However, how an enzyme lowers the barrier has been an area of extreme debate, with multiple hypotheses proposed over the years (reviewed in (*31*)). One of the more recent ideas put forth is enzyme dynamics, more specifically, it was proposed that all motions on the protein surface can alter the free energy profile of the enzyme and aid in transition state crossing. This contribution of dynamics to catalytic power has been questioned based upon experimental evidence of the time scales at which reactions and motions occur (summarized in (*32*)). To summarize, large-scale motions such as whole domain movements occur on the millisecond (ms) to second time scale, loop movements function on the nanosecond (ns) to microsecond (μs) time scale, and side chain rotamers occur on the picosecond (ps) to nanosecond (ns) time scale (Figure 1-7b) (*32*). While all of these motions are extremely fast they are still orders of magnitude slower than the amount of time it takes for bond vibration to occur, on the femtosecond (fs) time scale. The fact that dynamic motions are probably too slow to be directly involved in transition state crossing does not mean that these motions are not vital to the catalytic properties of an enzyme. The crossing of the transition state barrier is just one step in the catalytic cycle and the steps leading up to and after this event are of equal importance. In the case of PEPCK, crystallographic studies have revealed multiple motions (loops, rotamers, and whole domains) that undoubtedly act in concert in order for chemistry to occur.

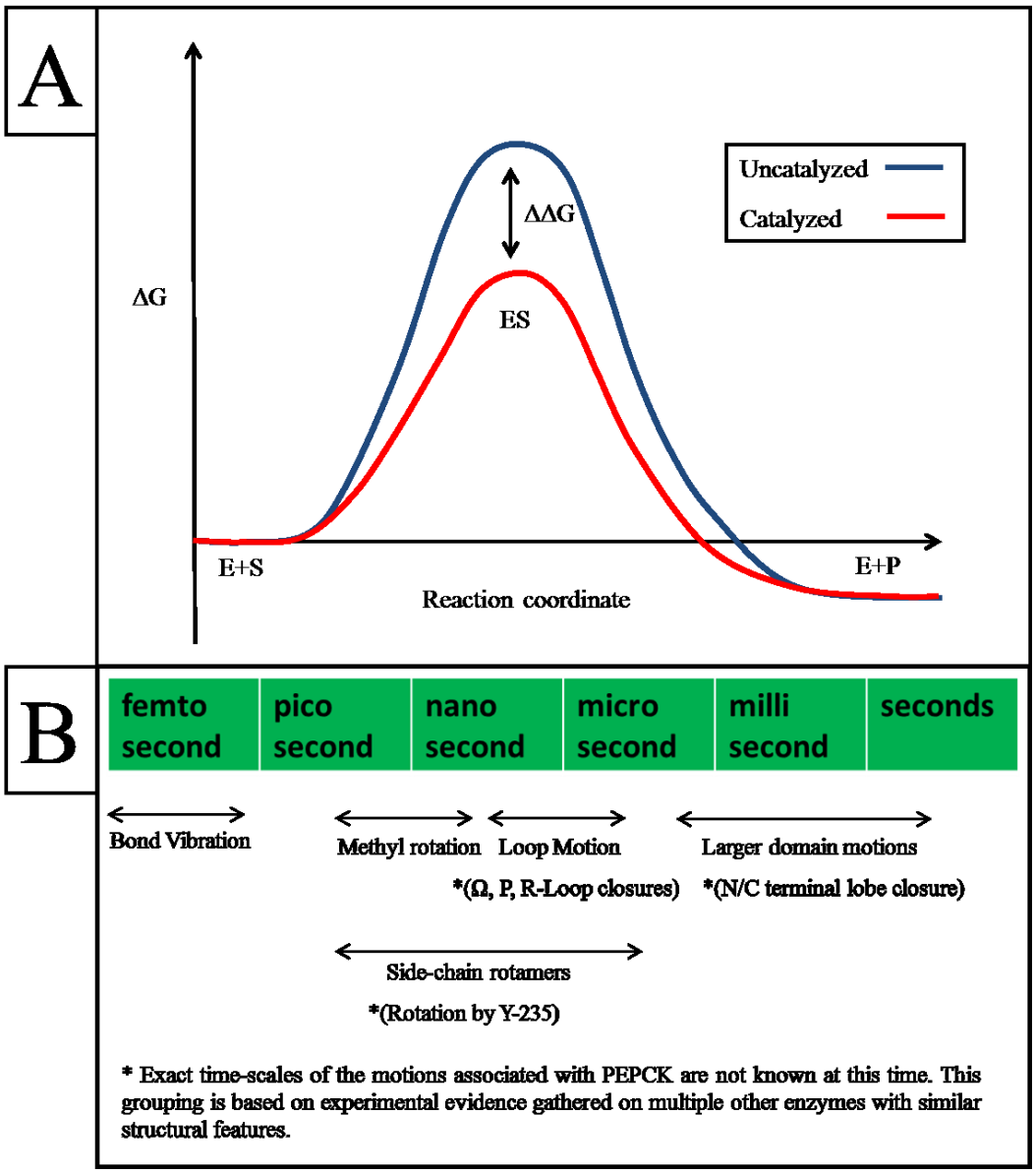

Figure 1-7. Free energy of chemical reactions and time scales of protein motions

In order for a chemical reaction to occur it must overcome the free energy barrier preventing bond breakage. In solution two substrates will eventually overcome this barrier; however, in a biological setting, the reaction must occur significantly faster so that life can exist. To overcome the free energy barrier quickly, nature has evolved to utilize enzymes to lower the barrier (A). How enzymes reduce this barrier is an area of extensive debate. What is known is that enzymes have mobile elements that contribute to their activity and these motions operate within a very narrow time regime (B). Adapted from Henzler-Wildman (*32*)

PEPCK dynamic motions during catalysis

As mentioned above the PEPCK reaction steps were deduced from a series of protein crystal structures. This structural series revealed multiple regions undergoing conformational changes at different times during the catalytic cycle. The structural work also gave detailed insight into the binding of both the nucleotide and ligands and how the interactions are connected to the mobile elements of the protein.

Substrate Binding- The first step in any enzyme catalyzed reaction is the binding of substrates in the active site. The crystallographic structure of PEPCK–Mn^{2+}–OAA (PDB ID: 2QF1) demonstrates that OAA binds to the enzyme by directly coordinating to the M1 manganese ion, which is absolutely required for PEPCK activity (Figure 1-8) (*25*). In addition to the interactions between OAA and the M1 Mn^{2+} ion, binding of OAA is facilitated by interactions with the side chains of Arg-87 and Ser-286 (Figure 1-8) (*25*). The structure of PEPCK–Mn^{2+}–Mn^{2+}GTP (PDB ID: 2QEY) shows that GTP binds to PEPCK within the unique nucleotide-binding site of GTP-dependent PEPCKs. This results in multiple interactions between the enzyme and both the guanosine ring and the phosphoryl groups (Figure 1-5) (*25*). One such interaction involves Lys-290, located in the P-loop, bridging the β- and γ-phosphoryl groups. This interaction, along with coordination of the γ-phosphate between the M1 and M2 metal ions, facilitates the ability of the γ-phosphate to act as a leaving group (*5*). Comparing the two structures (2QF1 and 2QEY) reveals that the Ω-loop lid is in an open/disordered orientation in both complexes, the R-loop is disordered when OAA is not bound, and lastly but most importantly, the substrates are not positioned close enough for catalysis to occur (*5*).

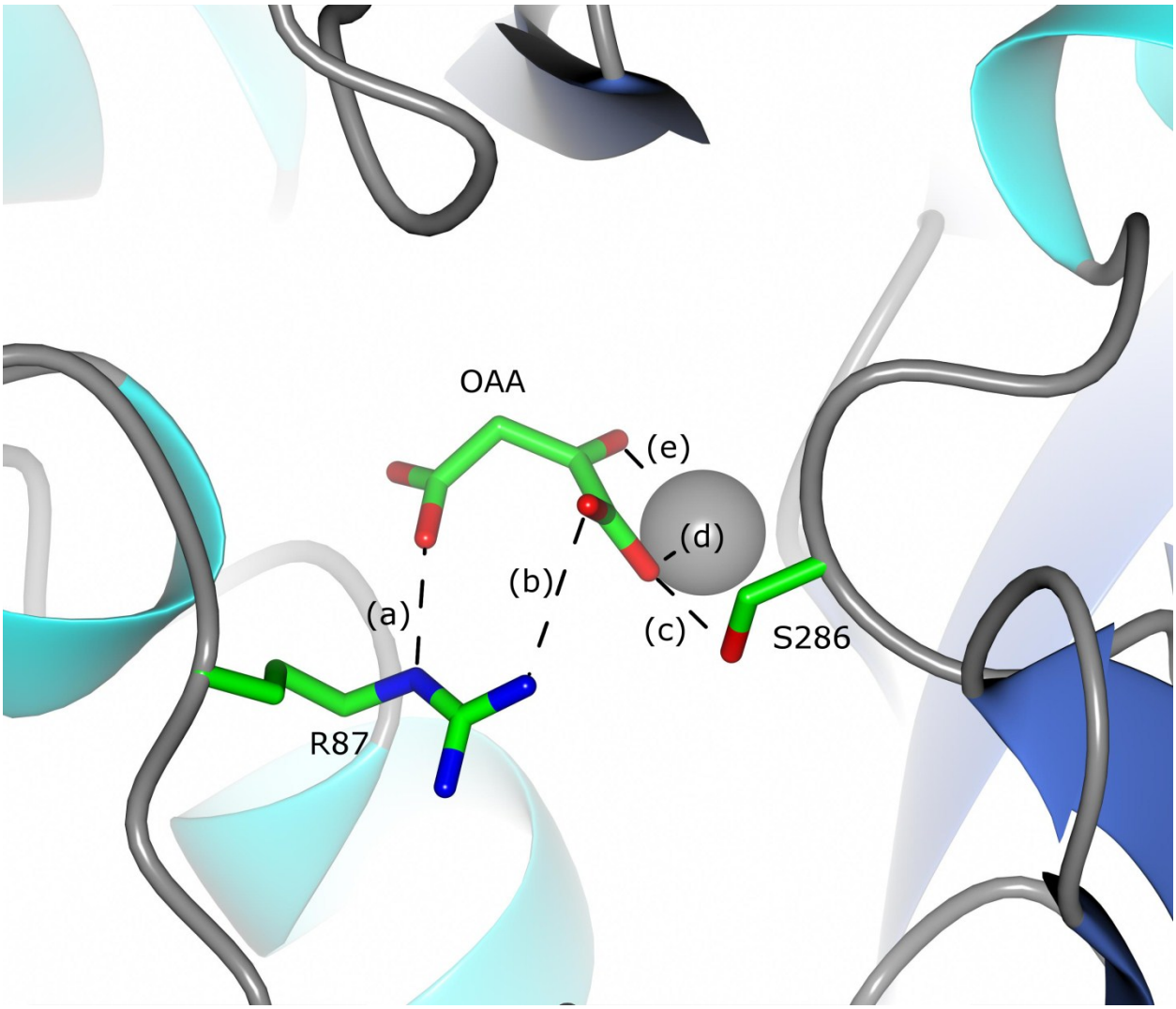

Figure 1-8. OAA binding site.

OAA binds to PEPCK through interactions with the M1 manganese ion (gray sphere), Arg-87, and Ser-286. The distance of each interaction is as follows: (a) 2.82Å (b) 3.54 Å (c) 3.39 Å (d) 2.28 Å (e) 2.26 Å.

Formation of the Michaelis Complex- After formation of one of the single substrate complexes, PEPCK binds the second ligand, forming the lid-open Michaelis complex (Figure 1-9A). This complex has OAA and GTP positioned for a direct in-line phosphoryl transfer, but at a distance that is too great for nucleophilic attack (*5*). To bring the substrates closer, the next step in the catalyzed reaction is the sampling of the lid-closed conformation by the Ω-loop (Figure 1-9B). In order for the Ω-loop lid open/closed transition to occur, certain motions must act in concert to remove a potential steric clash between Thr-465 in the Ω-loop and Ala-287 in the P-loop (*5*). The P-loop cradles the nucleotide and has to close/move by ~0.5 Å to remove the clash and allow the Ω-loop to close. The P-loop movement simultaneously repositions the GTP molecule towards OAA and the M1 metal, shortening the distance to allow in-line phosphoryl transfer (*5*). The second major motion that must occur is the closure of the N- and C-terminal lobes to reduce the size of the active site cleft and exclude solvent. Following closure of the P-loop and the inward movement of the N- and C-terminal lobes can the Ω-loop sample the closed conformation. Experimental evidence clearly demonstrates that each of these motions is essential for catalysis (*5*).

Chemistry- After forming the lid-closed Michaelis complex, the substrates are positioned for PEPCK catalysis. Based upon the structural information, residues Asn-403 and Arg-87 facilitate the decarboxylation of OAA forming the enolate intermediate. These two residues flank both sides of the carboxylate of OAA, causing polarization of this substrate and ultimately the CO_2 leaving group propensity (Figure 1-9-C) (*25*). Additionally, Tyr-235 rotates forward to interact with and stabilize the CO_2 product. This rotation forward by Tyr-235, to aid in stabilization, is not observed in the complexes with OAA (compare Figure 1-9-B & C) (*27*). The transfer of the

γ-phosphate to the resultant enolate occurs by positioning and stabilizing the phosphoryl group through electrostatic interactions with Arg-405, Lys-290, and the M1 and M2 metal ions (*5*).

Lid Opening and Product Release- Once the products PEP, GDP, and CO_2 are formed, the enzyme reverses the process described above, starting with the sampling of the lid open conformation (Figure 1-9-D & E). Upon sampling of the lid open state, the N- and C-terminal lobes open and Tyr-235 shifts to its rearward orientation, which allows for the release of the CO_2 (*27*). Next, the PEP product shifts away from direct coordination to the M1 and M2 metal ions into outer-sphere coordination, in which it interacts with the M1 metal, Arg-87, and Arg-405 (*27*). Once PEP shifts to outer-sphere coordination, the stabilizing interactions it made with the P-loop are removed, allowing for P-loop opening. This opening results in the shift of the GDP nucleotide away from the M1 metal. The combination of the shift by Tyr-235 to a rearward orientation, the shift of PEP to outer-sphere coordination, and the opening of the P-loop and Ω-loop allows for product release and ultimately the transition back to the beginning of the catalytic cycle (*5*).

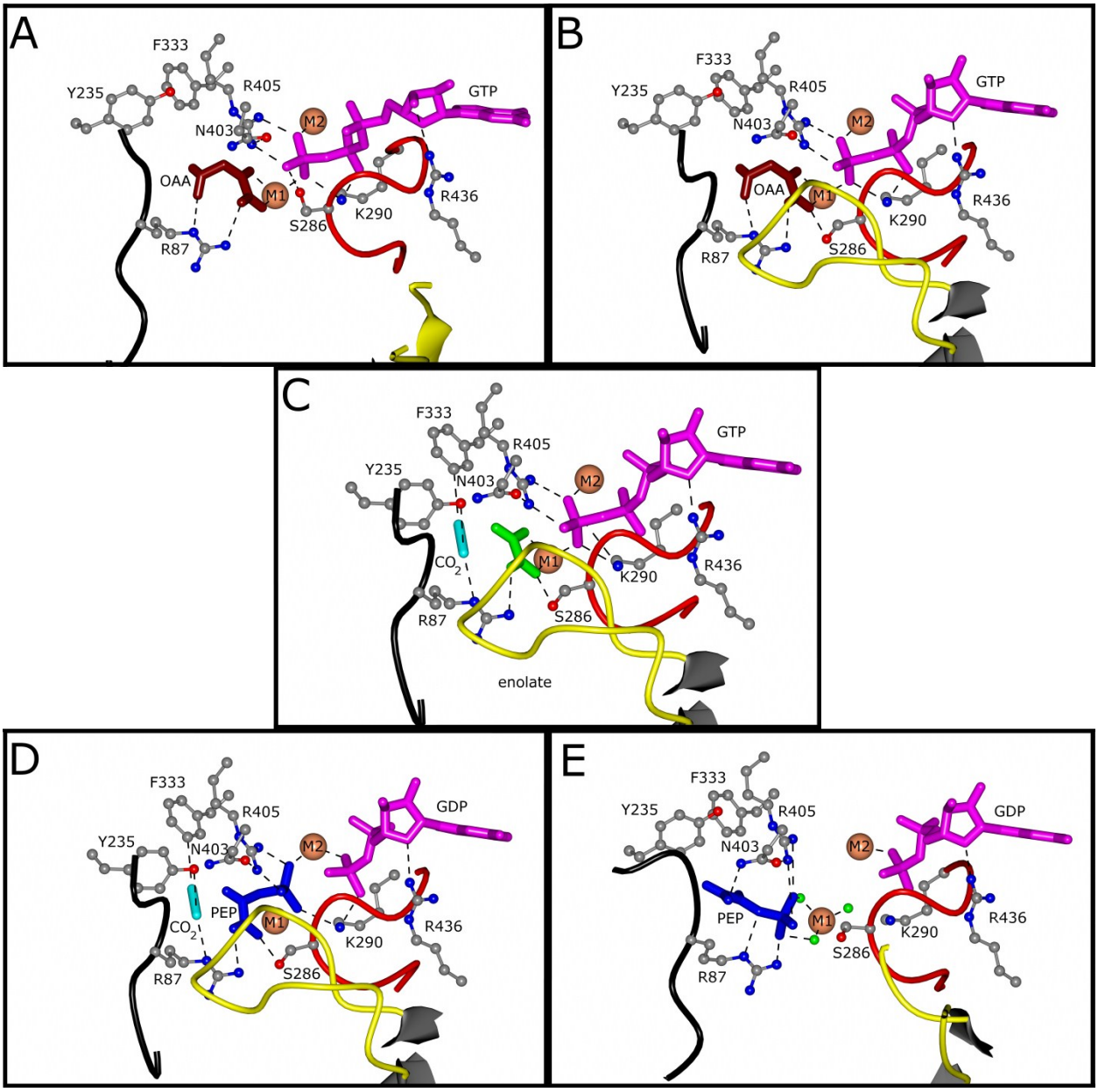

Figure 1-9. Structural look at the chemical reaction of PEPCK.

The substrates, products, and mobile elements are colored by molecule: M1 and M2 manganese ions (tan), GTP/GDP (magenta), OAA (burgundy), oxalate (green), CO_2 (cyan), PEP (blue), Ω-loop (yellow), P-loop (red), and the R-loop (black). The amino acid residues involved in substrate binding interactions are rendered as gray ball-and-stick models colored by atom type and labeled. Panels A and B are WT PEPCK–OAA–Mn^{2+}–Mn^{2+}GTP with 2 molecules (A and B). Panel C is WT PEPCK–enolate–Mn^{2+}–Mn^{2+}GTP. Panels D and E are WT PEPCK–PEP–Mn^{2+}–Mn^{2+}GDP with 2 molecules (A and B). In panel E the green spheres around the M1 metal are water molecules. Dashed lines represent substrate-protein interactions.

A Free Energy Landscape model for PEPCK catalysis

During protein synthesis, most proteins adapt a stable 3-dimensional fold, meaning an enzyme is rigid enough to maintain an overall structure, but flexible enough to allow substrate binding, chemical reaction, and product release (*33*). The driving force behind correct protein folding is the ability of the protein to adapt the lowest energy state or reach the bottom of the folding funnel (*34*). Once an enzyme has reached this final folded state, any dynamic elements on the protein surface will continue to sample multiple conformations until the relevant catalytic complex is formed (*33, 35*). However, the conformations sampled are dictated by the global free energy profile of the enzyme, as random sampling will hamper catalytic efficiency (*35*). Rather, the enzyme samples a select few conformations that are optimized for substrate binding (*35*). In the case of PEPCK all of the substrates bind to the lid open form of the enzyme (*27*). Upon binding, in a clear example of a classical induced-fit mechanism, the enzyme adapts a catalytically active conformation by altering the orientations of multiple mobile elements (*27*). It is only upon closure of these loops and domains that the substrates are positioned correctly to allow for catalysis to proceed (*27*). Furthermore, the structural data support a model in which the free energy profile for the enzyme is modified as ligands bind during progression through the catalytic cycle (Figure 1-10 A-C) (*5*). This model was developed by observing structures of PEPCK in complex with different substrates (OAA, PEP, GTP, and GDP). In these complexes, the mobile regions, specifically the Ω-loop lid, were always in an open conformation (Figure 1-10-A) (*25*). When the structure of the Michaelis complex was solved, there was a 50-50 distribution of lid states between open and closed (Figure 1-10-B) (*27*). Finally, the structure with the enolate intermediate bound always has the lid in the closed conformation (Figure 1-10-C) (*27*). These data suggest that the formation of the closed-lid state is increasingly favored as the enzyme progresses from the holo enzyme through the Michaelis and intermediate complexes.

This operates by a mechanism in which the entropic penalty of closing the lid is offset by the favorable Gibbs free energy of interaction between enzyme and ligands, building on the idea put forth by Fersht and Jencks (*36, 37*). To summarize, a portion of the enthalpic energy of binding is partitioned to the protein, offsetting an unfavorable entropic change that results from the lid assuming an ordered closed conformation rather than a conformationally dynamic open state.

Combining all of the structural and biochemical data on PEPCK has led to a proposed model for the role of the Ω-loop lid domain in catalysis. In this model, the Ω-loop is energetically coupled to ligand binding. The data further suggested a number of functional roles for the lid domain (*27*), the first being the correct positioning of the substrates, which only occurs upon the closure of the P-loop and Ω-loop domains (*5*). The other roles of the lid deal with the reaction intermediate, the enolate. Since the enolate is highly reactive, the chemical mechanism necessitates its protection from bulk solvent. Exposure of the enolate to water would result in its protonation resulting in the formation of pyruvate, a deleterious alternative chemistry (*27*). It is proposed that closure of the Ω-loop sequesters the enolate in the active site and protects the reaction until phosphoryl transfer can occur (*38*). Through the finely tuned dynamic motions, and particularly the motion of the lid element, PEPCK can catalyze the conversion of OAA to PEP.

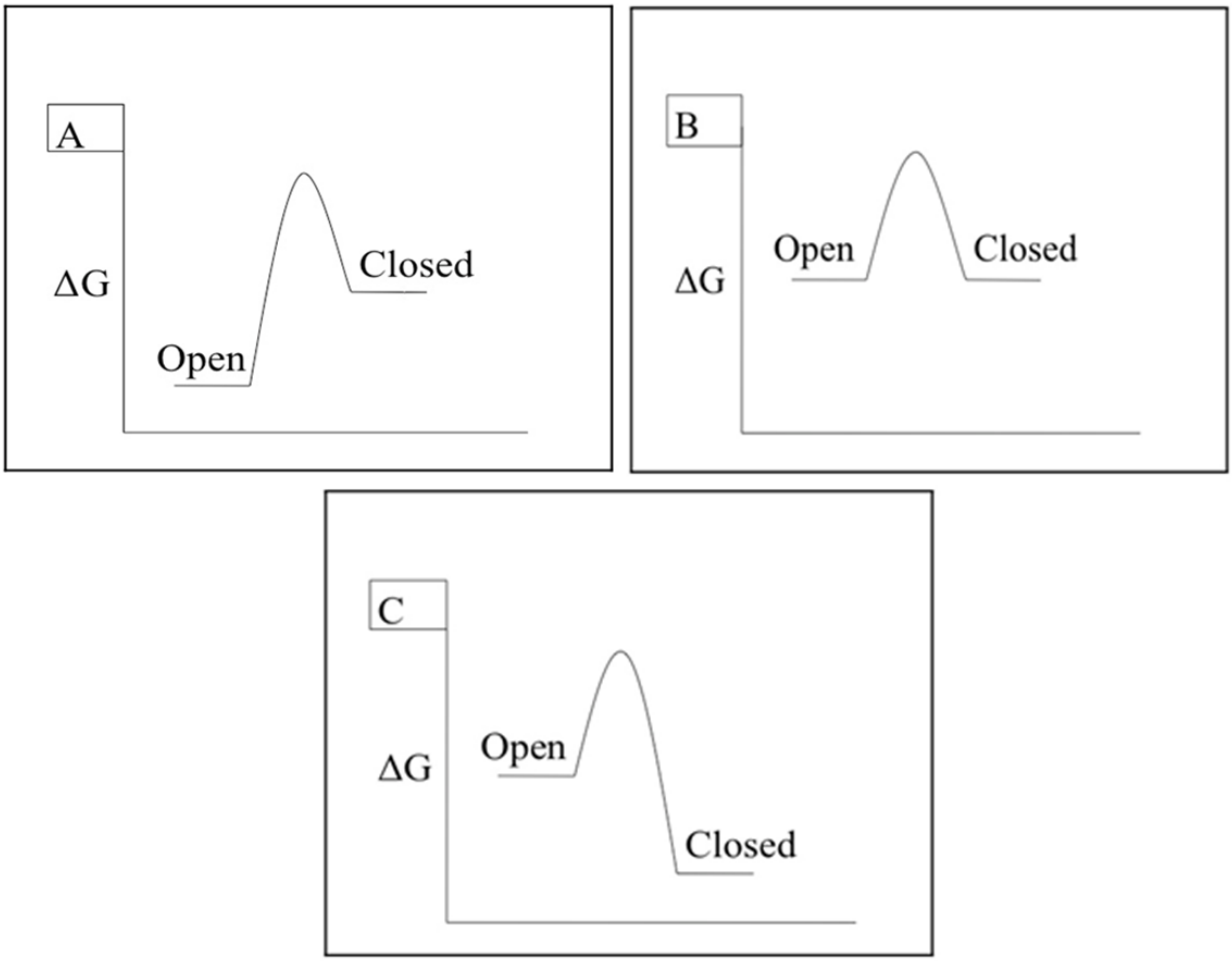

Figure 1-10. Free energy distribution of lid conformations

A cartoon representation of the free energy diagram for the conformational shift between the lid open and closed states in the (A) holo enzyme, (B) Michaelis complex, and (C) the enolate intermediate.

Chapter 2 Removal of the Ω-loop lid domain

Introduction

Enzymes catalyze a multitude of different chemical reactions. Understanding how they function has been an area of interest for many years. It is commonly accepted that proteins are not rigid in solution, but flexible and able to sample multiple conformations to adapt a catalytically active form (*33*). The ability to sample different conformations can vary widely between enzymes, meaning the mobile elements can theoretically be as small as a side chain rotameric shift, as large as a whole domain shift, or complete structural refolding. There are multiple different regular secondary structures that a protein region can fold into (α-helix, β-sheet, etc.) and these can have motional properties as well. One non-regular secondary structure element is an omega-loop which is a 10-20 amino acid region characterized by its resemblance to the Greek letter omega with a very narrow end-to-end distance (3-5 Å typically) (*39*). This type of loop is usually on the protein surface and can have a conformational movement of up to 10 Å at the tip (*40*). These different conformations are usually observed via X-ray crystallographic analysis when different substrates are bound to the enzyme. The open/closed transition can be ligand gated and is often essential for catalysis (*27, 40*). One enzyme that has been structurally characterized and found to have a catalytically important Ω-loop is PEPCK (*24, 25, 27*).

PEPCK catalyzes the first committed step of the gluconeogenesis pathway, the reversible decarboxylation and phosphorylation of OAA to form PEP (Figure 1-2). The reaction is freely reversible *in vitro,* but operates primarily in the direction of PEP synthesis *in vivo*. PEPCK requires two divalent cations for enzymatic activity, with the preferential cations being Mn^{2+} and Mg^{2+} (*18-20*). Manganese is the most activating cation in the GTP-dependent isoforms of PEPCK, but Mg^{2+} presumably fills the second cationic site, since the metal-nucleotide complex is the true substrate, there is more Mg^{2+} present than Mn^{2+}, and the nucleotide has a higher

affinity for Mg^{2+}. PEPCK has been extensively characterized biochemically and, more recently, structurally. The structural studies illustrated many previously unappreciated features of PEPCK, specifically the different mobile elements the Ω-loop lid, the P-loop, the R-loop and the bi-lobal fold (Figure 1-6 a/b) (reviewed in (*5*)). These features were identified by mapping the protein as it progressed through the catalytic cycle, utilizing substrate analogs to mimic the different complexes (*27*). As the enzyme transitions from the holo state to the Michaelis complex to the intermediate state, each mobile element moves in concert with the others to play their individual roles culminating in catalysis. The R-loop and the P-loop are involved in OAA and GTP binding, respectively. Further, the bi-lobal fold and the Ω-loop lid transition between an open/closed conformation without directly interacting with the substrates in the active site. However, in order for the Ω-loop and the bi-lobal motions to occur, the P-loop must first move forward by ~0.5 Å (*5*). This movement serves two purposes: one to remove the steric clash between Thr-465 on the Ω-loop and Ala-287 on the P-loop, and too, correctly position the γ-phosphate of GTP for direct inline phosphoryl transfer (*5*). As soon as the P-loop has repositioned the GTP, and OAA is bound, the N- and C-terminal lobes can sample the closed conformation, which effectively reduces the size of the active site, helping to protect the highly reactive enolate intermediate formed during the transition from OAA to PEP. Once the lobes have closed, the Ω-loop adapts the closed conformation, forming a stable salt bridge between His-470 on the lid and Glu-89 on the R-loop (Figure 3-1) (*25*). The structural data suggest that only upon closure of the Ω-loop are all substrates correctly positioned for catalysis to proceed. Furthermore, based on the step-wise reaction scheme for PEPCK and its progression through the highly reactive enolate another role for the Ω-loop is in the protection and sequestering of the enolate from alternative chemistries (*5*).

Multiple other enzymes, such as triosephosphate isomerase, glutathione synthetase, and ribulose-1,5-bisphosphate carboxylase/oxygenase, have also been shown to have an Ω-loop that transitions between an open and closed conformation (*40-43*). Based on the structural work on these enzymes, a role was proposed for the Ω-loop (similar to PEPCK) in which the loop acts to sequester and protect the reaction intermediate; however, after removal of the loop and subsequent functional assessment, additional roles for the Ω-loop were discovered, such as recruiting of charged groups to the active site, aiding in correctly positioning substrates and side chains, and stabilizing protein conformations (*40-42*). The realization that the structural information tightly constrained the role of the Ω-loop in these other enzymes and that only upon loop removal were the other functional roles elucidated, leads to the idea that in PEPCK the Ω-loop potentially has further roles during the catalytic cycle than currently recognized.

To investigate the proposed role of the Ω-loop lid in PEPCK catalysis and elucidate any further roles for it, a series of lid deletions were created (Figure 2-1). The loop in PEPCK is 11 amino acids starting at residue 464 and ending at 474. The distance between the Cα of Ala-464 and Val-474 is ~5 Å; knowing the normal Cα-Cα bond distance to be ~4.5 Å, it was hypothesized that it would take between 1-3 amino acids to successfully bridge the gap without distorting the overall fold and the region immediately before and after the Ω-loop. Three lid deletion mutants were created, each of which removed residues 464-474 and replaced them with one glycine (Ld_1g), two glycines (Ld_2g), or three glycine residues (Ld_3g). In order to elucidate further roles of the lid domain in PEPCK function the mutants were characterized via structural and thermodynamic techniques to further investigate the role of the active site lid.

	459		478
Wt	A M R S E *A T A A A E H K G K V*		I M H D
Ld_1g	A M R S E	***G***	I M H D
Ld_2g	A M R S E	***GG***	I M H D
Ld_3g	A M R S E	***GGG***	I M H D

Figure 2-1. Lid deletion amino acid sequence

Amino acid sequence of WT and Ld_1, 2, 3g PEPCK with the site of the mutation in bold and underlined. The Ω-loop amino acid sequence is italicized.

Results

Kinetic characterization of the lid deletion mutations

Kinetic experiments (Assays A-D see chapter 5 kinetic assays) were attempted for all three lid deletion mutants. However, due to the removal of the Ω-loop, the mutant enzymes were unable to catalyze the conversion of OAA to PEP, or vice versa, at a detectable rate. Furthermore, the mutant enzymes were unable to catalyze the first half-reaction (Assay C), the decarboxylation of OAA.

Nucleotide binding by fluorescence quenching.

Direct measurements of the K_D values for IDP and ITP were carried out by intrinsic protein fluorescence quenching. The inosine nucleotides were substituted in place of guanosine to reduce the inner filter effect observed when guanosine nucleotides are utilized, inosine absorbs less of the excitation energy than guanosine. PEPCK utilizes inosine and guanosine nucleotides with similar catalytic efficiency, while ITC experiments on the human enzyme have demonstrated the exocyclic C-2 amino group of guanosine nucleotides increases the affinity of the enzyme for those nucleotides by approximately an order of magnitude over that of the inosine analogue (*44*). As shown in Table 2-1, WT PEPCK has a K_D for ITP of 0.79 μM while Ld_1g has a K_D of 4.7 μM, Ld_2g has a K_D of 2.4, and Ld_3g has a K_D of 3.2. Meanwhile, the dissociation constants for IDP are 2.7 μM, 40 μM, 16 μM, and 32 μM for WT and Ld_1, 2, and 3g respectively. The curve fits of the raw data can be found in Appendix 3.

Table 2-1. Thermodynamic binding constants of lid deletion PEPCK

Characterization of the lid deletion mutants		
	Substrate Affinities	
Enzyme	**K_D (ITP) (μM)**	**K_D (IDP) (μM)**
Wt	**0.79 ± 0.07**	**2.7 ± 0.1**
Ld_1g	**4.7 ± 0.3**	**40 ± 4**
Ld_2g	**2.4 ± 0.3**	**16 ± 2**
Ld_3g	**3.2 ± 0.3**	**32 ± 3**

Structural characterization of lid deletion mutants

The removal of the Ω-loop and replacement with one, two, or three glycine residues left the mutant enzymes catalytically inactive. In order to determine the cause of the inactivity and investigate any additional roles for the Ω-loop lid, the structure of each lid deletion was solved in complex with βSP, PEP, or oxalate, plus either GTP or GDP, and Mn^{2+}. Data statistics can be found in Appendix four. The lack of enzymatic activity made it possible to utilize the physiological substrate PEP in place of its analog PGA (used in the WT studies). OAA could have been used in place of βSP, however, the non-enzymatic decarboxylation of OAA in the presence of metal would have caused a mixture of OAA and pyruvate in the active site. Assuming, the electron density maps were of sufficient resolution it would not be an issue to model in both substrates, but for the sake of clearly identifying what is affected by the lid removal, the OAA analog (βSP) was utilized. Structural studies on the WT enzyme in complex with βSP, PGA, and oxalate demonstrated that as the enzyme commits to catalysis the thermodynamic favorability of the enzyme adapting the closed lid conformation increases (*27*). In order for the enzyme to properly orient the active site for catalysis, a series of structural changes must occur. These motions include the closing of the P-loop, ordering of the R-loop, closing of the N- and C-terminal lobes, and the closing of the Ω-loop lid (*5*). A disruption of any of these motions will hamper catalysis (*28, 29, 38*). Crystals of each lid deletion were grown under similar conditions as previously used for the WT enzyme; however, the removal of the lid allowed the enzymes to pack in a different crystal lattice. The crystals had a different morphology upon inspection, which resulted in a different Bravais Lattice when indexing the diffraction data. The WT PEPCK co-crystallized with GTP/GDP and soaked with the substrate analog are observed to be in the $P2_1$ space group, while the lid deletion mutants grown identically

are in $P2_12_12_1$. The higher order space group is indicative of tighter packing and allows the data to be collected using a 90° wedge, as opposed to collecting a full 360° in the $P2_1$ crystals.

The structures of the lid deletion mutants in each individual complex were highly similar, allowing generalizations to be drawn for each structural complex. The first is the Michaelis complex in the physiological OAA→PEP reaction. In each of the mutant isoforms βSP and GTP are bound in the active site in an identical orientation observed in the lid open molecule of the WT enzyme of the same complex (for an example see Figure 1-9). There are no significant differences between the mutants and WT in this complex except the absence of the Ω-loop (there are no significant distortions of the regions before and after the lid) (Figure 2-2). In the Michaelis complex in the PEP→OAA reaction, PEP-GDP, a comparison between the WT and the mutants reveals no differences among the different mobile elements. The only difference observed is that in the mutants there is a mixture of GDP and GTP in the active site. HPLC purified GDP was utilized in the crystallization conditions, but a small contamination of the solution with GTP remains. The binding constants for the di- and tri-phosphates (Table 2-1) show a slightly higher affinity for the tri-phosphate, which could account for the mixture of the two in the active site. As a result of the contamination the PEP molecule has a slightly reduced occupancy of its phosphate, but it does bind in an identical orientation to that observed in the WT PEPCK-PEP-Mn^{2+} complex (PDB ID: 2QZY).

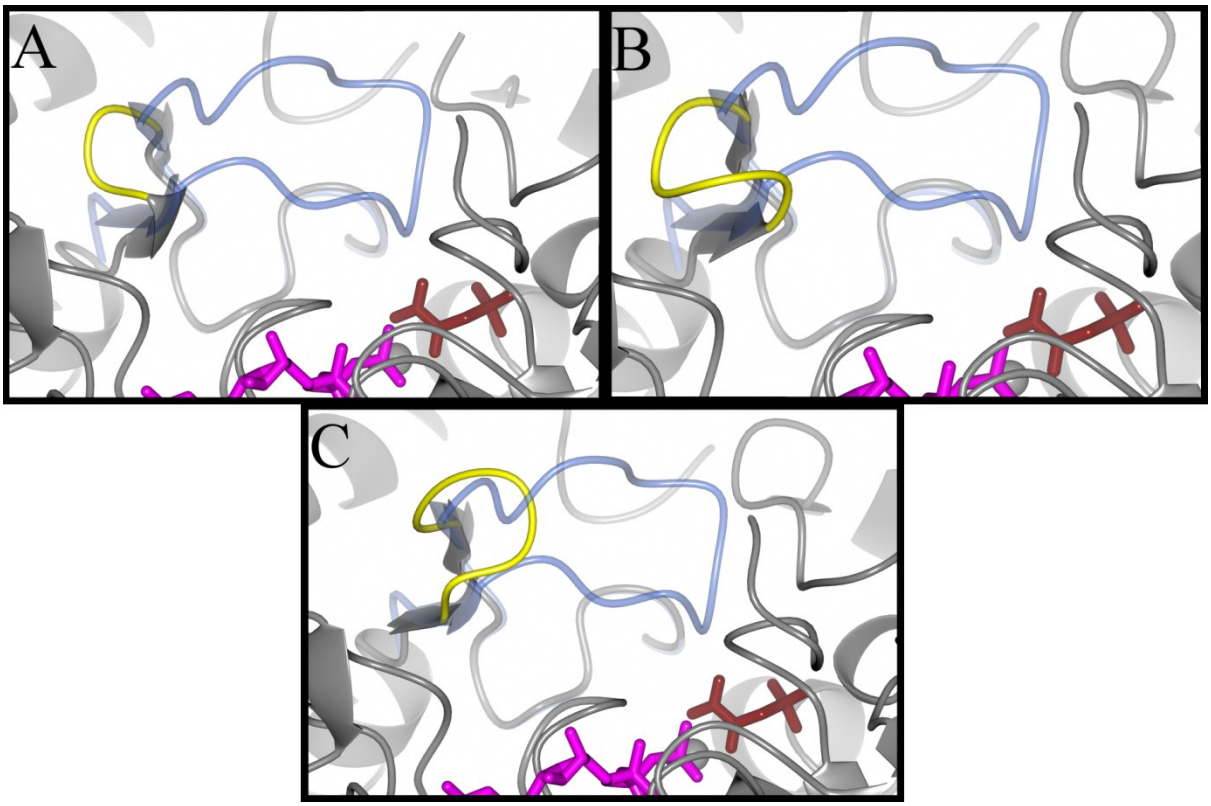

Figure 2-2. Active site lid region of Ld_1, 2, and 3g.

Upon lid removal the protein still adapts its native fold with no distortion around either hinge region (464 or 474). Each panel is a different lid deletion mutant in complex with βSP (tan) and GTP (magenta) A) Ld_1g, B) Ld_2g, C) Ld_3g. The small yellow loop is the glycine residues which replaced 464-474. The blue Ω-loop that is visible is from the WT enzyme in the same complex to show where the lid would normally reside.

The last set of structures solved for the lid deletion mutants were those obtained in complex with oxalate and GTP. In this complex with the WT enzyme all of the mobile elements are closed/ordered (R-loop, P-loop, Ω-loop, and the N/C terminal lobes) and Y235 is rotated forward aiding in the stabilization of the CO_2 leaving group and through it the enolate intermediate (See Figure 1-9). In the lid deletions the R-loop is observed in two conformations (Figure 2-3). The first orientation is normal compared to the WT enzyme, but the second is flipped out. The flipped conformation, with a minor occupancy less than 30%, results in a displacement of residues 86-89 with the Cα of R87 being moved the furthest at 6Å. The P-loop is occupying the rearward orientation, which in turn keeps GTP at a non-catalytically relevant distance from the enolate intermediate. This sampling is true for the N- and C-terminal lobes as well. A detailed look through the peptide backbone reveals positive difference density which could account for the shift in the lobes from open to closed, but the predominant orientation of the lobes is in the open conformation. The other interesting feature of the lid deletion complexes with oxalate and GTP is the split conformation of Y235. As shown in Figure 1-9 in the WT enzyme Y235 rotates forward to aid in stabilizing the CO_2 leaving group upon decarboxylation of OAA. In these mutants Y235 has a 50-50 occupancy of the forward and rearward orientations. Combining all of the structural data and keeping in mind the inactivity of the lid deletion mutants, additional roles for the Ω-loop can be proposed.

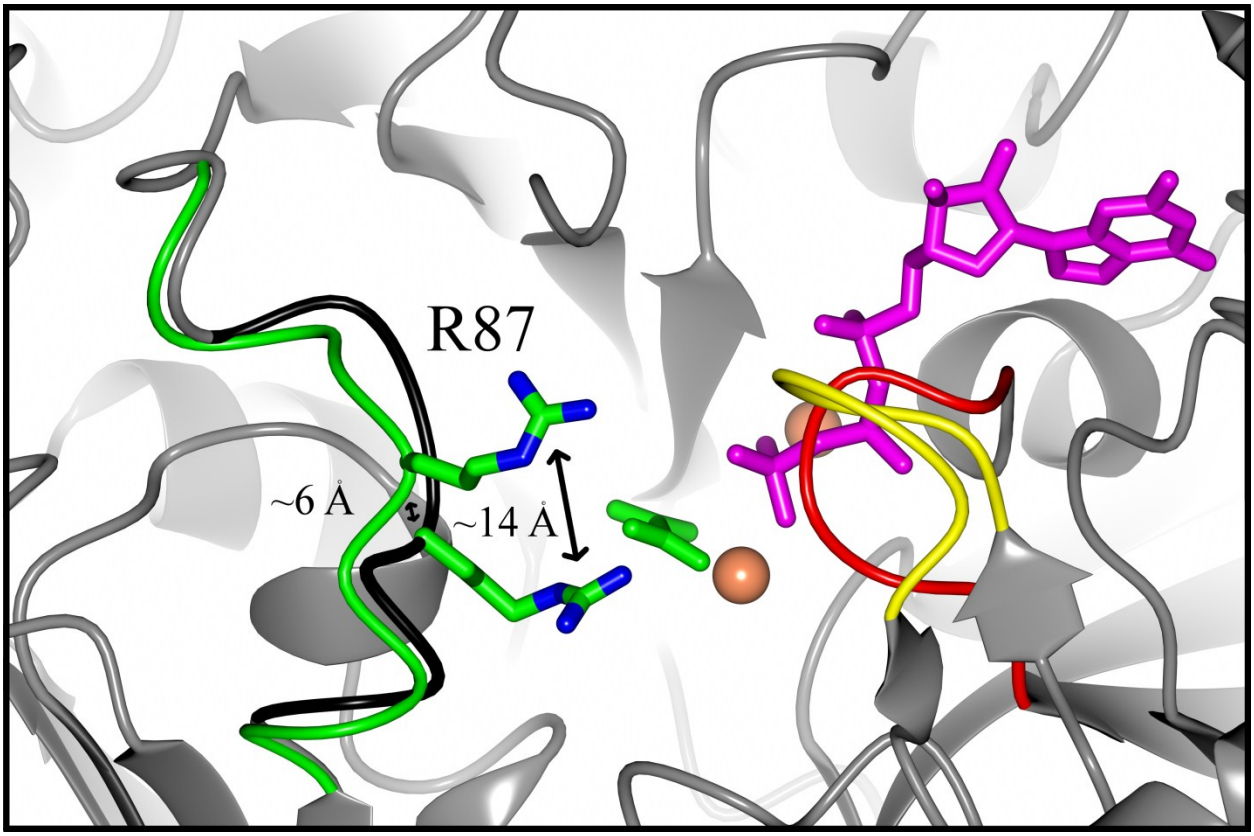

Figure 2-3. R-loop movement in Ld_3g

The lid deletion mutants in complex with GTP showed a minor occupancy for a "flipped" out orientation (green) with arginine 87 no longer positioned to interact with the enolate intermediate. The Ω-loop is yellow, P-loop is red, GTP is magenta, oxalate is green, manganese is coral, and the normal orientation for the R-loop is black.

Discussion

Structural characterization of proteins via X-ray crystallography and NMR has allowed scientists to visualize the protein surface at the molecular level. This has led to the observation that primary, secondary, and tertiary structural elements each have a certain inherent flexibility allowing them to sample multiple conformations (*33, 35*). One non-regular secondary structural element that has been observed in multiple enzyme systems to have mobile features that are critical to catalytic function is the omega-loop (Ω-loop) (*41, 42, 45-51*). This particular type of loop is characterized by its very narrow end-to-end distance, resulting in the structural domain, resembling the Greek letter omega (Figure 2-4). A number of enzymes with this type of loop undergo a transition from disordered to ordered as the enzyme binds substrates for catalysis (*39, 40, 42, 47*). This ligand gated transition is usually identified by crystallographic analysis when different substrates are bound to the enzyme (*24, 27, 39*). Utilization of crystallography limits the enzyme to the lowest energy state for a given enzyme-substrate complex, therefore, the involvement of the Ω-loop in catalysis is generalized by what is observed in the electron density for these WT structures. Previous studies carried out on the glycolytic enzyme triosephosphate isomerase, glutathione synthetase, and ribulose-1,5-bisphosphate carboxylase/oxygenase illustrate that structural information on the WT enzyme alone does not reveal the entire role for an Ω-loop in catalysis (*41-43*). To further probe the role of the Ω-loop in each respective enzyme the loop was removed. Upon functional assessment it was determined that additional roles for the Ω-loop existed in each enzyme system.

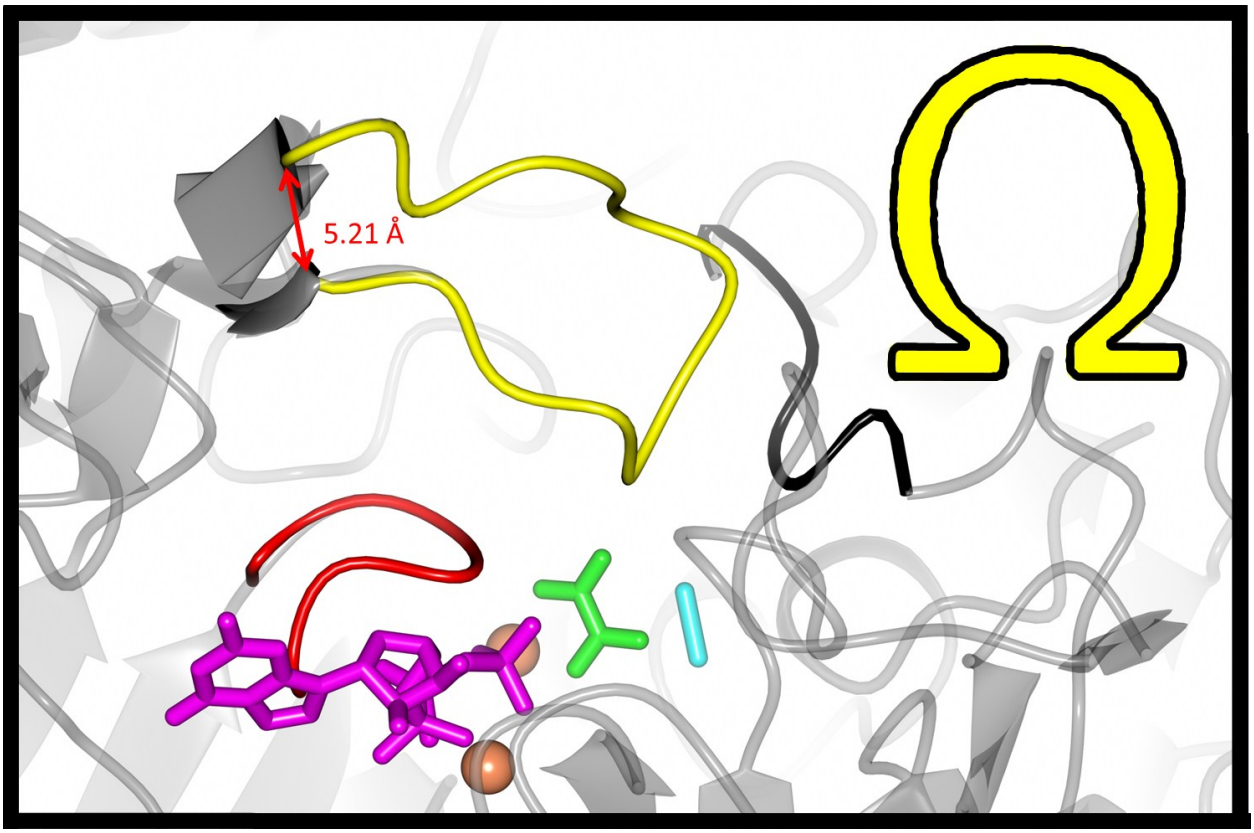

Figure 2-4. Architecture of an Ω-loop

An omega loop looks like the Greek letter Ω, shown in yellow, with a minimal distance separating the ends. In the case of PEPCK the end-to-end distance is 5.21Å. The other colored regions are the mobile P-loop (red) and R-loop (black) and the substrates GTP (magenta), oxalate (green), and CO_2 (teal).

The gluconeogenic enzyme PEPCK was discovered in the 1950's and has been extensively characterized metabolically and biochemically. It was only recently (15 years ago) that the first structure of PEPCK was solved, and only within the last five years that structural changes occurring during catalysis were mapped out (*23-25, 27*). It was from these more recent structural studies on PEPCK that the Ω-loop was identified. Based upon the ligand-gated nature of the Ω-loop and the chemical mechanism of PEPCK, progressing through an enolate intermediate, a model for Ω-loop function was put forth (*27*). In the model the Ω-loop of PEPCK acts as an active site lid and functions to sequester and protect the reaction intermediate, correctly position substrates, and aid in the transition between ground states. As previous studies have shown characterization of a WT enzyme does not necessarily reveal the entire scope of loop involvement in catalysis (*40, 42*). In order to fully probe the role of the active site lid in PEPCK catalysis, the 11 amino acid Ω-loop was removed and replaced with 1-3 glycine residues.

Rational behind lid removal

The unique architecture of an Ω-loop results in a narrow end-to-end distance (Figure 2-4). In the case of PEPCK the Cα of the loop hinge residues, Ala-464 and Val-474, are ~5 Å apart. Therefore, replacing the 11-amino acid loop in PEPCK with one, two, or three glycine residues should allow the loop to be removed without distorting the overall fold of the protein. Furthermore, the area directly around the hinge regions should have minimal distortion, if any at all. The removal of the loop will result in the loss of any stabilizing interactions between the Ω-loop and the body of the protein. The loss of stabilizing interactions will test the proposed model (Chapter 1. *A free energy landscape model for PEPCK catalysis*) for PEPCK Ω-loop function in substrate positioning and enolate protection, and allow additional roles to be elucidated.

Kinetic and thermodynamic characterization

PEPCK catalyzes the reversible OAA→PEP reaction at a reasonable rate *in vitro* (See Chapter 3 Table 3-1 for WT values). However, any mutation can have a profound effect on catalysis if that residue is involved in the enzyme's function. In the case of PEPCK the Ω-loop was predicted to play a role in the catalytic cycle by correctly positioning substrates and protecting and sequestering the reaction intermediate. Removal of the lid and replacement with one, two, or three glycines rendered the enzyme catalytically inactive in each of the four assays utilized in PEPCK characterization. To determine whether or not this was a result of loop removal and not a function of disrupted binding, fluorescence quenching experiments were performed to investigate nucleotide binding. The results of those experiments (Table 2-1) show that nucleotide binding is only slightly affected. The difference in ITP binding is 5-fold at the most (Ld_1g) but is still 4.7 μM, while the K_D for IDP is decreased 15-fold to 40 μM in the mutant with the biggest change (Ld_1g). While the values do differ, the degree to which they have been altered is not large enough to account for the total inactivity of the lid deletion mutants. At the present time there is not a reliable assay in which to measure direct ligand (OAA/PEP) binding to see if it has been disrupted. However, the crystallographic evidence illustrates that these ligands bind to the enzyme in their native orientations.

Structural characterization of Δ464-474 PEPCK

The lack of enzymatic activity in each of the kinetic assays for the Ld_1g, 2g, and 3g mutants suggests that lid removal equates to loss of activity, but the question how or why the enzyme is inactive remains. To try and answer this question the structure of each lid deletion mutant was solved in complex with βSP-GTP, PEP-GDP, and oxalate-GTP. These are the same substrates/analogs used when WT PEPCK was structurally characterized (*24, 25, 27*). Through this series of structures it was observed that PEPCK has a number of regions undergoing

dynamic changes dependent upon the ligation state of the enzyme (Figure 1-6A). One of these mobile elements, the P-loop, contains a reactive cysteine residue (C288) that upon modification (WT PEPCK) results in the inactivity of the enzyme (*28, 29*). At the time of the inactivation studies, the crystal structure of PEPCK had not been solved nor had the P-loop been identified; however, in light of the recent structural work, the inactivity is presumably due to the prevention of the P-loop from moving forward in the active site. The P-loop movement is required to correctly position the GTP/GDP nucleotide and remove a steric clash between Thr-465 on the Ω-loop and Ala-287 on the P-loop. PEPCK has two other motions that undergo an open/close transition upon ligand association, the N- and C-terminal lobes and the Ω-loop lid (Figure 1-6A&B). The motion of the lobes was not readily identified from the original study, for the simple fact that the motion of the lobes is not significantly large. Superposing the WT PEPCK–Mn^{2+} and WT PEPCK–oxalate–Mn^{2+}–Mn^{2+}GTP structures revealed that the N- and C-terminal lobes are offset from one another. Upon submission of these PDB files for normal mode analysis this motion was exaggerated and easily identified (Figure 1-6B) (*52*). The normal mode analysis server (*El Némo*) predicts possible conformations of a macromolecule in solution, or in the case of PEPCK the largest amplitude motion between the two different structures. What is observed in the crystal lattice is restrained by packing interactions between the molecules. The server is able to predict the freedom the enzyme would enjoy in solution and accurately predict its free range of motions. Although, the server is limited in its ability to predict when the motions occur, knowledge from the extensive crystallographic characterizations of WT PEPCK predicts that the lobes close upon ligand association. The last mobile element is the Ω-loop lid, which has been shown to change its conformation from open to closed, based on the ligation state of the enzyme (*27*). The importance of these transitions is critical to PEPCK function.

(i) βSP-GTP Michaelis-like complex and PEP-GDP Michaelis complex

The first structures solved for each of the lid-deletion mutants were the forward and reverse Michaelis complexes. The forward Michaelis complex is formed with βSP (Figure 3-4) and GTP; this is the same complex used in the WT enzyme (PDB ID: 3DT7). In the WT structure there were two molecules in the asymmetric unit (ASU), with one molecule occupying a closed lid conformation and the other an open lid. All of the lid deletion mutants mimic the lid open complex, with all active site substrates and residues in identical orientations to their WT counterpart. In the reverse Michaelis complex, PEP was used instead of the substrate analog PGA (used in WT PDB ID: 3DTB). Due to the kinetic inactivity observed with the mutant enzymes, the true complex with PEP-GDP could be utilized. In the WT enzyme with PGA-GDP it was observed, similar to the βSP-GTP complex, to have two molecules in the ASU, with one adapting an open lid conformation and the other a closed lid conformation. In the Ld_1, 2, and 3g structures the enzyme retains the lid open conformation. The biggest difference is that PEP binds in a different orientation compared to PGA. However, the structure of WT PEPCK has been solved in complex with PEP and a comparison of the orientations shows that in each of the lid deletions, PEP is oriented identical to the WT structure. The one unusual aspect of the PEP-GDP complexes was in each mutant a mixture of GTP and GDP can be found in the active site. This mixture of the two nucleotide species is thought to be a contamination of the GDP stock by GTP.

(ii) Oxalate-GTP Intermediate

As PEPCK progresses through the reaction coordinate the enolate intermediate is the most important step to protect from bulk solvent. A mimic of the enolate (oxalate; Figure 3-4) is utilized for the structural characterization, as it has been shown to bind the active site manganese similar to the C1 and C2 carbons of OAA. In the WT enzyme the structure in complex with

oxalate and GTP is always observed in the closed lid state. To make this transition happen, a number of mobile elements must change conformations (Figure 1-9). In contrast, the lid deletion mutants in complex with oxalate and GTP are observed primarily in the open lid conformation. What is different from the WT enzyme is that the R-Loop has a minor conformation in which it is flipped out of the active site toward bulk solvent, and the N- and C-terminal lobes of the enzyme are open (Figure 2-5A). The differences between the structures of the WT and mutant enzymes suggest additional roles for the Ω-loop lid. First, the flipping out of the R-loop has never been observed previously, which suggests that the interaction between His-470 and Glu-89, upon lid closure, aids in stabilizing the lid-closed conformation (suggested in (*24*)) and further stabilizes the R-loop to maintain ligand association. In the WT structures with oxalate the N- and C-terminal lobes are always observed to be closed. Lobe closure aids in the ability of the active site to exclude bulk solvent, aiding in protection of the reaction intermediate (Figure 2-5B), and more importantly, positions the phosphoryl donor and acceptor close enough for phosphoryl transfer. In the lid deletion enzymes the lobes are observed to be in the open conformation, which suggests that lid closure acts as a latch between the lobes allowing them to remain closed during the chemical steps of the reaction. The results from this study allow a new model for Ω-loop function during PEPCK catalysis to be proposed. The Ω-loop lid on the surface of PEPCK has a role during catalysis that consists of stabilization of the R-loop and lobe closure, correctly positioning substrates in the active site, and sequestering and protecting the reaction intermediate.

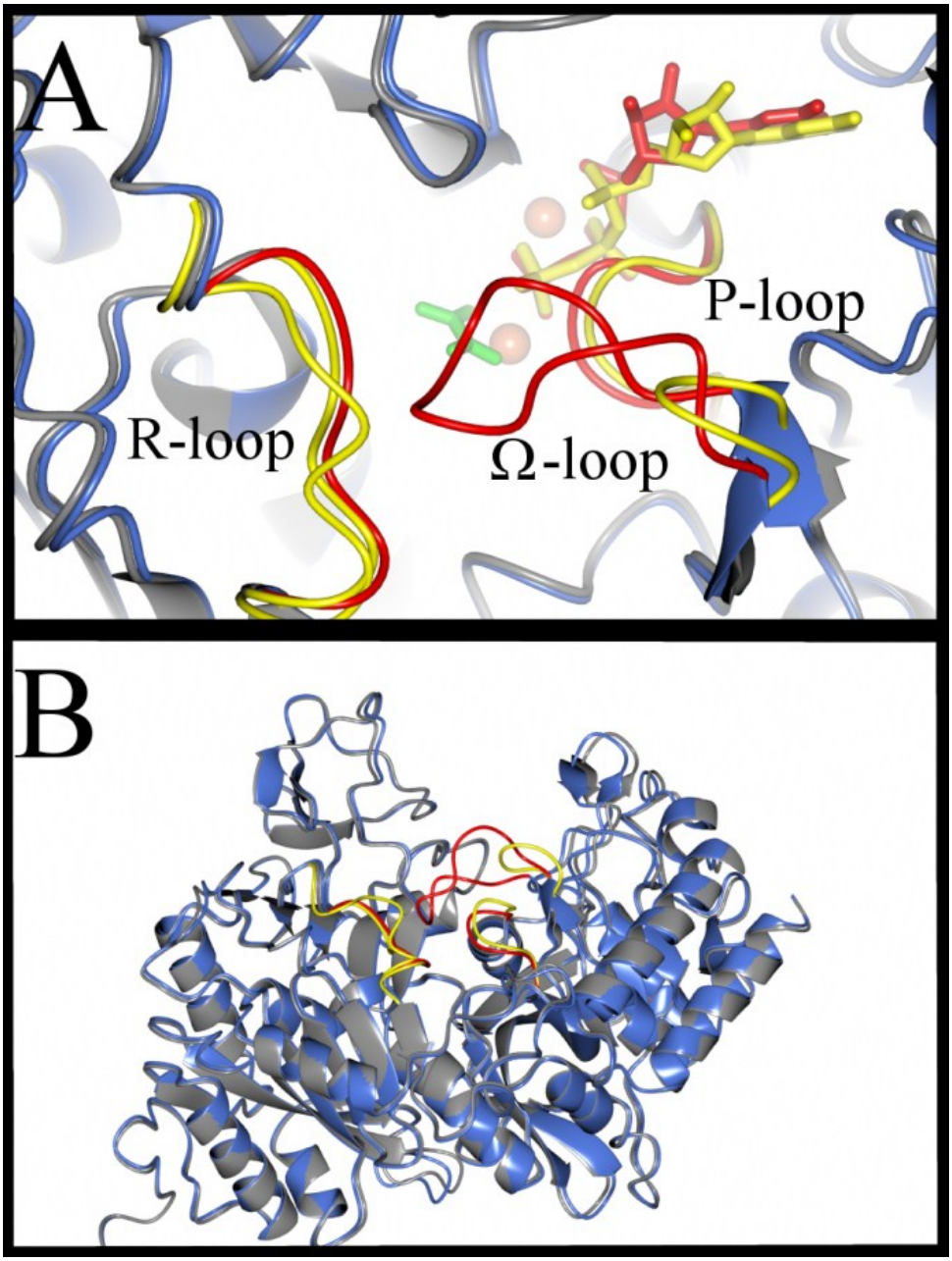

Figure 2-5. Active site and whole protein overlay of Ld_3g and Wt

Overlay of Ld_3g and WT PEPCK in complex with oxalate and GTP. Removal of the lid region alters the ability of the enzyme to stabilize the structural changes necessary for PEPCK catalysis to occur. Above the WT whole protein is blue, with the loops and substrates in red. Ld_3g whole protein is grey, the loops and substrates in yellow (note the R-loop is observed in two conformations). A) zoomed in look at the mobile regions, B) whole protein view.

Chapter 3 Disruption of the free energy profile by mutagenesis

Introduction

Phosphoenolpyruvate carboxykinase (PEPCK) catalyzes the reversible decarboxylation of oxaloacetate (OAA) with subsequent phosphorylation to form PEP, utilizing GTP as the phosphate donor as shown in Figure 1-2. Bacteria, yeast, and certain plants use ATP. While *in vitro* the reaction is freely reversible, the consensus is that in most organisms PEPCK operates primarily in the direction of PEP synthesis. One of the exceptions is *Ascari Suum,* which fixes CO_2 and synthesizes OAA to replenish the TCA cycle (*22*). PEPCK is a metal-requiring enzyme demonstrating an absolute requirement on divalent cations for activity. Mn^{2+} is the most activating cation in the GTP dependent isoforms (*18-20*). In addition a second divalent metal ion is required for the reaction, as the metal-nucleotide complex is the true substrate; Mg^{2+} and/or Mn^{2+} is able to fulfill this role. In higher eukaryotes PEPCK is present as both a cytosolic and mitochondrial isoform, with the relative distribution in the liver of the two isoforms being species dependent (Table 1-1) (*2, 3, 6*). Biologically cPEPCK functions as a key cataplerotic enzyme, removing TCA cycle anions for usage in downstream metabolic pathways. In addition to PEPCKs well-characterized role in gluconeogenesis, it also participates in the lesser known pathways of glyceroneogenesis and triglyceride biosynthesis, as well as the synthesis of serine (reviewed in (*9*)) (Figure 1-1). In contrast, the role of mPEPCK in metabolism is relatively unknown.

The recent structural studies on PEPCK have revealed many details about the enzyme during the catalytic cycle. First and foremost, the structures illustrated the cationic active site, composed of the two divalent metal ions, and specific lysine and arginine residues that are positioned to readily carry out the reversible decarboxylation/carboxylation and phosphoryl transfer half-reactions (Figure 1-9) (*5*). Based on the stepwise reaction pathway (Figure 1-2), it was postulated

that the enzyme forms a highly reactive enolate intermediate that must be stabilized and protected for catalysis to proceed. It has been suggested that this protection/stabilization is what allows for the reversible nature of the PEPCK catalyzed reaction (*5*). Another informative aspect of the structural studies was the revelation that conformational changes are occurring at the active site during the catalytic cycle (*5, 24-27*). These previously unappreciated movements included an eleven-residue Ω-loop lid domain, reminiscent of a similar domain found in TIM (*53-56*). The data suggest that only upon lid closure are the substrates correctly positioned for phosphoryl transfer. Furthermore, closure of the lid may result in the sequestering/protection of the reactive enolate, allowing PEPCK catalysis to proceed via the stepwise mechanism illustrated in Figure 1-2.

The dynamic nature of lid opening and closing raises the questions of what is the energetic driving force for lid closure and what specific role lid closure plays in the catalytic cycle. The structural data on PEPCK demonstrated that no direct contacts are made between the lid when it closes and the substrates in the active site. This is in contrast to the Ω-loop on TIM which directly interacts with its substrate through the phosphate "gripper" (*46*). The single interaction the Ω-loop lid of PEPCK makes upon closing is between His-470 and Glu-89 (Figure 3-1). Glu-89 makes a second interaction with Arg-87, which directly stabilizes the OAA substrate in the active site. Observing this indirect interaction pathway between the Ω-loop and the substrates led us to propose a model consistent with the notion put forth by Fersht and Jencks (*36, 37*). In this model, as the ligands add to the enzyme a portion of their Gibbs free energy of binding is partitioned to the protein, resulting in a shift in the thermodynamic favorability of the enzyme adapting an alternative conformation. In the case of PEPCK this alternative conformational state would be the energetically unfavorable closed lid conformation. The remodeling of the free

energy profile via the energy partitioning can offset the entropic penalty the lid pays when assuming an ordered closed conformation rather than a mobile open (inactive) state (*27*). Recent NMR studies on TIM suggest that it operates under a similar mechanism in which the open-close equilibrium is ligand dependent (*46*). These results are consistent with the proposed model for PEPCK lid motion.

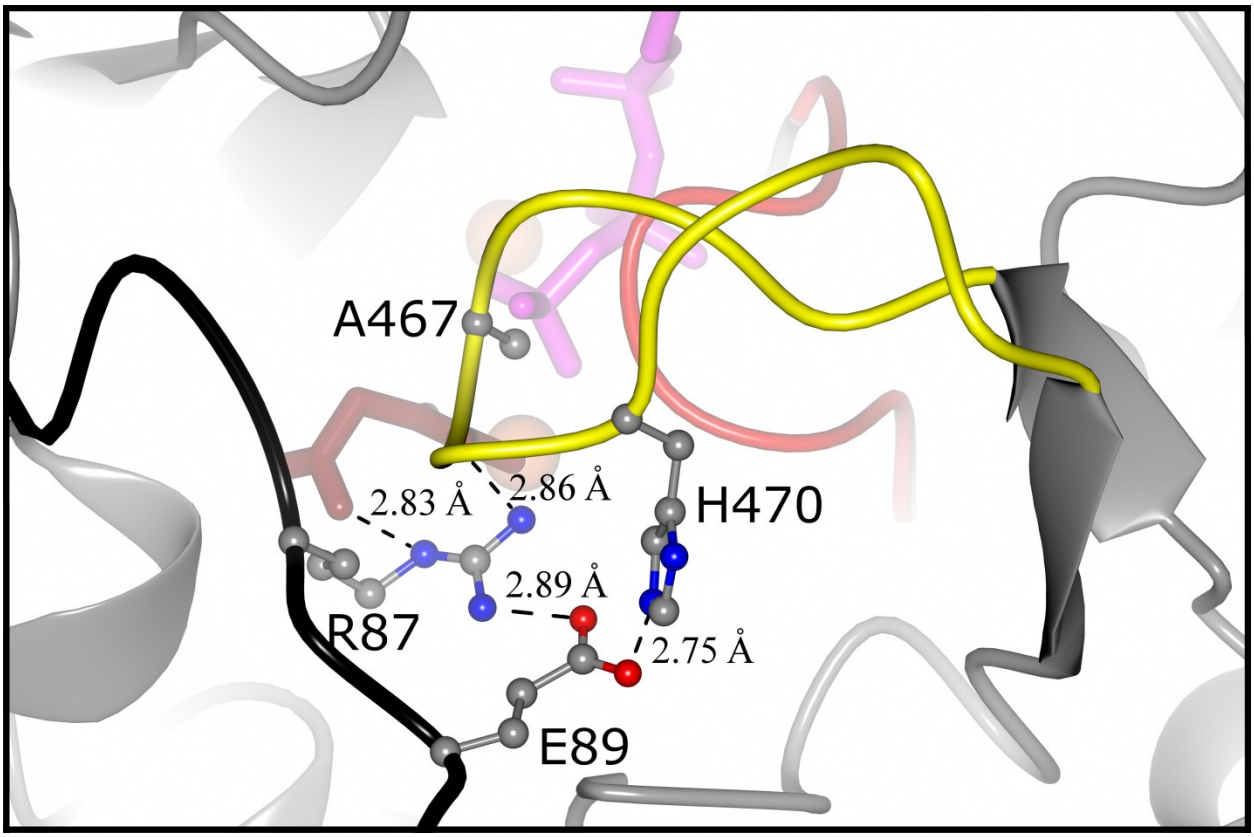

Figure 3-1. Ω-loop interactions in closed conformation.

A potential energetic pathway between the Ω-loop and the active site ligand with the residues involved, shown as ball-and-stick (carbon-gray, nitrogen-blue, and oxygen-red), and the interactions, between OAA (burgundy) and the Ω-loop (yellow), shown as dashed lines. The other structural features and cofactors are shaded as follows: P-loop is red, R-loop is black, GTP is magenta, and the M1 and M2 Mn^{2+} ions are coral.

In order to test our model, that a portion of the Gibbs free energy of binding is partitioned to the enzyme to offset the reduction in conformational entropy upon lid ordering, and to further probe the role of lid closure, I have generated two sets of mutants. The first mutant is a lid mutation (A467G - Figures 3-1 & 3-2) designed to increase the entropic penalty for ordering the lid in the closed conformation. The second set is three R-loop mutations (E89A, D, Q - Figure 3-1 & 3-3) designed to disrupt the free energy pathway between ligands binding at the OAA/PEP site and the lid domain. Structural, kinetic, and thermodynamic characterization was performed on each of the four mutants.

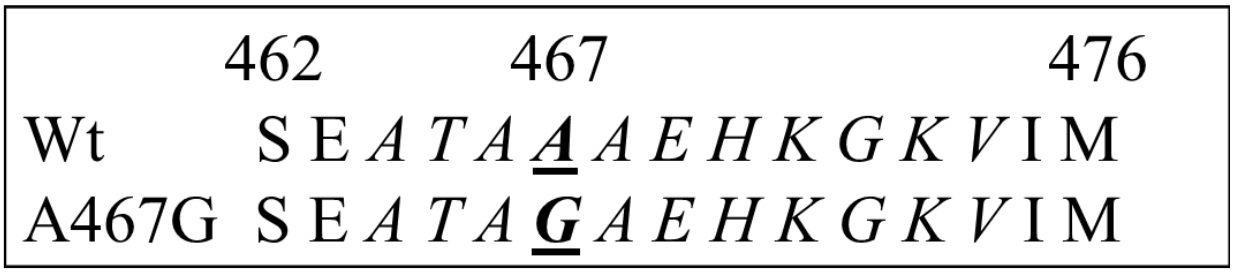

Figure 3-2. A467G mutation

Amino acid sequence of WT and A467G PEPCK with the site of the mutation in bold and underlined. The Ω-loop amino acid sequence is italicized.

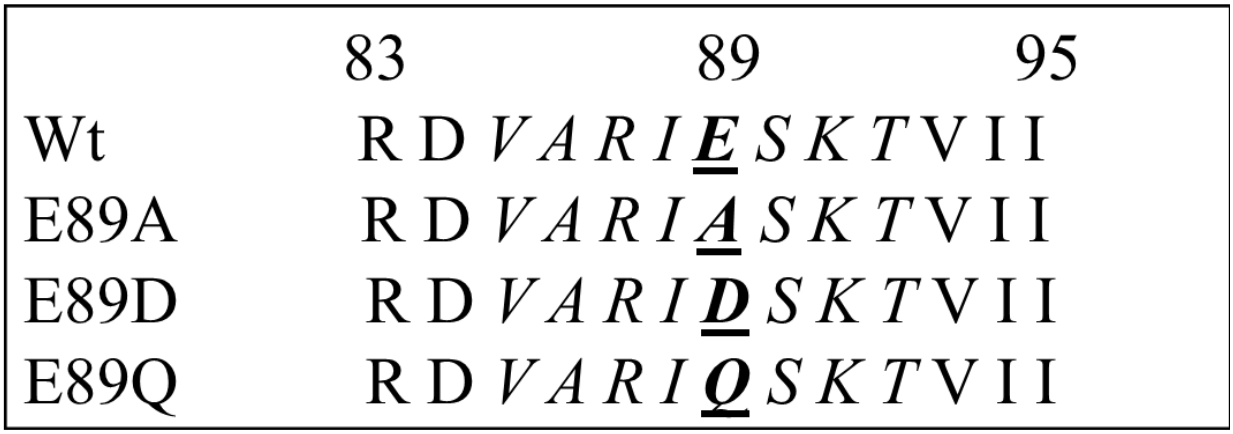

Figure 3-3. E89 mutants

Amino acid sequence of WT and E89A, D, & Q PEPCK with the site of the mutation in bold and underlined. The R-loop amino acid sequence is italicized.

Results

Kinetic experiments were performed to determine the effect of mutation upon the kinetic constants for the reaction in both the direction of PEP formation and OAA formation, as well as the OAA decarboxylase activity (Table 3-1 and 3-2). Further kinetic experiments were carried out to determine inhibition constants for the substrate analogues in lieu of a true thermodynamic measurement (Table 3-2C). However, thermodynamic experiments were utilized to determine binding constants for the GTP and GDP nucleotides via intrinsic protein fluorescence quenching (Table 3-2C). The data presented in the tables show two different WT values for each measurement, due to a change in the expression/purification of PEPCK between the A467 (pGEX vector) and the E89 (pSUMO vector) mutants and also a change in conditions for certain assays. The change in expression system changed the full length enzyme; pGEX has additional glycine and serine residues on its N-terminus due to how the GST tag is cleaved from PEPCK by thrombin. Fits for all of the primary kinetic and thermodynamic data can be found in Appendix three. The structural data and refinement statistics can be found in Appendix four.

Kinetic Characterization of recombinant WT and mutant PEPCK enzymes.

OAA → PEP. In the physiological direction, where OAA is converted to PEP, a mixed metal assay (assay A) was utilized, as the background rate of non-enzymatic OAA decarboxylation is lower in the presence of high concentrations of magnesium when compared to using manganese as the sole divalent cation. Utilizing this assay, A467G PEPCK has a 14-fold higher K_M value for OAA than WT (Table 3-1A); E89A has a 23-fold higher K_M; E89D has a 32-fold higher K_M value; and E89Q has a 29-fold increase in the K_M for OAA versus WT. This increase in K_M is coupled with a reduction in k_{cat} (26% 8%, 29%, and 19% of WT, respectively), resulting in a reduction in catalytic efficiency ($k_{cat}/K_{M,OAA}$) by two to three orders of magnitude (1.9%, 0.4%, 0.9%, and 0.7% of WT). Conversely, there is little change in the K_M for GTP resulting in the

$k_{cat}/K_{M,GTP}$ decreasing by less than a factor of three for A467G, decreasing 8-fold for E89A, 3-fold for E89D, and by less than one for E89Q. As described below, all of these mutants produce pyruvate during the turnover of OAA to PEP. The data for the formation of PEP that is coupled to pyruvate kinase and lactate dehydrogenase was corrected for this pyruvate formation activity.

PEP → OAA. In the reverse direction PEPCK catalyzes the formation of OAA from PEP (assay B). The mutant A467G and the E89 mutants (A and Q) showed a decrease in the K_M value for PEP (21%, 32%, and 32% of WT respectively), while the E89D mutant had no change in the K_M for PEP compared to WT (Table 3-1B). In contrast, all of the mutants have drastically reduced k_{cat} values (1-5% of WT). The combination of a decrease in K_M and a decrease in k_{cat} results in only a factor of four reduction in the k_{cat}/K_M for A467G, while the E89 mutants have a 20-fold reduction relative to WT. On the other hand, the K_M values for GDP were elevated slightly, which resulted in the $k_{cat}/ K_{M,GDP}$ being decreased to less than 1% of WT for E89A and Q and less than 3% of WT for A467G and E89D.

Table 3-1. Kinetic characterization in the physiological direction and its reverse.

(A) Physiological Assay (OAA + GTP → PEP + GDP + CO_2)					
	K_M (μM)			k_{cat}/K_M ($M^{-1}s^{-1}$)	
Enzyme	OAA	GTP	k_{cat} (s^{-1})	OAA	GTP
Wt[a]	52 ± 6	68 ± 4	54 ± 0.2	1.0 x 10^6	7.9 x 10^5
A467G[a]	749 ± 67	47 ± 17	14 ± 0.1	1.9 x 10^4	2.7 x 10^5
Wt[b]	51 ± 4	55 ± 5	52 ± 1	1.0 x 10^6	9.5 x 10^5
E89A[b]	1190 ± 190	25 ± 3	4.4 ± 0.8	3.7 x 10^3	1.2 x 10^5
E89D[b]	1640 ± 300	27 ± 3	15 ± 3	8.9 x 10^3	3.0 x 10^5
E89Q[b]	1470 ± 270	11 ± 2	10 ± 2	6.6 x 10^3	5.7 x 10^5

(B) Reverse Physiological Assay (PEP + CO_2 + GDP → OAA + GTP)							
	K_M (μM)				k_{cat}/K_M ($M^{-1}s^{-1}$)		
Enzyme	PEP	GDP	CO_2	k_{cat} (s^{-1})	PEP	GDP	CO_2
Wt[a]	294 ± 16	39 ± 2	11000 ± 109	19 ± 0.8	6.6 x 10^4	5.1 x 10^5	2.0 x 10^3
A467G[a]	63 ± 11	70 ± 8	7500 ± 900	1 ± 0.1	1.5 x 10^4	1.4 x 10^4	1.4 x 10^2
Wt[b]	475 ± 14	207 ± 23	4000 ± 400	18.5 ± 0.4	3.7 x 10^4	9.2 x 10^4	4.6 x 10^3
E89A[b]	149 ± 8	390 ± 30	5100 ± 500	0.28 ± 0.01	1.9 x 10^3	7.3 x 10^2	5.6 x 10^1
E89D[b]	507 ± 25	265 ± 24	3900 ± 500	0.65 ± 0.01	1.3 x 10^3	2.4 x 10^3	1.7 x 10^2
E89Q[b]	153 ± 7	291 ± 25	2190 ± 160	0.28 ± 0.01	1.9 x 10^3	9.3 x 10^2	1.1 x 10^2

[a] PEPCK enzyme from the pGEX expression vector
[b] PEPCK enzyme from the pSUMO expression vector

Pyruvate formation. It has been well documented that PEPCK catalyzes the production of pyruvate from OAA (*57-60*). With rat cPEPCK at 25°C, this activity is dependent on the presence of GDP (assay D). When comparing the mutant and WT enzymes, A467G has a K_M value seven-fold higher than WT with a modest reduction in k_{cat} (57% of WT). The E89 mutants have K_M values that are slightly elevated (all three are less than 2-fold) and a modest reduction in k_{cat} (A-65%, D-59%, and Q-56% of WT). This results in the WT enzyme being 20-fold more efficient at catalyzing the decarboxylation of OAA than the A467G mutant but only 2-fold more efficient than the E89 mutants (Table 3-2B).

All of the mutations were designed to reduce the favorability of the enzyme adapting the lid closed state and test our proposed role for the lid in protecting the enolate intermediate, once formed, from favorable protonation (*vide infra*). To this end, we investigated the ability of the enzyme to catalyze the formation of pyruvate during the catalyzed formation of PEP from OAA (assay C). In the WT enzyme there was no measurable formation of pyruvate at 25 °C. However, each of the point mutations showed a measureable amount of pyruvate formation, albeit with a K_M value similar to the elevated K_M observed in both the decarboxylation reaction and the overall reaction in the direction of PEP formation, both described above (Table 3-2A).

Inhibition of WT and A467G PEPCK by substrate analogs. The competitive inhibition of PEPCK by the substrate analogues βSP and PGA and the enolate mimic oxalate have been illustrated previously on both mitochondrial and cytosolic isoforms of PEPCK (Figure 3-4) (*26, 61*). The kinetic and structural data demonstrate that all three inhibitors are excellent mimics of the respective substrate/intermediate (Figure 3-4). We utilized the binding constants determined from the inhibition experiments to assess whether the mutations had any effect on substrate and enolate affinity. For the OAA analogue (βSP) the affinity in A467G is roughly unchanged,

however, the affinity in all three E89 mutants is increased by ~6-fold (Table 3-2C). For the PEP analogue (PGA) only the A467G and WT were tested, with the resultant affinity values being unchanged. In contrast, the reduction in the affinity of oxalate is significant in all mutants, with A467G being increased by ~8-fold, while the E89 mutants are altered by at least 200 times, with the largest, E89Q, differing from the WT by a factor of 660.

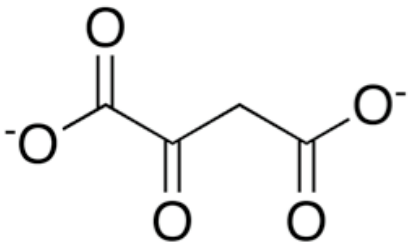

oxaloacetate

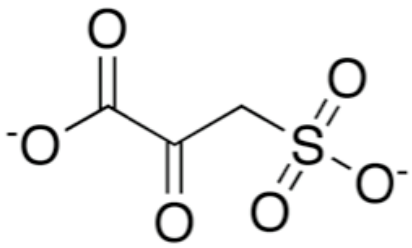

β-sulfopyruvate

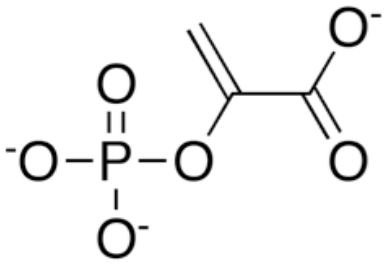

phosphoenolpyruvate

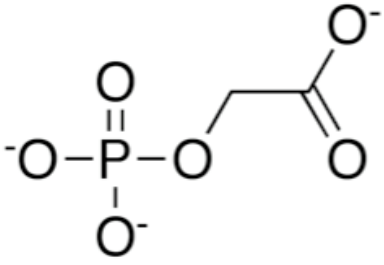

2-phosphoglycolate

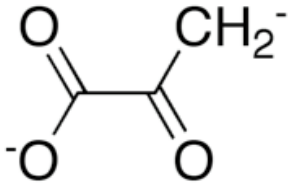

enolate of pyruvate

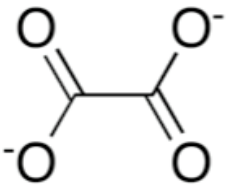

oxalate

Figure 3-4. Substrates and analogues

The physiological substrates are shown on the left with the corresponding analog show in the right handle column.

Nucleotide binding by fluorescence quenching.

The K_M values for GDP and GTP suggest that the mutations have little effect on the relative affinity of PEPCK for the nucleotide substrates. This conclusion was confirmed by the direct measurement of the K_D values for IDP and ITP by intrinsic protein fluorescence quenching experiments. The inosine nucleotides were substituted in place of guanosine to reduce the inner filter effect observed when guanosine nucleotides are utilized. PEPCK utilizes inosine and guanosine nucleotides with similar catalytic efficiency, while ITC experiments on the human enzyme have demonstrated the exocyclic C-2 amino group of guanosine nucleotides increases the affinity of the enzyme for guanosine nucleotides by approximately an order of magnitude over that of the inosine analogue. As shown in Table 3-2C, WT PEPCK and all of the mutants have similar K_D values for ITP and IDP.

Table 3-2. Pyruvate production and substrate affinities.

(A) Pyruvate Production during the OAA + GTP → PEP + GDP + CO_2 reaction			
Enzyme	K_M (OAA) (μM)	k_{cat} (s^{-1})	k_{cat}/K_M ($M^{-1}s^{-1}$)
Wt[a]	Not detectable	Not detectable	Not detectable
A467G[a]	512 ± 43	2.6 ± 0.1	5.0 x 10^3
Wt[b]	Not detectable	Not detectable	Not detectable
E89A[b]	1100 ± 220	3.5 ± 0.8	3.2 x 10^3
E89D[b]	860 ± 120	1.1 ± 0.2	1.2 x 10^3
E89Q[b]	1000 ± 300	3 ± 1	3.1 x 10^3
(B) Decarboxylation Half-Reaction (OAA + GDP → pyruvate + GDP + CO_2)			
Enzyme	K_M (OAA) (μM)	k_{cat} (s^{-1})	k_{cat}/K_M ($M^{-1}s^{-1}$)
Wt[a]	117 ± 11	2.3 ± 0.1	2.0 x 10^4
A467G[a]	970 ± 118	1.3 ± 0.1	1.0 x 10^3
Wt[b]	404 ± 28	2.00 ± 0.06	5.0 x 10^3
E89A[b]	732 ± 65	1.31 ± 0.06	1.8 x 10^3
E89D[b]	497 ± 38	1.18 ± 0.03	2.4 x 10^3
E89Q[b]	554 ± 66	1.12 ± 0.06	2.0 x 10^3

(C) Substrate and Substrate Analogue Affinities					
Enzyme	K_D (ITP) (μM)	K_D (IDP) (μM)	K_I (BSP) (μM)	K_I (PGA) (μM)	K_I (oxalate) (μM)[c]
Wt[a]	0.34 ± 0.01	11.6 ± 0.4	25 ± 6	2605 ± 171	78 ± 6
A467G[a]	0.50 ± 0.03	8.0 ± 0.3	46 ± 4	1375 ± 105	890 ± 110
Wt[b]	0.79 ± 0.07	2.7 ± 0.1	25 ± 6	Not determined	4.6[d]
E89A[b]	0.67 ± 0.06	4.1 ± 0.3	165 ± 12	Not determined	970 ± 74
E89D[b]	3.2 ± 0.5	6.9 ± 0.4	174 ± 12	Not determined	2100 ± 225
E89Q[b]	1.3 ± 0.1	5.9 ± 0.4	156 ± 11	Not determined	2650 ± 240

[a] PEPCK enzyme from the pGEX expression vector
[b] PEPCK enzyme from the pSUMO expression vector
[c] Wt and A467G from pGEX were carried out under Assay B conditions. Wt and the E89 mutants from pSUMO were carried out with Assay A conditions.
[d] As reported in Ash et.al. 1990. JBC.

Structural characterization of A467G, E89A, E89D, and E89Q.

In order to demonstrate that the mutations created decrease the thermodynamic favorability of the enzyme adapting the closed lid conformation, the structures of each mutant PEPCK were solved in complex with βSP, PGA, and oxalate and either GTP or GDP. Final data statistics for A467G can be found in Appendix 4. The statistics for the E89 mutants are not as complete as the A467G mutant due to an inherent property of the protein within the crystal lattice in which the N- and C-terminal domains are not in a single conformation, resulting in C-terminal lobe disorder and that makes refinement difficult. However, the electron density at the active site of each structure is well defined allowing for observations to be drawn from the data (Figure 3-5).

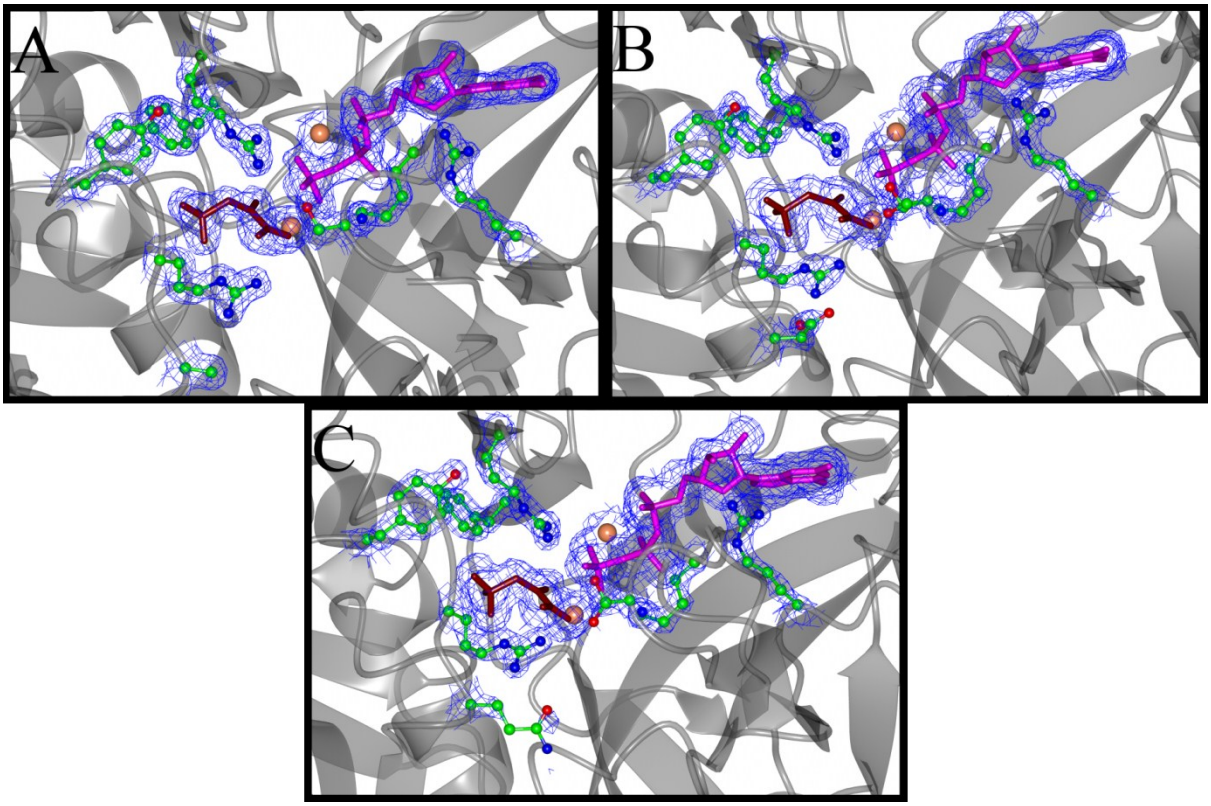

Figure 3-5. Active site region of E89A, D, and Q with electron density.

The unique nature of the E89 mutants has resulted in the enzyme sampling the closed conformation. This has made refinement of the data more difficult, however, the active site is well ordered in each of the three mutants. Structures of PEPCK-βSP–Mn^{2+}–Mn^{2+}GTP A) E89A, B) E89D, C) E89Q. βSP, GTP and the active site residues involved in binding are modeled with electron density (rendered at 1.3σ).

As mentioned above, the structures of each mutant in the Michaelis-like and the enolate-intermediate-like complexes were solved. Identical structural studies on the WT enzyme demonstrated that as the enzyme commits to catalysis the thermodynamic favorability of the enzyme adapting the closed lid conformation increases (see lid changes in Figure 1-9) (*27*). In the forward and reverse Michaelis complexes, βSP-GTP and PGA-GDP, respectively, the WT enzyme contains two molecules in the ASU, with one adapting a closed lid conformation and the other one remaining open. In the oxalate-GTP complex with WT enzyme, the lid was always found to be in a closed conformation. In contrast to those results, and consistent with the design of the mutations, the structures of A467G, E89A, E89D, and E89Q with βSP-GTP and PGA-GDP were found to only adapt the open lid conformation, consistent with a destabilization of the closed lid state. In a similar fashion to the WT, the A467G–oxalate–Mn^{2+}–Mn^{2+}GTP structure contains two molecules in the ASU in which molecule B possess an open lid conformation. Molecule A was found to partially adapt a closed lid conformation that was manually adjusted to an occupancy of 70% (Figure 3-6). This results in an overall occupancy of the closed lid conformation for the crystal of 35%, compared to 100% in the WT enzyme. Upon comparison of the closed lid conformation observed in molecule A with the conformation of the closed lid in the WT PEPCK-oxalate-GTP structure (PDB ID: 3DT4), it is observed that the substitution of glycine for alanine does not change the low energy conformation of the closed lid (Figure 3-6).

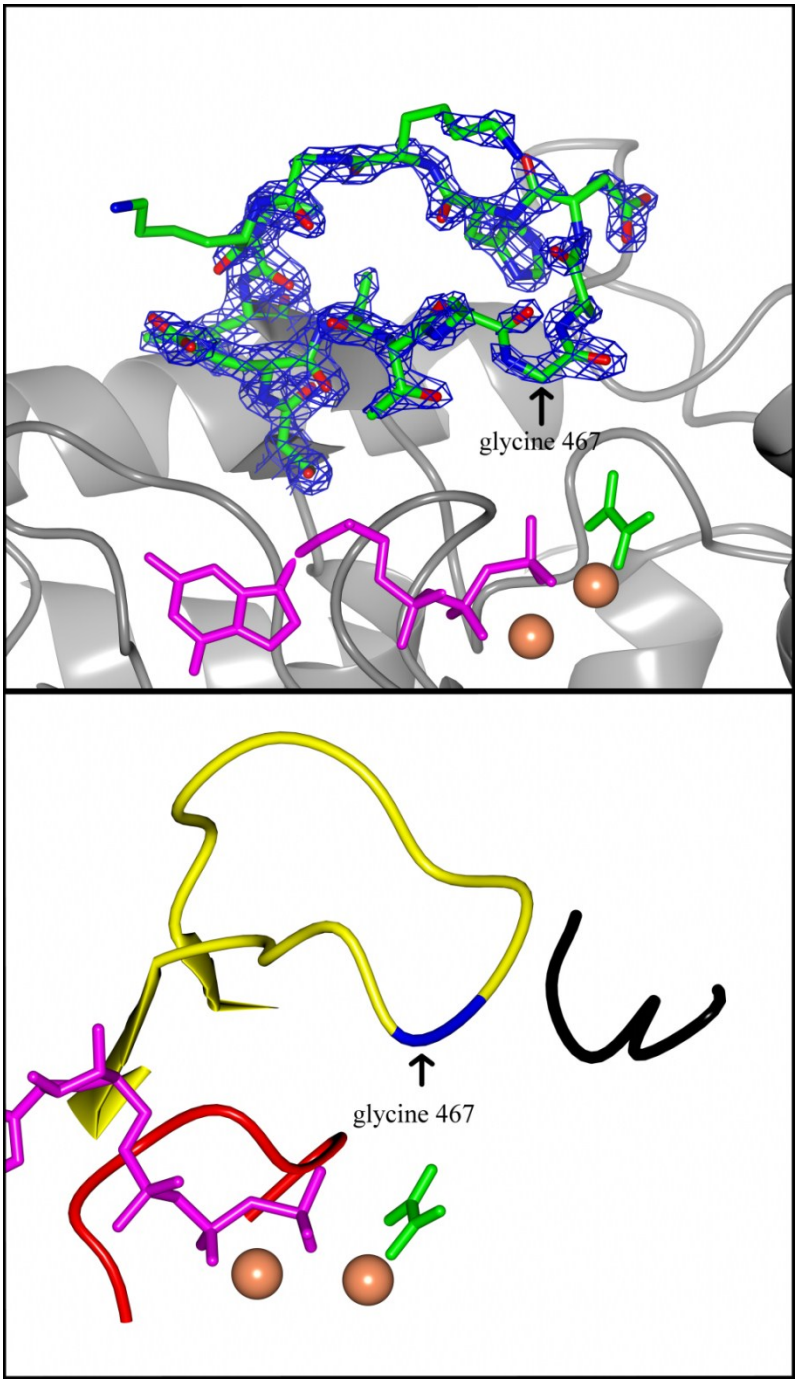

Figure 3-6. A467G lid closed complex

The substitution of a glycine for alanine 467 has not altered the low energy conformation of the Ω-loop lid. The left panel has the amino acid residues displayed with the electron density rendered at 1.5σ. Right-hand panel is the ribbon diagram of the active site mobile elements.

On the other hand, not a single E89 mutant adapts a closed lid conformation (even partially) in the structure with oxalate and GTP. In fact the structural data for two of these mutants (E89A and E89Q) illustrated the motional properties of the R-loop (discussed in Chapter 2), it flips out by 6 Å (Cα to Cα distance of R87) (Figure 3-7). This movement results in arginine 87 occupying space where the Ω-loop lid would normally reside when in the closed conformation. The R-loop in the E89D structure with oxalate-GTP is not observed to be flipped out; but the B-factors are extremely high compared to other regions of the structure, and the electron density in the R-loop region is not as complete as other less mobile areas of the structure. While the closed lid state is not observed in the E89 mutants, the kinetic results presented in Table 3-1 can only result if the lid is stabilized in the closed conformation to correctly position the substrates and amino acid side chains within the active site. Combining all of the structural data, and keeping in mind the kinetic results, confirms that the introduction of the individual point mutations allows the perturbation of the thermodynamic favorability of the enzyme adapting the closed lid conformation, necessary for catalysis, without altering the low energy conformation of the closed lid.

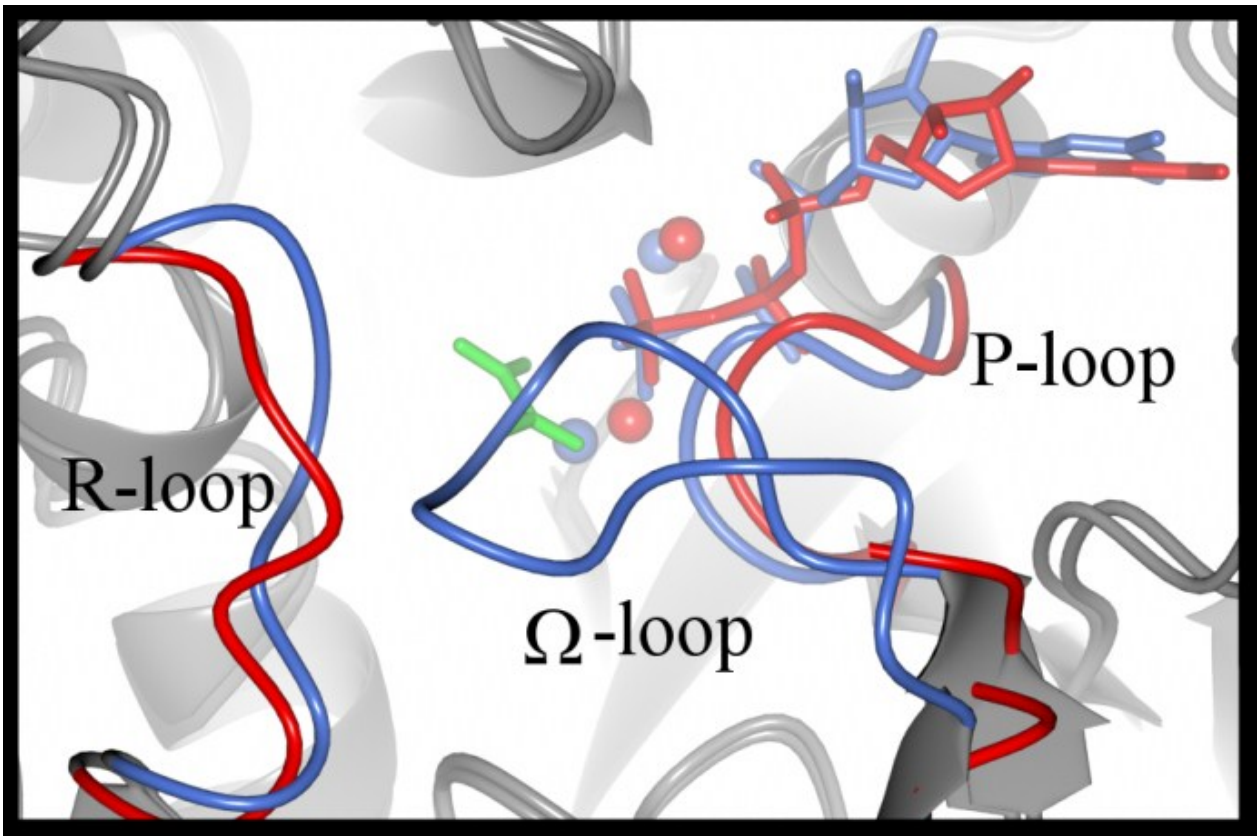

Figure 3-7. E89A and WT PEPCK active site overlay

Overlay of WT (blue) and E89A (red) PEPCK–oxalate–Mn^{2+}–Mn^{2+}GTP complexes. The changes in the position of the mobile elements due to the introduction of the mutation at Glu-89 is illustrated.

Discussion

Mobile loop regions have been observed in multiple enzymes (PEPCK, TIM, and S-adenosylmethionie synthetase) and shown to be essential for enzymatic activity (*45-50*). One enzyme in particular, TIM has a mobile Ω-loop lid domain that has been extensively characterized. In one study a portion of the lid was removed, which led to an increase in production of the reaction side product methylglyoxal and negatively affected catalytic function, by no longer stabilizing the reaction intermediate (*43*). In another study, mutations designed to increase the motional freedom of the lid were introduced in the hinge region of the Ω-loop of TIM. This set of mutations significantly impaired catalytic activity, but did not result in an increase in the production of methylglyoxal (*46, 47*). In general, these studies on TIM may demonstrate a common feature of mobile loop domains, in which a balance between rigidity and flexibility is necessary for catalytic function (*46, 47, 62*).

PEPCK and TIM catalyze two different chemical reactions. However, both PEPCK and TIM catalyze their respective reactions via a mechanism in which the chemistry proceeds through an unstable enolate intermediate. The intermediate from either reaction is highly reactive and will rapidly decompose in solution. Based upon the common structural feature of a mobile Ω-loop that is coupled to ligand binding, two hypotheses can be made for the role of the Ω-loop lid in PEPCK. First, the mobility of the lid is necessary for ligand association/disassociation; and second, during catalysis the lid closes over the active site to sequester and/or stabilize the reactive intermediate and prevent its favorable protonation.

While the two enzymes have the common structural feature, the mechanism of lid-closure stabilization is different. In TIM the lid domain forms a hydrogen bond with the phosphate of dihydroxyacetone phosphate (*54, 55*). In contrast, when the lid of PEPCK closes it makes no direct contacts with the bound substrates or the enolate intermediate. Therefore, in PEPCK, lid-

closure cannot be stabilized by new interactions between the lid and the substrates. In light of this difference, an alternative mechanism is needed to explain how the transition between open and closed lid states is driven, energetically.

The current model for the dynamic motions of PEPCK, in particular the Ω-loop, proposes that the free energy of substrate association is split between forming a tight binding E-S complex and being partitioned to the protein to offset any unfavorable entropic penalties for ordering of mobile elements. The energy that is partitioned to the protein, upon substrate binding, alters the free energy landscape. The free energy change allows the closed lid state to become thermodynamically favorable (*27*). This general idea has been presented previously (*36, 37*). In order to understand the role of the lid domain in the reaction mediated by PEPCK, I have undertaken structural and kinetic studies of four mutant isoforms of the enzyme. The mutations were designed to alter the equilibrium of the open/closed transition while probing the pathway by which the free energy is partitioned.

The rationale behind the A467 and E89 mutations

To test the free energy model of lid dynamics in PEPCK catalysis described above, two approaches were devised. The first was to increase the entropic penalty for lid closure, and the second to disrupt the free energy pathway between the active site and the Ω-loop. To test the model by these methods, the available interaction energy was kept constant by utilizing the same substrates and analogues previously used to characterize the WT enzyme. To achieve the first goal, a modified lid domain was engineered by the replacement of Ala-467 with the more conformationally flexible glycine to increase the entropic penalty for lid closure while maintaining the ability of the Ω-loop to function as a singular rigid domain. To disrupt the free energy pathway, three separate mutations at Glu-89 were introduced: an alanine (to completely remove the side chain beyond Cβ), aspartate (to maintain the polar charged head group but

shorten the length by one carbon), and glutamine (to maintain the size of the side chain but eliminate electrostatic interactions). Glu-89 was chosen as the site to mutate because it interacts with both His-470 on the Ω-loop, and Arg-87 on the R-loop (R87 directly interacts with OAA/PEP). A mutation at this location will disrupt the only interaction the Ω-loop makes when it closes, therefore, the transfer of free energy will be disrupted. Upon expression and purification of each mutant (A467G, E89A, E89D, E89Q), structural and functional studies were performed to determine if the mutation provided data are consistent with our model of loop function.

Structures of the Michaelis and enolate intermediate-like complexes

The structures of A467G, E89A, E89D, and E89Q-PEPCK mimicking the forward (βSP-GTP) and reverse (PGA-GDP) Michaelis complexes and the enolate intermediate complex were determined under identical conditions as the previously determined WT structures (PDB ID: 3DTB, 3DT2, 3DT7) (*27*). All twelve structures illustrate that no gross structural changes have been induced by the introduction of the mutations (Figure 3-8). However, consistent with the design of these mutations, the lid-closed state has become less thermodynamically favorable. This results in the closed lid state only being observed at a low population (35% of total molecules) in the A467G–oxalate–Mn^{2+}–Mn^{2+}GTP complex (Figure 3-6), and not at all in the E89A, D, & Q oxalate-GTP complexes. Similarly, the Ω-loop in the two Michaelis-like complexes is observed to be open 100% of the time in all of the mutant enzymes. These results contrast identical experiments on the WT enzyme in which the forward and reverse Michaelis-like complexes have a 50-50 distribution of lid open/closed states, and the intermediate complex only possess a closed lid conformation. There are two important structural features that warrant addressing. First, the population of molecules in the A467G–oxalate–Mn^{2+}–Mn^{2+}GTP structure that do adapt the closed lid conformation demonstrate that the substitution of glycine for alanine

has not altered the structure of the Ω-loop (Figure 3-6). This allows the kinetic data to be interpreted in the context of the mutation disrupting the favorability of the closed lid state without other structural effects. The second observation from the structural work involves two of the E89 mutants (E89A and E89Q). In the structures with oxalate and GTP, the Ω-loop is open as mentioned above, but the R-loop adapts a new conformation. The move involves residues 86-89 being displaced or flipped out (Figure 3-7). At the furthest point the Cα of R87 is 6 Å from its normal orientation. This flipping out, combined with the removal of the interaction between E89 and H470, disrupts the ability of the Ω-loop to form a stable closed-lid complex and allows water molecules to fill the void left by R87. This rearrangement is only observed in the oxalate-GTP structures of the E89A and E89Q mutants, which suggests that the polar charged head group of glutamate and the interactions it makes with R87 and the Ω-loop play a role in stabilizing/orienting the R-loop. The flipped out R-loop is not observed in the E89D mutation because the polar charged head group is available to interact with R87, but the crystallographic B-factors for this region are high compared to the rest of the structure. The combination of the B-factors being high and the electron density not being complete suggests that the R-loop has a certain amount of disorder in this structure. This is due to the shortening of the amino acid by one carbon, presumably creating a gap that is too large for the stabilizing interaction with H470 to be made. The stabilization of the R-loop consequently aids in the stabilization of the enolate intermediate so that phosphoryl transfer can occur. Unfortunately, the crystallographic data are limited to observing the low energy conformation due to packing in the crystal lattice. This limitation prevents the determination of whether the shift in equilibrium towards the lid open conformation is due to a decrease in the closing rate or an increase in the opening rate. A previous study on TIM increased the entropic freedom of the Ω-loop, with the results showing

that the increased freedom did not lead to an increased rate of lid opening, but did lead to a decreased frequency of lid closure (*47*). Therefore, further studies on PEPCK will be necessary to see what effect increasing the entropy of the lid domain and decreasing the free energy transfer has on lid domain opening and closing rates.

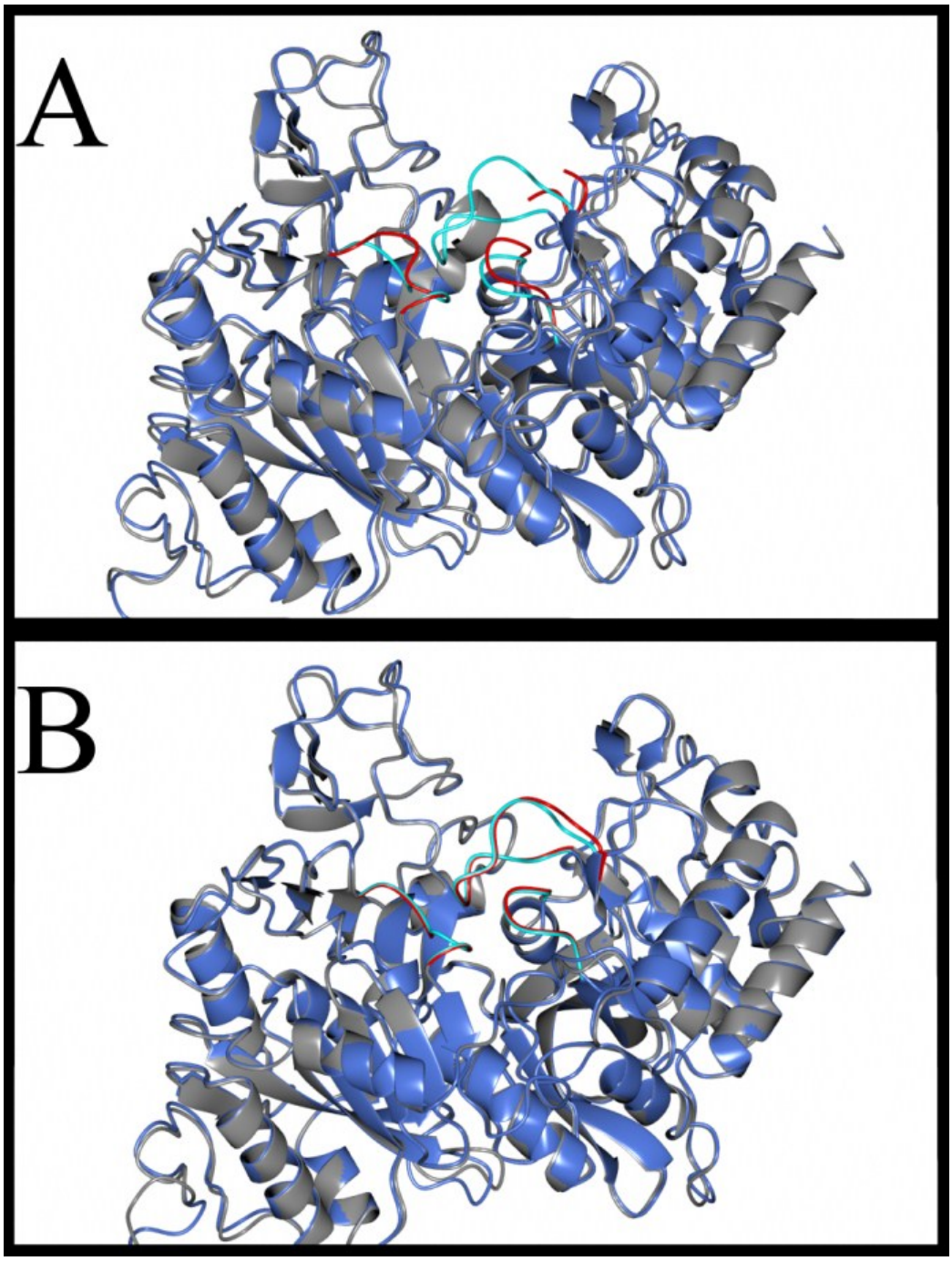

Figure 3-8. Whole protein overlay between WT and A467G or E89A

Structures of E89A (A-grey, mobile elements are red) and A467G (B-grey, mobile elements are red) solved in complex with oxalate and GTP superposed on the identical structure of WT PEPCK (Blue, mobile elements in cyan).

Lid closure stabilizes the enolate intermediate

The enolate of pyruvate is a highly reactive intermediate formed during the conversion of OAA to PEP. As such, its stabilization and protection from protonation is a requirement for this conversion to occur. In the WT PEPCK–oxalate–Mn^{2+}–Mn^{2+}GTP structure, it was observed that stabilization of oxalate arises from the rotation forward of Y235, and its interactions with R87, and coordination to the M1 manganese ion. When the lid is closed, Y235 is observed to occupy a rotameric position in which the phenolic side chain is oriented towards the oxalate and the M1 manganese (Figure 1-9C & D) (*27*). In a study of Y235 mutants it was proposed that an anion quadrapole interaction is formed between the tyrosine in the forward orientation and the enolate, aiding in stabilization (*59*). In molecule B of the A467G PEPCK–oxalate–Mn^{2+}–Mn^{2+}GTP, structure oxalate is bound at the active site, yet Y235 occupies a rearward orientation, too far away to form a stable interaction. This orientation of Y235 is also observed in all of the E89 mutants when oxalate is bound. The coincident nature of lid closure and the stabilization of the forward rotamers of Y235 in the presence of oxalate are illustrated by molecule A of the A467G PEPCK–oxalate–Mn^{2+}–Mn^{2+}GTP structure. Molecule A possesses a mixture of open and closed-lid states and a mixture of forward and rearward Y235 rotameric states. This shift in the low energy conformation of Y235 would appear to play a role in the observed increase in K_i for all four mutant PEPCK's (Table 3-2). The structural studies on the E89 mutations gave further insight into the mechanism of stabilization for the enolate intermediate. As detailed in Figure 1-9, the interactions between R87 and the OAA/enolate/PEP ligand are required for enzymatic activity (R87 mutations resulted in an enzymatically inactive isoform of PEPCK, data not shown). It was observed from the E89 mutant structures with oxalate-GTP that the R-loop has a higher level of disorder than the WT or has completely flipped, out occupying space where the Ω-loop lid would reside in the closed conformation. This results in the loss of R87 interaction

with oxalate, and by extrapolation, with the enolate intermediate. The loss of interaction with R87 coupled with the rearward rotameric state of Y235 results in an increased K_i (8-600 times that of WT) being observed for all mutants (Table 3-2). Furthermore, the decrease in affinity for oxalate, by the E89 mutants, could be due to the enzyme requiring more binding energy to stabilize the R-loop, as it is no longer stabilized through its interactions with H470. A related observation is that the hydration state of the active site has been altered when Y235 is in the rearward orientation and the R-loop flips out. This alteration may not contribute to the weakened affinity of the enzyme for the enolate/oxalate, but the change in water structure could account for the pyruvate formation observed in each of the mutants. The repositioned water molecules could potentially create an environment in which they are able to protonate the enolate intermediate. The protonation event is not observed in the WT enzyme at 25 °C. Currently it is not known whether the enolate is protonated on the enzyme or in solution upon release, but considering the K_D for pyruvate is nine mM (*61*) a protonation event on the enzyme would provide a mechanism by which the tightly bound enolate intermediate could be released.

Kinetic consequences of the disruption of lid dynamics

Previous structural data on PEPCK demonstrate that the enzyme follows an induced fit mechanism of substrate binding. This results in the true enzyme-substrate not being formed until the Ω-loop lid closes over the active site. Based upon this observation, the kinetic schemes in Figures 3-10, 11, 12 are proposed to interpret the kinetic data for the WT and mutant (A467G, E89A, E89D, and E89Q) enzymes. These schemes may be an oversimplification but a two-state model would incorrectly define the open/closed conformations and a more in depth look at the different ensemble of protein states is excessive. The low energy trajectory illustrated by Figures 3-10, 11, 12 is reasonable for the interpretation of the kinetic data in Tables 3-1 and 3-2.

The decarboxylation of OAA

The reaction catalyzed by PEPCK can be split into two half-reactions, the decarboxylation of OAA and the phosphoryl transfer from GTP to the enolate intermediate. It was observed from measurements of the decarboxylation half-reaction that the mutations at A467 and E89 only modestly affect (A467G ~8-fold, E89 less than 2-fold) the K_M for OAA (Table 3-2B) and slightly decrease the rate of decarboxylation. As illustrated in the kinetic scheme (Figure 3-9), this K_M value represents the binding of OAA to the PEPCK-GDP complex and the opening/closing of the Ω-loop. This conclusion is reached based upon two pieces of data: 1) the decarboxylation activity is only observed in the presence of GDP and 2) structural data on the WT–OAA–Mn^{2+}–Mn^{2+}GDP complex demonstrates it has an increased propensity for lid-closure (PDB ID: 2QF2), similar to the WT Michaelis-like complexes (PDB ID: 3DTB and 3DT7) (*27*). This shift in equilibrium to the closed conformation stimulates the decarboxylation of OAA generating the enolate and CO_2. Both of these pieces of data are consistent with the idea that decarboxylation is only initiated after lid-closure. However, since GDP is utilized in this assay there is no transferable phosphoryl group available to phosphorylate the enolate. This results in pyruvate being formed and released the next time the lid samples the open conformation. Based upon the proposed kinetic scheme (Figure 3-9), the observed increase in the K_M for OAA in all of the mutants could result from either an increase in k_2, k_{open}, or k_{off}, or a decrease in k_{on} or k_{close}. All of the values obtained for k_2 in the mutant enzymes were slightly decreased compared to WT, therefore in the wrong direction to cause an increase in K_M. To try to better understand if the k_{on}/k_{off} or k_{close}/k_{open} step is the reason for the modest increase in the K_M, inhibition studies of PEPCK by βSP (OAA analog) were undertaken. The inhibition data for A467G suggest that k_{on} and k_{off} are only modestly affected, since the binding of βSP only differs by a factor of 2 between the WT and A467G. This minimal effect on binding could be a bi-product of altered lid

dynamics, k_{open}/k_{close} rates, in the PEPCK-GTP state. The altered rates of opening and/or closing can affect k_{on}/k_{off}, as the structural studies illustrated that binding of substrates cannot occur after lid closure (*27*). Inhibition of the E89 mutants resulted in a decrease in affinity for βSP (~6 times WT), suggesting that k_{on} and k_{off} are slightly more affected by a mutation at glutamate 89. The change in affinity is not totally unexpected due to the proximity of the mutation to R87 on the R-loop. However, this slight change in k_{on} and k_{off} does not result in a significant increase in the K_M for OAA. On the contrary, the K_M's for OAA measured for the E89 mutants were not even elevated 2-fold, which suggests that the mutation alters the k_{open} and k_{close} step leaving the K_M relatively unchanged. This explanation for the disrupted lid behavior has been used before on kinetic data of hinge mutations in TIM(*47*). Therefore, the structural and kinetic data are consistent with the modest increase in K_M resulting from a shift in the open-closed lid equilibrium favoring the open lid conformation.

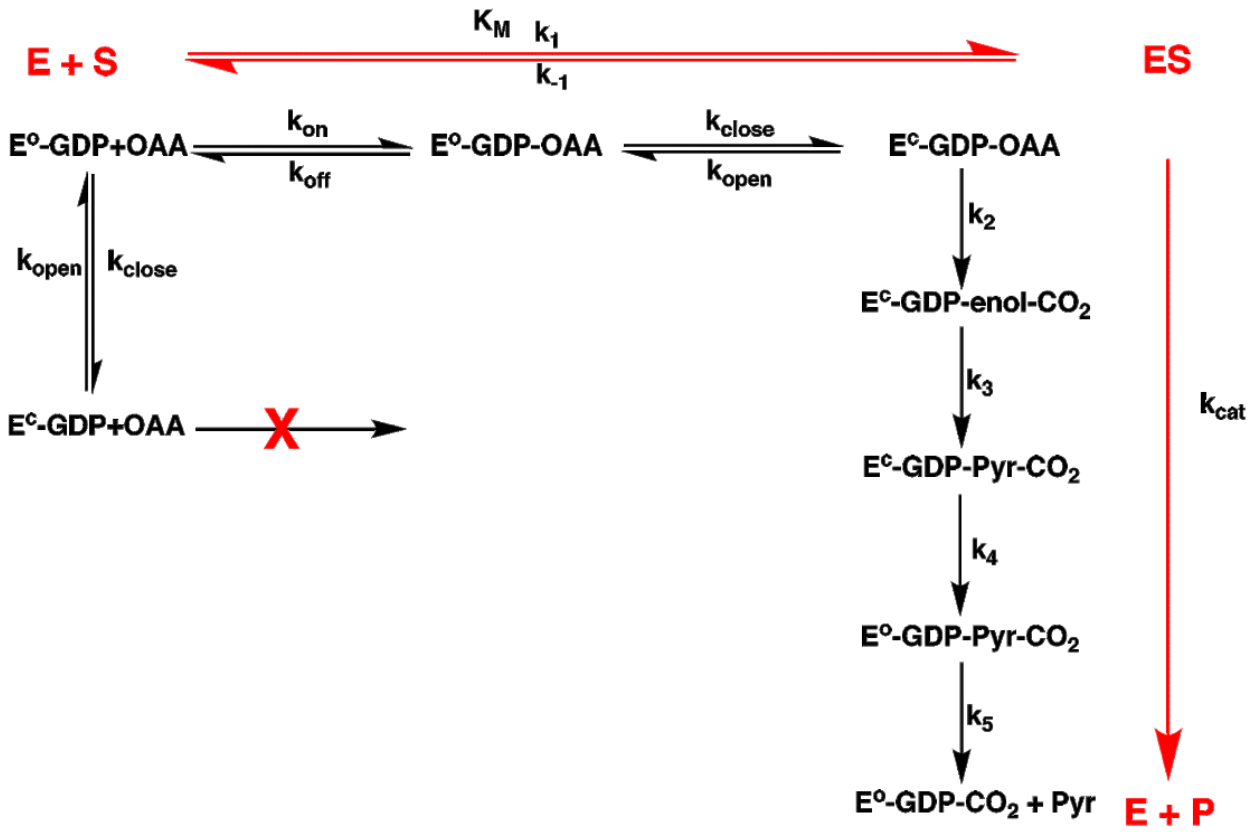

Figure 3-9.Decarboxylation kinetic scheme.

The OAA → PEP reaction

In the physiological reaction catalyzed by PEPCK, the mutations introduced result in a 14-32 fold increase in the K_M for OAA, coupled with a decrease in k_{cat} (8-29% of WT) (Table 3-1). Similar to what was discussed above for the decarboxylation half-reaction, the change in the K_M value is due to either a decrease in the rate of lid-closure or an increase in the rate of lid-opening (Figure 3-10), effectively shifting the equilibrium of lid states to the open conformation, which is consistent with the design of the mutations and the structural data. All four of the mutant enzymes will form a stable lid-closed conformation in order to initiate catalysis. Assuming $k_{cat} \sim k_3$, the phosphorylation of the enolate intermediate is the potential rate limiting step of the reaction, since, it is envisioned that this step is the most energetically costly (Figure 3-12). Therefore, the observation of pyruvate formation by each of the mutant enzymes suggests that the rate of k_3 has been altered (Figure 3-10). In WT k_3 is fast compared to k_{reopen}, as no pyruvate formation is observed, but in the mutants the equilibrium between the rates has shifted. The shift is caused by either a reduction in the phosphoryl transfer rate or an increase in the k_{reopen} rate. This change results in pyruvate being produced at a rate of one molecule per five turnover events in A467G, 1:1 in E89A, 1:15 in E89D, and 1:3 in E89Q. To address whether pyruvate formation is caused by a slowing of the phosphoryl transfer step, kinetic studies on were carried out on WT PEPCK using the slowly hyrdrolyzable substrate 5'-O-(γ-thio)triphosphate (GTPγS). Usage of GTPγS reduces k_{cat} ($13 s^{-1}$) and the K_M is 39 μM. However, no pyruvate formation was observed using GTPγS. Therefore, the data suggest that the phosphoryl transfer step is not responsible for the decoupling of the reaction in the absence of a destabilization of the lid-closed conformation.

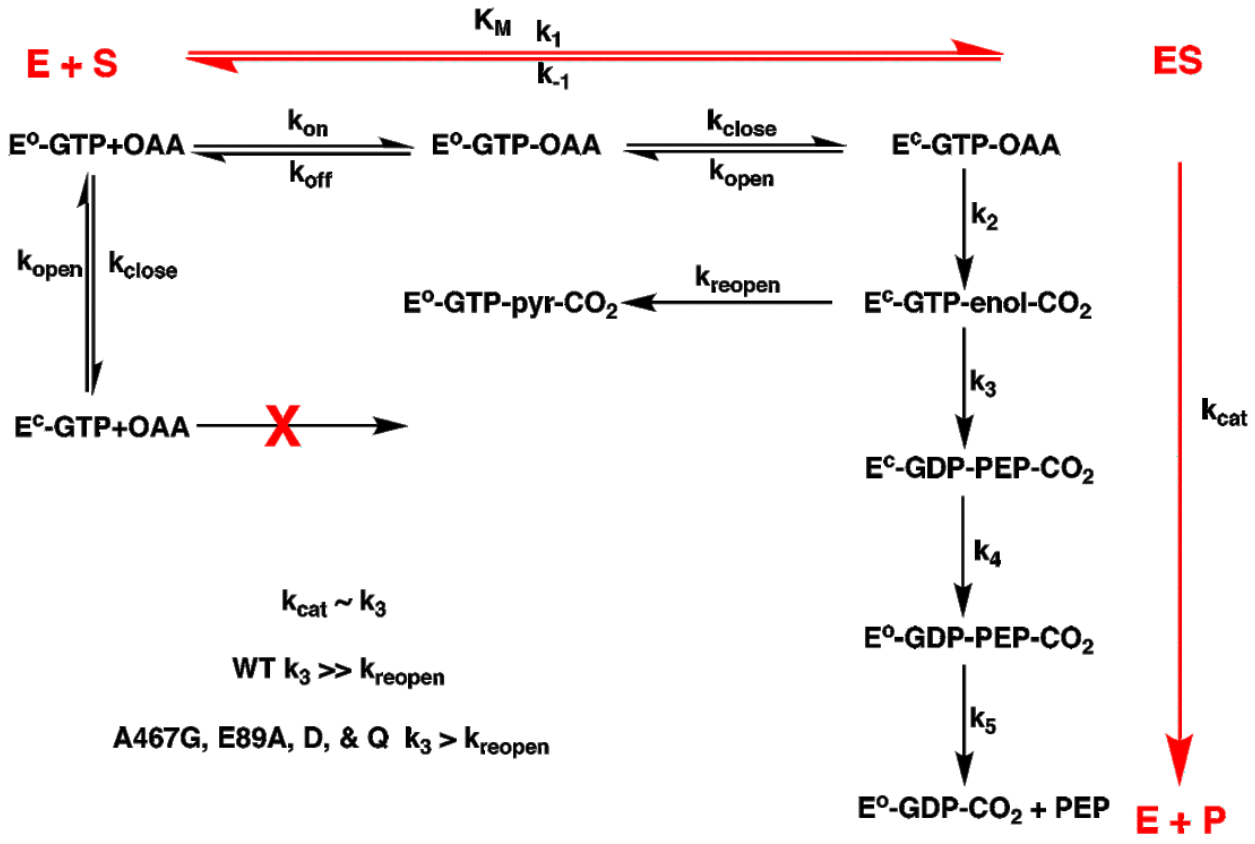

Figure 3-10.Physiological direction kinetic scheme

The PEP → OAA reaction

In contrast to the decarboxylation and physiological assays, the results from the reaction in the direction of OAA synthesis results in a decrease in K_M, in three of four mutants, and a significant decrease in k_{cat} for all four mutants. The data can be interpreted by the model presented in Figure 3-11. Based upon the proposed kinetic scheme, the observed decrease in the K_M for OAA (A467G, E89A, and E89Q) could result from either a decrease in k_2, k_{open}, or k_{off}, or an increase in k_{on} or k_{close}. All of the values obtained for k_2 with the mutant enzymes were significantly decreased compared to WT (A467G-5%, E89A-1%, E89D-3%, E89Q-1% of WT). Inhibition data were collected for WT and A467G using the substrate analog PGA. The results of that assay indicate that the affinity for PEP is slightly increased in the mutant enzyme, but increases by less than a factor of two (Table 3-2). The E89 mutants were not tested with PGA, as the substrate is no longer commercially available; however, the assumption is made that these mutants will act similarly to the A467G mutant (affinity for PGA slightly increased), as the other kinetic results have been similar. The minimal change in PGA affinity observed in the A467G mutant is not believed to cause the decrease in K_M. In the kinetic scheme for PEPCK in the direction of OAA synthesis, lid closure does not stimulate decarboxylation and formation of the enolate, rather lid closure stimulates phosphoryl transfer from PEP to GDP. Based on the standard free energies for the reversible OAA to PEP reaction, it is envisioned that the phosphoryl transfer step is the most energetically costly (Figure 3-12). As a result the destabilization of the enolate intermediate by all of the mutant isoforms has a more drastic effect on the activation energy barrier for the reaction in the PEP to OAA direction. As a consequence, the reduction in k_2 observed in A467G, E89A, and E89Q leads to the reduction in K_M. However, the E89D mutant PEPCK had a K_M value that is roughly equal to the WT, but yet still has a drastic reduction in k_2. The explanation for this difference is that the rate of k_{close}/k_{open} or k_{on}/k_{off} has been altered to a different degree

than the A467G, E89A, and E89Q mutants. Further studies are needed to determine which step is affected. This interpretation of the data is also consistent with the lack of observed pyruvate formation during turnover by these mutant isoforms in the PEP→OAA direction. On the basis of the free energy diagram the slow step, phosphoryl transfer, precedes enolate formation. The carboxylation step (k_3) is expected to be significantly faster than the lid reopening rate (k_{reopen}), resulting in a lack of pyruvate formation in this direction.

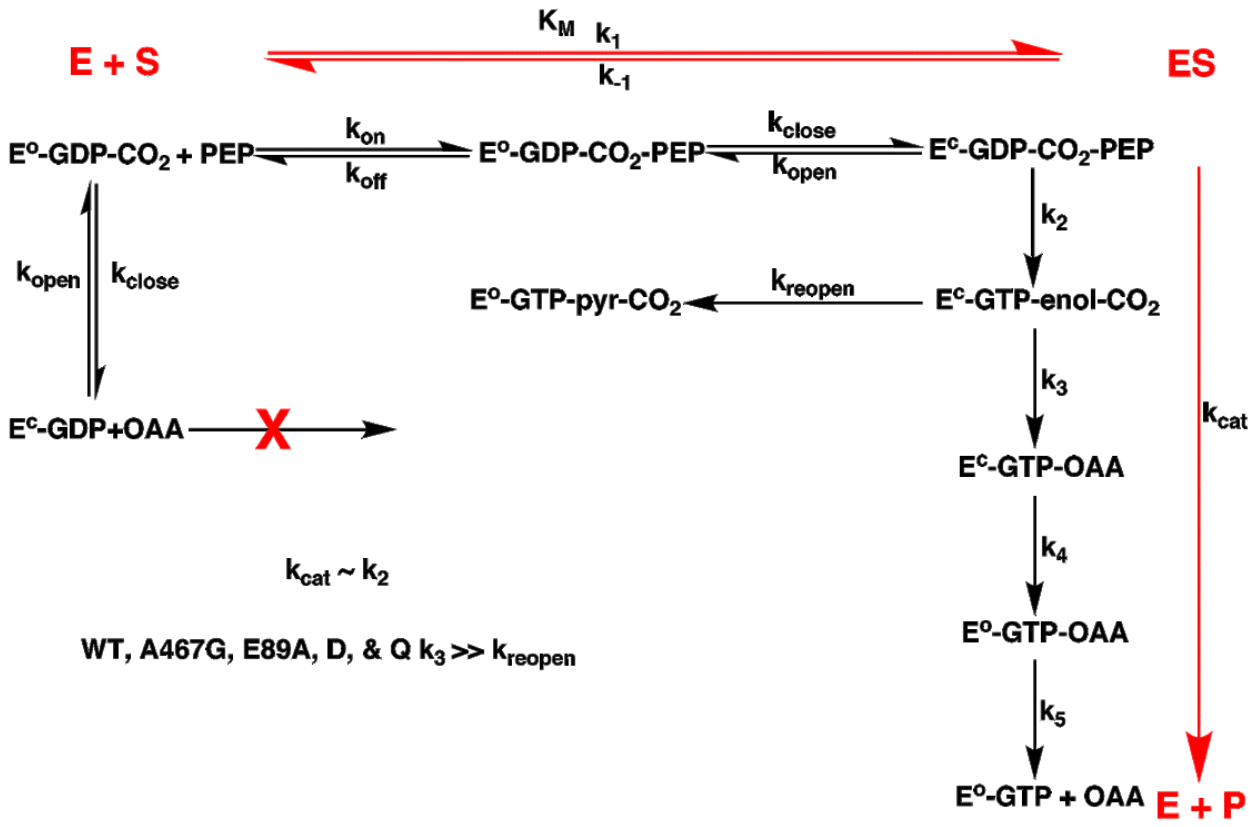

Figure 3-11. Reverse Physiological reaction kinetic scheme.

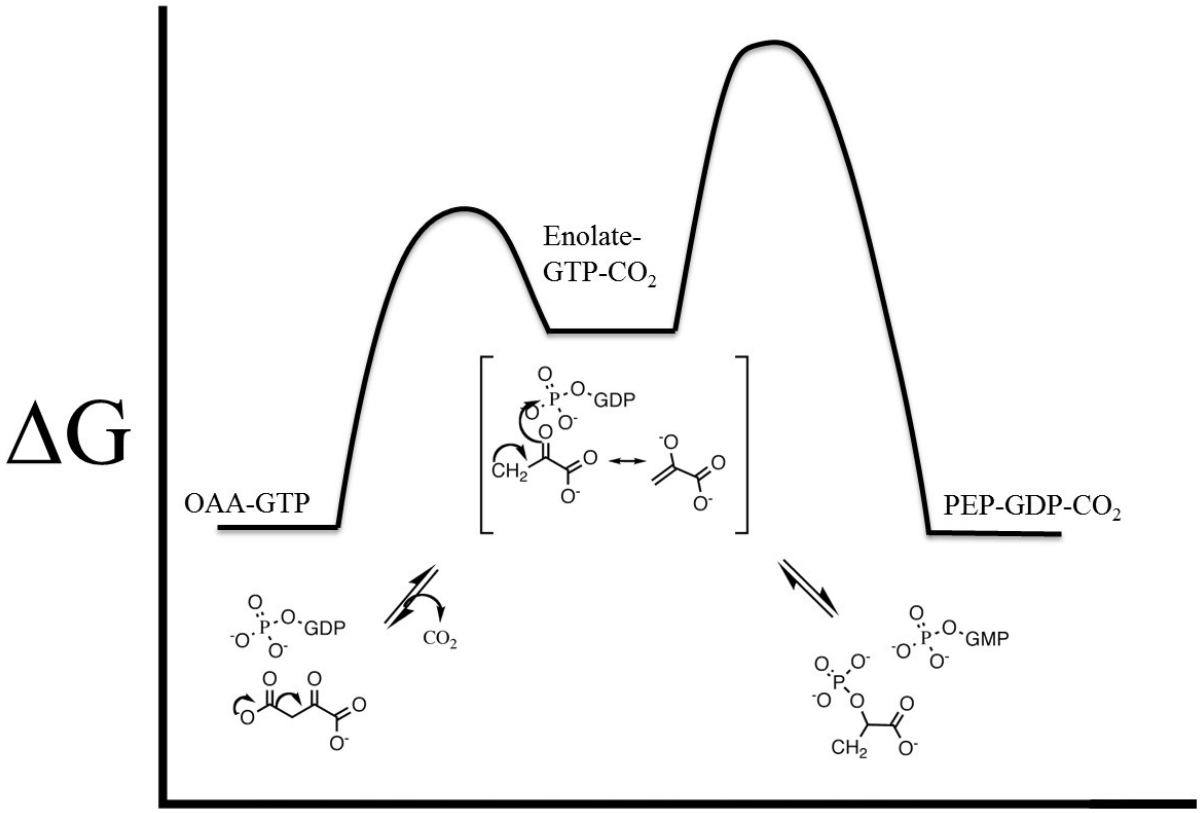

Figure 3-12. Cartoon free energy diagram of PEPCK catalysis.

Chapter 4 Conclusion and Future directions

Phosphoenolpyruvate carboxykinase is an important metabolic enzyme discovered in the 1950's. Since that time it has been extensively characterized both metabolically and biochemically. In the mid 1990's the first structure of PEPCK was solved by X-ray crystallography. Within the next decade over 40 structures had been solved of PEPCK in complex with multiple different small molecules. This led to PEPCK being mapped structurally along the reaction coordinate, with the intention of revealing any mobile regions that may be important for function. From these studies it was discovered that PEPCK has a number of structural features that have conformational flexibility. The structures revealed that as the enzyme progresses from the holo (metals bound) state, to the Michaelis complex, to the intermediate state certain structural features undergo a disordered/ordered (open/closed) transition. One of these mobile elements is an 11 amino acid Ω-loop, reminiscent of a similar structure in TIM, which acts like an active site lid. From the structural work a role in catalysis for the Ω-loop was proposed: the open/closing motion acts to correctly position substrates in the active site, sequester and protect the reaction intermediate, and aid in the transition between ground states. Furthermore, the transition is ligand gated, meaning the loop closure only occurs as substrates associate with the enzyme. This observation led to the question what is the energetic driving force behind lid closure. Unlike the loop in TIM, when the PEPCK Ω-loop closes it does not make any interaction with the substrates in the active site. However, the Ω-loop has a histidine residue (470) that forms a stable salt bridge with a glutamate (89) in the R-loop. The glutamate further interacts with arginine 87, which is directly involved in ligand binding. Upon seeing this interaction pathway, it was proposed that the energetic driving force for Ω-loop lid closure was the partitioning of enthalpic energy from ligand binding to offset any entropic penalty the lid must pay to close. To test this model I came up with a multi-faceted approach: first to investigate additional roles for the lid in

catalysis, I removed the lid; and second, to test the free energy partitioning, I created a lid mutant to increase the entropic penalty for lid closure and a mutation at Glu-89 to disrupt the proposed enthalpic energetic pathway.

The results of my studies shed light on how the Ω-loop in PEPCK operates and allows a revised model to be proposed. From the lid removal mutants, it was observed that the Ω-loop is absolutely required for catalysis. More specifically, closure of the lid stabilizes the R-loop when the intermediate is bound and acts like a latch for N- and C-terminal lobe closure. The Glu-89 and Ala-467 mutations illustrated that a very fine energetic balance exists and that at least a portion of the enthalpic energy partitioned to the lid from the OAA/PEP goes through the R87-E89-H470 pathway. Taking into consideration all of the data from WT and each set of mutants, a revised model for PEPCK catalysis is proposed. The roles of the Ω-loop during the catalytic cycle are to aid in correctly positioning the substrates, stabilize the R-loop when the reaction intermediate is present, stabilize the N- and C-terminal lobe closure, and as a culmination of these other roles to sequester and protect the reactive enolate intermediate.

The one piece of information really lacking from a complete understanding of the Ω-loop lid is the time-scale on which lid opening and closing occurs, and how the mutations affect these rates. At the present time multiple attempts have been made to obtain rate values with no success. As new techniques are devised and/or instrumentation becomes more sensitive, these measurements will be obtainable. The most recent attempt utilized NMR to measure a change in Met-476, which is in the hinge region of the Ω-loop lid. The preliminary results of this experiment suggest that this methodology may allow for the measurements of Ω-loop lid rates. The A467G mutation was designed to increase the entropy of the system; to further test the free energy balance, crystallographic and kinetic experiments utilizing a temperature change would lend support to

the enthalpy/entropy balance. The Glu-89 mutations disrupted the enthalpic free energy transfer, to build upon this and see if the pathway could be reestablished His-470 could be mutated to an arginine in the E89D mutant. This could allow the electrostatic interactions to reform, returning PEPCK to normal enzymatic function. Finally, the lid deletions created were extreme; if the lid was systematically shortened by removal of A466, A467, and A468, the role of the loop in positioning the substrates and protecting the reaction could be tested through structure function characterization.

Chapter 5 Materials and Methods

Creation of mutations

Recombinant rat cPEPCK in pGEX-4T-2 (*E. coli)* was used as the starting vector to create the A467G mutation. Recombinant rat cPEPCK in pSUMO (*E. coli)* was used as the starting vector to create the Glu-89 mutants (E89A, D, Q), as well as the lid removal with subsequent replacement by one, two, or three glycine mutants (Ld_1,2,3g). The forward primer (Figure 5-1) and its reverse complement were utilized with the Stratagene Quik Change protocol. The resultant mutated DNA was isolated with a Hurricane cleanup kit from Gerard Biotech and subsequently sequenced to confirm the presence of the desired mutation and the absence of any additional mutations introduced via the PCR protocol. The plasmid DNA was transformed into *E. Coli* BL-21(DE3) electro-competent cells for expression.

Mutation	5’-3’ Primer sequence
A467G	GAGGCCACCGCTGGTGCAGAGCATAAGG
E89A	GTGGCCAGGATCGCAAGCAAGACGGTC
E89D	GTGGCCAGGATCGACAGCAAGACGGTC
E89Q	GTGGCCAGGATCCAAAGCAAGACGGTC
Ld_1g	GCCATGAGATCAGAGGGCATCATGCACGACCCCTTCGC
Ld_2g	GCCATGAGATCAGAGGGCGGTATCATGCACGACC
Ld_3g	GCCATGAGATCAGAGGGCGGAGGTATCATGCACGACC

Figure 5-1. Primers for mutagenesis.

The 5’-3’ primers utilized to create the mutations discussed in chapters 2 and 3 are shown here. The 3’-5’ reverse complement was also synthesized.

Expression and Purification

GSH tagged PEPCK

Overnight cultures of BL-21(DE3) Escherichia coli cells containing the WT or A467G plasmid DNA in pGEX-4T-2 were grown at 37 °C at 225rpm in LB media supplemented with 200 μg/mL ampicillin. The cells were pelleted by centrifugation at 6000rpm for 15 min. The resultant cell pellet was resuspended and grown in 1.5L of LB-200 μg/mL ampicillin at 37 °C until the OD_{600} reached 1.0-1.5. The cells were subsequently induced with 1mM IPTG and grown for an additional 4h. The cells were harvested by centrifugation at 6000rpm for 15 min and then stored at -80 °C. The frozen pellet was resuspended in buffer A [25mM HEPES, pH 7.5, 10mM DTT, 10% glycerol 0.1% Synperonic NP30, 100mM NaCl, and 0.1mM EDTA] and lysed by two passages through a French pressure cell. The cell debris was pelleted by centrifugation at 9000rpm for 15 min at 4 °C. Protamine sulfate at a final concentration of 0.1% was added to the supernatant and allowed to incubate for 20-30 min, after which the solution is centrifuged 3 times at 14,000 rpm for 15min at 4 °C. After the final spin the supernatant was collected and incubated with glutathione-Uniflow resin for 1-2 h at 4 °C with stirring. The resin was poured into a column, allowed to settle, then washed with buffer A until the A_{280} was 0.1 or less. The resin was incubated overnight at 4 °C with 10 unit of thrombin (Bovine plasma). The resin was returned to the column and rinsed with Buffer 1 until the A280 was less than 0.1. The eluent was concentrated to ~15mL in an Amicon stirred cell, nitrogen concentrator using a 30 kDa filter and then loaded onto an anion exchange column (Hi-Q) attached to a Biorad DuoFlow. PEPCK was eluted from this column using a gradient of buffers B [25mM HEPES, pH 7.5, 10mM DTT] and C [25mM HEPES, pH 7.5, 10mM DTT, 500mM NaCl]. The fractions containing the protein were pooled together and concentrated in the Amicon concentrator to a final volume of 3mL or less. The concentrated enzyme was subsequently loaded onto a P6DG column equilibrated in

buffer B for desalting. The fractions with an A280 above 0.3 were pooled and concentrated with a 30 kDa centricon to a final concentration of 10mg/ml, determined by absorbance at A_{280} using a molar extinction coefficient of 1.65 mL mg^{-1}. The protein was then flash frozen by pipetting 30μL drops directly into liquid nitrogen.

pSUMO tagged PEPCK

Overnight cultures of BL-21(DE3) Escherichia coli cells containing WT, E89, or Ld mutant DNA in pSUMO were grown at 37 °C, 225rpm in LB media supplemented with 50 μg/mL kanamycin. The cells were pelleted by centrifugation at 6000rpm for 15 min. The resultant cell pellet was resuspended and grown in 1.5L of LB-50 μg/mL kanamycin at 37 °C until the OD_{600} reached 1.0-1.5. The cells were subsequently induced with 1mM IPTG and grown for an additional 4h. The cells were harvested by centrifugation at 6000rpm for 15 min and then stored at -80 °C. The frozen pellet was resuspended in buffer A [25mM HEPES, pH 7.5, 2mM TCEP, 10% glycerol, 10mM imidazole and 300mM NaCl] and lysed by two passages through a French pressure cell. The cell debris was pelleted by centrifugation at 9000rpm for 15 min at 4 °C. Protamine sulfate at a final concentration of 0.1% was added to the supernatant and allowed to incubate for 20-30 m, after which the solution is centrifuged 3 times at 14,000 rpm for 15min at 4 °C. After the final spin, the supernatant was collected and incubated with Ni-NTA resin for 0.1-1 h at 4 °C. After incubation, the resin was poured into a column, allowed to settle and washed with buffer A until the A_{280} was 0.1 or less. The protein was subsequently eluted from the Ni-NTA with buffer B [25mM HEPES, pH 7.5, 2mM TCEP, and 300mM imidazole]. The eluted protein was then incubated with 2.5mg of pSUMO protease for 1 h, concentrated to ~4mL in an Amicon concentrator with a 30kDa filter. The concentrated solution was applied to a P6DG desalting column equilibrated in buffer C [25mM HEPES, pH 7.5 and 2mM TCEP] to remove the imidazole. The fractions containing protein were pooled and reincubated with the Ni-NTA

resin (to remove the hydrolyzed pSUMO tag) for 30min and washed with buffer C till the A_{280} was 0.1 or less as PEPCK was collected in the flow through. The sample was then concentrated to ~15mL and loaded onto an anion exchange column (Hi-Q) equilibrated in buffer D [25mM HEPES, pH 7.5, 10mM DTT] and eluted using a gradient of buffers D and E [25mM HEPES, pH 7.5, 10mM DTT, 500mM NaCl]. The fractions containing the protein were pooled and concentrated in an Amicon concentrator to a final volume of 3mL or less. The concentrated enzyme is next loaded onto a P6DG desalting column equilibrated in buffer D to exchange the buffer. The fractions with an A280 above 0.3 were pooled and concentrated with a 30 kDa centricon till a final concentration of 10mg/ml, determined by absorbance at A_{280} using a molar extinction coefficient of 1.65 mL mg^{-1}. The protein was then flash frozen by pipetting 30µL drops directly into liquid nitrogen.

Kinetic assays

All kinetic data were collected on a Cary 100 spectrophotometer equipped with a multi-cell changer and a temperature bath. PEPCK activity was assayed in both the physiological direction of PEP formation and the reverse direction of OAA formation using modifications of previously published assays (*19, 57, 58, 61*). All assays were performed at 25˚ C, in a final volume of 1 mL and monitored spectrophotometrically by following the decrease in absorbance at 340 nm due to the oxidation of NADH. The oxidation of NADH was recorded in real time so as to allow the calculation of a rate of enzyme activity from the extinction coefficient for NADH (?). In all kinetic assays the concentration of PEPCK utilized was as follows 14-36 nM for WT, 43-86 nM for A467G, 75-125nM for the E89, and 25-35nM for the lid deletion mutants.

Assay A: OAA+GTP→PEP+CO_2+GDP.

The decarboxylation and phosphorylation of OAA to form PEP was carried out utilizing two slightly different reaction mixtures. The WT and A467G mutant (from the pGEX construct)

reaction mixture contained 50mM HEPES pH 7.5, 10mM DTT, 4mM $MgCl_2$, 500 µM GTP, 1mM ADP, 200 µM $MnCl_2$, 150 µM NADH, 30 units of LDH, 50 µg PK, and 350 µM (2mM for A467G) OAA. The WT and E89 mutant(s) (from the pSUMO construct reaction mixture contained 50mM HEPES pH 7.5, 10mM DTT, 5.8mM $MgCl_2$, 450 µM GTP, 1mM ADP, 20 µM $MnCl_2$, 150 µM NADH, 30 units of LDH, 50 µg PK, and 350 µM (2 mM for E89A,D,Q) OAA. All enzyme-catalyzed rates that use OAA as the substrate have been corrected for the non-enzymatic decarboxylation of OAA forming pyruvate (Assays A, C, and D). This assay was started by the addition of OAA to each cuvette. OAA and GTP concentrations were varied from 0.04-2mM and 6-450µM respectively to obtain the respective Michaelis constants. When OAA was varied, the reaction was performed as above. When GTP was the varied substrate, $MgCl_2$ was also varied to keep a constant 4:1 ratio of metal to nucleotide. The reaction mixture was preincubated at 25˚ C for 5 min prior to addition of OAA.

Assay B: PEP+GDP+CO_2→OAA+GTP.

The dephosphorylation and carboxylation of PEP to form OAA was measured using two different reaction mixtures, one for the WT and A467G from pGEX and the other for WT and E89A,D,Q from the pSUMO vector. For the WT and A467G the reaction mixture consisted of 50mM HEPES pH 7.5, 10mM DTT, 4mM $MnCl_2$, 500 µM GDP, 150 µM NADH, 2mM PEP, 10 units of MDH, and 50mM $KHCO_3$. For the pSUMO vector enzymes the assay mixture contained 50mM HEPES pH 7.5, 10mM DTT, 17mM $MgCl_2$, 20 µM $MnCl_2$, 4 mM GDP, 150 µM NADH, 5mM PEP, 10 units of MDH, and 50mM $KHCO_3$. This assay was started by the addition of PEPCK to the reaction mix in the cuvette. PEP and GDP concentrations were varied in turn, 0.04-5mM and 0.07-4mM respectively, to obtain the Michaelis constants. When GDP was the varied substrate $MnCl_2$ (pGEX constructs) and $MgCl_2$ (pSUMO construct) was also varied to keep a constant metal to nucleotide ratio of 4:1.

Assay C: OAA+GTP → pyruvate+GTP+CO_2.
The decoupling of the PEPCK catalyzed reaction (Assay A) through the production of pyruvate was measured in the same reaction mix as *assay A*. The only exception was that the coupling enzyme pyruvate kinase (PK) and its required nucleotide (ADP) were omitted from the reaction mix so that the direct production of pyruvate by PEPCK could be monitored. For the A467G mutant each cuvette consisted of 50mM HEPES pH 7.5, 10mM DTT, 4mM $MgCl_2$, 500 μM GTP, 200 μM $MnCl_2$, 150 μM NADH, 30 units of LDH, and variable (0.04-2 mM) OAA. For the E89 mutants the reaction mixture contained 50mM HEPES pH 7.5, 10mM DTT, 1.8mM $MgCl_2$, 450 μM GTP, 20 μM $MnCl_2$, 150 μM NADH, 30 units of LDH, and variable (0.04-2 mM) OAA. The reaction mixture was preincubated at 25˚ C for 5 min prior to addition of OAA to initiate the reaction.

Assay D: OAA+GDP →pyruvate+GDP+CO_2.
The PEPCK catalyzed decarboxylation of OAA without subsequent phosphoryl transfer was carried out under identical reaction conditions to *assay C* except that for A467G 500 μM GDP was substituted for GTP and for the E89 mutants 4.2mM GDP was substituted and the $MgCl_2$ concentration increased to 17 mM. A Michaelis constant for OAA was determined by varying OAA concentration. The reaction mixture was preincubated at 25˚ C for 5 min prior to the addition of OAA to initiate the reaction.

Inhibition Assays.
Inhibition experiments with oxalate and PGA were carried out using assay B for A467G and WT from pGEX. A Michaelis constant for PEP was determined at several fixed concentrations of each inhibitor. The inhibition by oxalate for the E89 mutants was carried out using *assay A*. Again, a Michaelis constant for OAA was determined at several fixed concentrations of oxalate. The inhibition by β-SP was carried out using *assay A,* for all of the mutants, as β-SP is a

substrate for the malate dehyrodgenase (MDH) coupling enzyme. Again, a Michaelis constant for OAA was determined at several concentration of β-SP.

Data analysis for WT and A467G pGEX purified enzymes.
All kinetic data was analyzed using SigmaPlot® 11. In assays A-D the slope of the line was used to calculate a rate of enzyme activity. Due to the production of pyruvate during the OAA → PEP reaction (Assay A) in the mutant enzyme, the data were corrected for this activity using the K_M and V_{max} values obtained for the enzyme from Assay C for the A467G enzyme. These two values were used in equation 1 to calculate the theoretical rate of catalyzed pyruvate formation at each substrate concentration used in Assay A for the A467G enzyme. This calculated rate was subtracted from the observed activity after correction for non-enzymatic, spontaneous OAA decarboxylation as described above. All kinetic data were fit nonlinearly to the Henri-Michaelis-Menten relationship (equation 1) to determine K_M and V_{max} values. A k_{cat} value was calculated from the V_{max} using a molecular weight of 69 415 Da. For the inhibition studies, all of the data were globally fit by the enzyme kinetics module in SigmaPlot® 11. For the inhibition of PEPCK by PGA and oxalate, the rate data was fit to equation 5-3 for competitive inhibition. For β-SP the data was fit to equation 5-4 for mixed inhibition. This is due to a contamination of the β-SP by sulfate. The value reported is the competitive inhibition portion of the data fit.

Data analysis for pSUMO purified enzymes.
All kinetic data was analyzed using SigmaPlot® 11. In assays A-D the slope of the line was used to calculate a rate of enzyme activity. Due to the production of pyruvate during the OAA → PEP reaction (Assay A) in the mutant enzymes, the data were corrected for this activity using the K_M and V_{max} values obtained for the enzyme from Assay C for the E89 mutants. These two values were used in equation 1 to calculate the theoretical rate of catalyzed pyruvate formation at each substrate concentration used in Assay A for the E89A,D,Q enzymes. This calculated rate was

subtracted from the observed activity after correction for non-enzymatic, spontaneous OAA decarboxylation as described above. All kinetic data for the WT enzyme, except *Assay D*, were fit nonlinearly to the Henri-Michaelis-Menten relationship (equation 5-1) to determine K_M and V_{max} values. Data from *Assay D* were fit linearly to a Lineweaver-Burk relationship (equation 5-2) to determine K_M and V_{max} values. Data from *Assays A, C, and D* were fit linearly to a Lineweaver-Burk relationship to obtain K_M and V_{max} values, with one exception *Assay A* for GTP. The data collected to obtain constants for GTP and *Assay B* were fit nonlinearly to the Henri-Michaelis-Menten relationship (equation 5-1) to determine K_M and V_{max} values. A k_{cat} value was calculated from the V_{max} using a molecular weight of 69 415 Da. For the inhibition studies on PEPCK by oxalate and β-SP, the rate data was plotted together and globally fit using equation 5-3 in the enzymes kinetic module for SigmaPlot® 11, resulting in a K_i value for the competitive inhibition of each substrate analog.

Equation 5-1. Henri-Michaelis-Menten relationship

υ is the initial velocity, V_{max} is the maximal velocity achieved, [S] is the concentration of substrate at each velocity, and K_M is the Michaelis constant for each respective substrate.

$$v = \frac{V_{max}[S]}{K_M + [S]}$$

Equation 5-2. Lineweaver-Burk relationship

υ is the initial velocity, V_{max} is the maximal velocity achieved, [S] is the concentration of substrate at each velocity, and K_M is the Michaelis constant for each respective substrate.

$$\frac{1}{v_0} = \left(\frac{K_M}{V_{\max}}\right)\frac{1}{[S]} + \frac{1}{V_{\max}}$$

Equation 5-3. Competitive inhibition

υ is the initial velocity, V_{max} is the maximal velocity achieved, [S] is the concentration of substrate at each velocity, K_M is the Michaelis constant for each respective substrate, [I] is the inhibitor concentration, and K_i is the inhibition constant.

$$v_o = \frac{V_{max}}{\left(1 + \left(\frac{K_M}{[S]}\right)\left(1 + \frac{[I]}{K_i}\right)\right)}$$

Equation 5-4. Mixed inhibition

υ is the initial velocity, V_{max} is the maximal velocity achieved, [S] is the concentration of substrate at each velocity, K_M is the Michaelis constant for each respective substrate, [I] is the inhibitor concentration, and K_i is the inhibition constant.

$$v_o = \frac{V_{max}}{\left(\left(\frac{K_M}{[S]}\right)\left(1+\frac{I}{K_I}\right)+\left(1+\frac{I}{(\alpha K_I)}\right)\right)}$$

Nucleotide Binding

PEPCK's affinity for nucleotide was determined using intrinsic fluorescence quenching experiments which were performed on a steady state PTI instrument with temperature control. Each assay was carried out in a triangular cuvette at 15˚ C with constant stirring. The reaction mixture for the pGEX enzymes contained 50mM HEPES, pH 7.5, 10mM DTT, 1mM $MnCl_2$, 200 μM KCl, and PEPCK (1-5 μM). The reaction mixture for the pSUMO enzymes contained 50mM HEPES, pH 7.5, 10mM DTT, 1.4mM $MgCl_2$, and PEPCK (1-5 μM). The emission was monitored at 330 nm after excitation at 295 nm. The sample was titrated with an identical solution, which also contained IDP or ITP. Inosine nucleotides were substituted for the guanosine nucleotides utilized in the kinetic studies to reduce inner filter effects. The binding constants and quenching maximums were determined by a nonlinear least squares fit of the titration data to equation 4 (IDP) or equation 5 (ITP).

Equation 5-5. Flourescence quenching

Q_L is the quenching at each ligand concentration, Q_M is the maximal quenching observed, K_D is the dissociation constant of the complex, L_T is the ligand concentration titrated into the sample, and P_T is the protein concentration.

$$Q_L = Q_M \left[\frac{K_D + L_T + P_T - \left(\sqrt{\left(K_D + L_T + P_T\right)^2 - 4P_T L_T} \right)}{2P_T} \right]$$

Equation 5-6. Fluorescence quenching 2.

Q_L is the quenching at each ligand concentration, Q_M is the maximal quenching observed, K_D is the dissociation constant of the complex, L_T is the ligand concentration titrated into the sample.

$$Q_L = \frac{Q_M L_T}{K_D + L_T}$$

Structural Studies

Crystallization.

Crystals of the complexes of A467G PEPCK were grown by vapor diffusion using the hanging drop method. The well solution consisted of 24-34% PEG 3350, 100mM HEPES pH 7.4, and water to obtain a final volume of 700µL. The crystals were grown on a siliconized cover slide in a liquid drop that contained 4µL of 10mg/mL protein, 2µL of the well solution, 0.5µL of 100mM GDP or GTP, and 0.5µL of 100mM $MnCl_2$. The crystals were cryoprotected by soaking the crystal for 30min in a solution containing 25% PEG 3350, 10% PEG 400, 100mM HEPES pH 7.4, 2mM $MnCl_2$, 10mM GDP or GTP, and 10mM of the nucleotides corresponding ligand (PGA-GDP, βSP-GTP, or Ox-GTP). While cryoprotection occurs within seconds of immersing the crystal in the cryoprotectant the crystals were soaked for 30min to allow binding of the ligand in the active site. After the soaking period the crystals were cryo-cooled by immersion in liquid nitrogen.

Crystals of the complexes of E89A,D,Q and Ld_1,2,3g PEPCK were grown by vapor diffusion using the hanging drop method. The well solution consisted of 22-26% PEG 3350, 100mM HEPES pH 7.4, and water to obtain a final volume of 700µL. The crystals were grown on a siliconized cover slide in a liquid drop that contained 4µL of 10mg/mL protein, 2µL of the well solution, 0.5µL of 30mM GDP or GTP, and 0.5µL of 75mM. The crystals were cryoprotected by soaking the crystal for 30-60 min in a solution containing 25% PEG 3350, 10% PEG 400, 100mM HEPES pH 7.4, 2mM $MnCl_2$, 5mM GDP or GTP, and 10mM of the nucleotides corresponding ligand (PGA-GDP, βSP-GTP, or Ox-GTP). The crystals were cryo-cooled by immersion in liquid nitrogen.

Data Collection

Data on the cryo-cooled A467G PEPCK-Mn^{2+}-βSP-Mn^{2+}GTP, and A467G PEPCK-Mn^{2+}-oxalate-Mn^{2+}GTP complexes maintained at 100K were collected at the Stanford Synchrotron Radiation Laboratory, Beamline 11-1, Menlo Park, CA. Data on the cryo-cooled E89A,D,Q PEPCK-Mn^{2+}-βSP-Mn^{2+}GTP, E89A,D,Q PEPCK-Mn^{2+}-PGA-Mn^{2+}GDP, and E89A,D,Q PEPCK-Mn^{2+}-oxalate-Mn^{2+}GTP complexes maintained at 100K were collected at the Stanford Synchrotron Radiation Laboratory, Beamlines 9-2 and 7-1, Menlo Park, CA. Data on the cryo-cooled Ld_1,2,3g PEPCK-Mn^{2+}-βSP-Mn^{2+}GTP, Ld_1,2,3g PEPCK-Mn^{2+}-PEP-Mn^{2+}GDP and Ld_1,2,3g PEPCK-Mn^{2+}-oxalate-Mn^{2+}GTP complexes maintained at 100K were collected at the Stanford Synchrotron Radiation Laboratory, Beamlines 9-2 and 7-1, Menlo Park, CA. The Data on the A467G PEPCK-Mn^{2+}-PGA-Mn^{2+}GDP crystal maintained at 100K were collected using a RU-H3R rotating copper anode X-ray generator with Blue Confocal Osmic mirrors and a Rigaku Raxis IV^{++} detector. All data were integrated and scaled with HKL-2000 (*63*).

Structure determination and refinement.
The A467G, E89A,D,Q, and Ld_1,2,3g mutant enzyme structures were solved by the molecular replacement method using MOLREP (*64*) in the CCP4 package (*65*) and the previously solved rat cPEPCK structures of the same complexes (PDB ID: 3DT4, 3DT7 and 3DTB) (*27*). For each complex, the molecular replacement solution was refined using Refmac5 followed by manual model adjustment and rebuilding using COOT (*66*). Ligand, metal, water addition and validation were also performed in COOT. A final round TLS refinement was performed for all models in Refmac5. A total of 5 groups per chain for the A467G PEPCK-Mn^{2+}-βSP-Mn^{2+}GTP, A467G PEPCK-Mn^{2+}-oxalate-Mn^{2+}GTP, Ld_1g PEPCK-Mn^{2+}-βSP-Mn^{2+}GTP, Ld_1g PEPCK-Mn^{2+}-oxalate-Mn^{2+}GTP, Ld_1g PEPCK-Mn^{2+}-PEP-Mn^{2+}GDP, Ld_2g PEPCK-Mn^{2+}-βSP-Mn^{2+}GTP, Ld_2g PEPCK-Mn^{2+}-oxalate-Mn^{2+}GTP, Ld_2g PEPCK-Mn^{2+}-PEP-Mn^{2+}GDP, Ld_3g PEPCK-Mn^{2+}-βSP-Mn^{2+}GTP, Ld_3g PEPCK-Mn^{2+}-oxalate-Mn^{2+}GTP, Ld_3g PEPCK-Mn^{2+}-PEP-

Mn^{2+}GDP, E89A PEPCK-Mn^{2+}-βSP-Mn^{2+}GTP, E89A PEPCK-Mn^{2+}-oxalate-Mn^{2+}GTP, E89A PEPCK-Mn^{2+}-PGA-Mn^{2+}GDP, E89D PEPCK-Mn^{2+}-βSP-Mn^{2+}GTP, E89D PEPCK-Mn^{2+}-oxalate-Mn^{2+}GTP, E89D PEPCK-Mn^{2+}-PGA-Mn^{2+}GDP, E89Q PEPCK-Mn^{2+}-βSP-Mn^{2+}GTP, E89Q PEPCK-Mn^{2+}-oxalate-Mn^{2+}GTP, E89Q PEPCK-Mn^{2+}-PGA-Mn^{2+}GDP models were used as refinements using greater than five groups per chain did not significantly improve R/R_{free}. A total of 20 groups per chain for the A467G PEPCK-Mn^{2+}-PGA-Mn^{2+}GDP model were used. The optimum TLS groups were determined by submission of the PDB files to the TLSMD server [http://skuld.bmsc.washington.edu/~tlsmd/] (*67-69*).

Chapter 6 References

1. Utter, M. F., and Kurahashi, K. (1954) PURIFICATION OF OXALACETIC CARBOXYLASE FROM CHICKEN LIVER, *J. Biol. Chem. 207*, 787-802.
2. Hanson, R. W., and Garber, A. J. (1972) Phosphoenolpyruvate carboxykinase. I. Its role in gluconeogenesis, *Am J Clin Nutr 25*, 1010-1021.
3. Soling, H. D., Kleineke, J., Willms, B., Janson, G., and Kuhn, A. (1973) Relationship between intracellular distribution of phosphoenolpyruvate carboxykinase, regulation of gluconeogenesis, and energy cost of glucose formation, *Eur J Biochem 37*, 233-243.
4. Nordlie, R. C., and Lardy, H. A. (1963) Mammalian Liver Phosphoenolpyruvate Carboxykinase Activities, *J. Biol. Chem. 238*, 2259-2263.
5. Carlson, G. M., and Holyoak, T. (2009) Structural insights into the mechanism of phosphoenolpyruvate carboxykinase catalysis, *J Biol Chem 284*, 27037-27041.
6. Colleen M. Croniger, Y. O. L. R. S. C. K. S. M. T. R. W. H. (2002) Phosphoenolpyruvate carboxykinase revisited: Insights into its metabolic role, *Biochemistry and Molecular Biology Education 30*, 14-20.
7. Modaressi, S., Christ, B., Bratke, J., Zahn, S., Heise, T., and Jungermann, K. (1996) Molecular cloning, sequencing and expression of the cDNA of the mitochondrial form of phosphoenolpyruvate carboxykinase from human liver, *Biochem J 315 (Pt 3)*, 807-814.
8. Modaressi, S., Brechtel, K., Christ, B., and Jungermann, K. (1998) Human mitochondrial phosphoenolpyruvate carboxykinase 2 gene. Structure, chromosomal localization and tissue-specific expression, *Biochem J 333 (Pt 2)*, 359-366.
9. Yang, J., Kalhan, S. C., and Hanson, R. W. (2009) What is the metabolic role of phosphoenolpyruvate carboxykinase?, *J Biol Chem 284*, 27025-27029.
10. Chakravarty, K., Cassuto, H., Reshef, L., and Hanson, R. W. (2005) Factors that control the tissue-specific transcription of the gene for phosphoenolpyruvate carboxykinase-C, *Crit Rev Biochem Mol Biol 40*, 129-154.
11. Yang, J., Reshef, L., Cassuto, H., Aleman, G., and Hanson, R. W. (2009) Aspects of the control of phosphoenolpyruvate carboxykinase gene transcription, *J Biol Chem 284*, 27031-27035.
12. Jiang, W., Wang, S., Xiao, M., Lin, Y., Zhou, L., Lei, Q., Xiong, Y., Guan, K.-L., and Zhao, S. (2011) Acetylation Regulates Gluconeogenesis by Promoting PEPCK1 Degradation via Recruiting the UBR5 Ubiquitin Ligase, *Molecular Cell 43*, 33-44.
13. Zhao, S., Xu, W., Jiang, W., Yu, W., Lin, Y., Zhang, T., Yao, J., Zhou, L., Zeng, Y., Li, H., Li, Y., Shi, J., An, W., Hancock, S. M., He, F., Qin, L., Chin, J., Yang, P., Chen, X., Lei, Q., Xiong, Y., and Guan, K.-L. (2010) Regulation of Cellular Metabolism by Protein Lysine Acetylation, *Science 327*, 1000-1004.
14. Lin, Y.-y., Lu, J.-y., Zhang, J., Walter, W., Dang, W., Wan, J., Tao, S.-C., Qian, J., Zhao, Y., Boeke, J. D., Berger, S. L., and Zhu, H. (2009) Protein Acetylation Microarray Reveals that NuA4 Controls Key Metabolic Target Regulating Gluconeogenesis, *Cell 136*, 1073-1084.
15. Zimmer, D. B., and Magnuson, M. A. (1990) Immunohistochemical localization of phosphoenolpyruvate carboxykinase in adult and developing mouse tissues, *J Histochem Cytochem 38*, 171-178.
16. Franckhauser, S., Munoz, S., Pujol, A., Casellas, A., Riu, E., Otaegui, P., Su, B., and Bosch, F. (2002) Increased fatty acid re-esterification by PEPCK overexpression in adipose tissue leads to obesity without insulin resistance, *Diabetes 51*, 624-630.

17. Olswang, Y., Cohen, H., Papo, O., Cassuto, H., Croniger, C. M., Hakimi, P., Tilghman, S. M., Hanson, R. W., and Reshef, L. (2002) A mutation in the peroxisome proliferator-activated receptor gamma-binding site in the gene for the cytosolic form of phosphoenolpyruvate carboxykinase reduces adipose tissue size and fat content in mice, *Proc Natl Acad Sci U S A 99*, 625-630.
18. Colombo, G., Carlson, G. M., and Lardy, H. A. (1981) Phosphoenolpyruvate carboxykinase (guanosine 5'-triphosphate) from rat liver cytosol. Dual-cation requirement for the carboxylation reaction, *Biochemistry 20*, 2749-2757.
19. Lee, M. H., Hebda, C. A., and Nowak, T. (1981) The role of cations in avian liver phosphoenolpyruvate carboxykinase catalysis. Activation and regulation, *J Biol Chem 256*, 12793-12801.
20. Hebda, C. A., and Nowak, T. (1982) Phosphoenolpyruvate carboxykinase. Mn2+ and Mn2+ substrate complexes, *J Biol Chem 257*, 5515-5522.
21. Arnelle, D. R., and O'Leary, M. H. (1992) Binding of carbon dioxide to phosphoenolpyruvate carboxykinase deduced from carbon kinetic isotope effects, *Biochemistry 31*, 4363-4368.
22. Ríos, S. E., and Nowak, T. (2002) Role of cysteine 306 in the catalytic mechanism of Ascaris suum phosphoenolpyruvate carboxykinase, *Archives of Biochemistry and Biophysics 404*, 25-37.
23. Matte, A., Goldie, H., Sweet, R. M., and Delbaere, L. T. (1996) Crystal structure of Escherichia coli phosphoenolpyruvate carboxykinase: a new structural family with the P-loop nucleoside triphosphate hydrolase fold, *J Mol Biol 256*, 126-143.
24. Holyoak, T., Sullivan, S. M., and Nowak, T. (2006) Structural insights into the mechanism of PEPCK catalysis, *Biochemistry 45*, 8254-8263.
25. Sullivan, S. M., and Holyoak, T. (2007) Structures of rat cytosolic PEPCK: insight into the mechanism of phosphorylation and decarboxylation of oxaloacetic acid, *Biochemistry 46*, 10078-10088.
26. Stiffin, R. M., Sullivan, S. M., Carlson, G. M., and Holyoak, T. (2008) Differential Inhibition of Cytosolic PEPCK by Substrate Analogues. Kinetic and Structural Characterization of Inhibitor Recognition, *Biochemistry 47*, 2099-2109.
27. Sullivan, S. M., and Holyoak, T. (2008) Enzymes with lid-gated active sites must operate by an induced fit mechanism instead of conformational selection, *Proc Natl Acad Sci U S A 105*, 13829-13834.
28. Carlson, G. M., Colombo, G., and Lardy, H. A. (1978) A vicinal dithiol containing an essential cysteine in phosphoenolpyruvate carboxykinase (guanosine triphosphate) from cytosol of rat liver, *Biochemistry 17*, 5329-5338.
29. Lewis, C. T., Seyer, J. M., and Carlson, G. M. (1989) Cysteine 288: an essential hyperreactive thiol of cytosolic phosphoenolpyruvate carboxykinase (GTP), *J Biol Chem 264*, 27-33.
30. Makinen, A. L., and Nowak, T. (1989) A reactive cysteine in avian liver phosphoenolpyruvate carboxykinase, *J Biol Chem 264*, 12148-12157.
31. Kamerlin, S. C. L., and Warshel, A. (2010) At the dawn of the 21st century: Is dynamics the missing link for understanding enzyme catalysis?, *Proteins: Structure, Function, and Bioinformatics 78*, 1339-1375.
32. Henzler-Wildman, K., and Kern, D. (2007) Dynamic personalities of proteins, *Nature 450*, 964-972.

33. Ma, B., and Nussinov, R. (2010) Enzyme dynamics point to stepwise conformational selection in catalysis, *Current Opinion in Chemical Biology 14*, 652-659.
34. Bryngelson, J. D., Onuchic, J.N., Socci, N.D., and P.G. Wolynes. (1995) Funnels, Pathways, and the Energy Landscape of Protein Folding: A Synthesis, *Proteins: Structure, Function, and Genetics 21*, 167-195.
35. Henzler-Wildman, K. A., Thai, V., Lei, M., Ott, M., Wolf-Watz, M., Fenn, T., Pozharski, E., Wilson, M. A., Petsko, G. A., Karplus, M., Hubner, C. G., and Kern, D. (2007) Intrinsic motions along an enzymatic reaction trajectory, *Nature 450*, 838-844.
36. Jencks, W. P. (1975) Binding Energy, Specificity, and Enzymic Catalysis: The Circe Effect, *Advances in Enzymology and Related Areas of Molecular Biology 43*.
37. Fersht, A. R. (1974) Catalysis, Binding and Enzyme-Substrate Complementarity, *Proceedings of the Royal Society of London. Series B, Biological Sciences 187*, 397-407.
38. Johnson, T. A., and Holyoak, T. (2010) Increasing the conformational entropy of the Omega-loop lid domain in phosphoenolpyruvate carboxykinase impairs catalysis and decreases catalytic fidelity, *Biochemistry 49*, 5176-5187.
39. Fetrow, J. (1995) Omega loops: nonregular secondary structures significant in protein function and stability, *The FASEB Journal 9*, 708-717.
40. Sampson, N. S., Kass, I. J., and Ghoshroy, K. B. (1998) Assessment of the Role of an Ω Loop of Cholesterol Oxidase: A Truncated Loop Mutant Has Altered Substrate Specificity†, *Biochemistry 37*, 5770-5778.
41. Larson, E. M., Larimer, F. W., and Hartman, F. C. (1995) Mechanistic insights provided by deletion of a flexible loop at the active site of ribulose-1,5-bisphosphate carboxylase/oxygenase, *Biochemistry 34*, 4531-4537.
42. Kato, H., Tanaka, T., Yamaguchi, H., Hara, T., Nishioka, T., Katsube, Y., and Oda, J. i. (1994) Flexible Loop That Is Novel Catalytic Machinery in a Ligase. Atomic Structure and Function of the Loopless Glutathione Synthetase, *Biochemistry 33*, 4995-4999.
43. Pompliano, D. L., Peyman, A., and Knowles, J. R. (1990) Stabilization of a reaction intermediate as a catalytic device: definition of the functional role of the flexible loop in triosephosphate isomerase, *Biochemistry 29*, 3186-3194.
44. Dunten, P., Belunis, C., Crowther, R., Hollfelder, K., Kammlott, U., Levin, W., Michel, H., Ramsey, G. B., Swain, A., Weber, D., and Wertheimer, S. J. (2002) Crystal structure of human cytosolic phosphoenolpyruvate carboxykinase reveals a new GTP-binding site, *Journal of Molecular Biology 316*, 257-264.
45. Williams, J. C., and McDermott, A. E. (1995) Dynamics of the flexible loop of triosephosphate isomerase: the loop motion is not ligand gated, *Biochemistry 34*, 8309-8319.
46. Kempf, J. G., Jung, J. Y., Ragain, C., Sampson, N. S., and Loria, J. P. (2007) Dynamic requirements for a functional protein hinge, *J Mol Biol 368*, 131-149.
47. Xiang, J., Jung, J.-y., and Sampson, N. S. (2004) Entropy Effects on Protein Hinges: The Reaction Catalyzed by Triosephosphate Isomerase†, *Biochemistry 43*, 11436-11445.
48. Johnson, T. A., Qiu, J., Plaut, A. G., and Holyoak, T. (2009) Active-Site Gating Regulates Substrate Selectivity in a Chymotrypsin-Like Serine Protease The Structure of Haemophilus influenzae Immunoglobulin A1 Protease, *J Mol Biol*.
49. Sampson, N. S., and Knowles, J. R. (1992) Segmental motion in catalysis: investigation of a hydrogen bond critical for loop closure in the reaction of triosephosphate isomerase, *Biochemistry 31*, 8488-8494.

50. Sampson, N. S., and Knowles, J. R. (1992) Segmental movement: definition of the structural requirements for loop closure in catalysis by triosephosphate isomerase, *Biochemistry 31*, 8482-8487.
51. Banerjee, S., Pieper, U., Kapadia, G., Pannell, L. K., and Herzberg, O. (1998) Role of the Ω-Loop in the Activity, Substrate Specificity, and Structure of Class A β-Lactamase†,‡, *Biochemistry 37*, 3286-3296.
52. Suhre, K., and Sanejouand, Y.-H. (2004) ElNémo: a normal mode web server for protein movement analysis and the generation of templates for molecular replacement, *Nucleic Acids Research 32*, W610-W614.
53. Joseph, D., Petsko, G. A., and Karplus, M. (1990) Anatomy of a conformational change: hinged "lid" motion of the triosephosphate isomerase loop, *Science 249*, 1425-1428.
54. Lolis, E., and Petsko, G. A. (1990) Crystallographic analysis of the complex between triosephosphate isomerase and 2-phosphoglycolate at 2.5-A resolution: implications for catalysis, *Biochemistry 29*, 6619-6625.
55. Alber, T., Banner, D. W., Bloomer, A. C., Petsko, G. A., Phillips, D., Rivers, P. S., and Wilson, I. A. (1981) On the three-dimensional structure and catalytic mechanism of triose phosphate isomerase, *Philos Trans R Soc Lond B Biol Sci 293*, 159-171.
56. Banner, D. W., Bloomer, A. C., Petsko, G. A., Phillips, D. C., Pogson, C. I., Wilson, I. A., Corran, P. H., Furth, A. J., Milman, J. D., Offord, R. E., Priddle, J. D., and Waley, S. G. (1975) Structure of chicken muscle triose phosphate isomerase determined crystallographically at 2.5 angstrom resolution using amino acid sequence data, *Nature 255*, 609-614.
57. Colombo, G., Carlson, G. M., and Lardy, H. A. (1978) Phosphoenolpyruvate carboxykinase (guanosine triphosphate) from rat liver cytosol. Separation of homogeneous forms of the enzyme with high and low activity by chromatography on agarose-hexane-guanosine triphosphate, *Biochemistry 17*, 5321-5329.
58. Noce, P. S., Utter, M.F. (1975) Decarboxlyation of Oxalacetate to pyruvate by purified avian liver phosphoenolpyruvate carboxykinase, *J. Biol. Chem. 250*, 9099-9105.
59. Dharmarajan, L., Case, C. L., Dunten, P., and Mukhopadhyay, B. (2008) Tyr235 of human cytosolic phosphoenolpyruvate carboxykinase influences catalysis through an anion-quadrupole interaction with phosphoenolpyruvate carboxylate, *FEBS J 275*, 5810-5819.
60. Jabalquinto, A. M., Laivenieks, M., Zeikus, J. G., and Cardemil, E. (1999) Characterization of the oxaloacetate decarboxylase and pyruvate kinase-like activities of Saccharomyces cerevisiae and Anaerobiospirillum succiniciproducens phosphoenolpyruvate carboxykinases, *J Protein Chem 18*, 659-664.
61. Ash, D. E., Emig, F. A., Chowdhury, S. A., Satoh, Y., and Schramm, V. L. (1990) Mammalian and avian liver phosphoenolpyruvate carboxykinase. Alternate substrates and inhibition by analogues of oxaloacetate, *J Biol Chem 265*, 7377-7384.
62. Watt, E. D., Shimada, H., Kovrigin, E. L., and Loria, J. P. (2007) The mechanism of rate-limiting motions in enzyme function, *Proc Natl Acad Sci U S A 104*, 11981-11986.
63. Otwinowski, Z., Minor W. (1997) Processing of X-ray diffraction data collected in oscillation mode, *Methods in Enzymology 276*, 307-326.
64. Vagin, A., and Teplyakov, A. (1997) MOLREP: an Automated Program for Molecular Replacement, *Journal of Applied Crystallography 30*, 1022-1025.

65. Collaborative. (1994) The CCP4 suite: programs for protein crystallography, *Acta Crystallographica Section D 50*, 760-763.
66. Emsley, P., Lohkamp, B., Scott, W. G., and Cowtan, K. (2010) Features and development of Coot, *Acta Crystallogr D Biol Crystallogr 66*, 486-501.
67. Painter, J., and Merritt, E. A. (2005) A molecular viewer for the analysis of TLS rigid-body motion in macromolecules, *Acta Crystallographica Section D 61*, 465-471.
68. Painter, J., and Merritt, E. A. (2006) Optimal description of a protein structure in terms of multiple groups undergoing TLS motion, *Acta Crystallographica Section D 62*, 439-450.
69. Painter, J., and Merritt, E. A. (2006) TLSMD web server for the generation of multi-group TLS models, *Journal of Applied Crystallography 39*, 109-111.

Appendices

Appendix 1. Sequence alignment of 4 isoforms of PEPCK.

The sequence alignment below is from four isoforms of PEPCK whose 3D structures have been solved; human and rat cytosolic PEPCK, chicken mitochondrial PEPCK, and E. Coli PEPCK. The sequence identity percentage is shown at the bottom. Active site residues and the Ω-loop lid are highlighted in blue. The RMSD calculation from the structures of each enzyme are at the bottom as well.

```
HcPEPCK       ---------------MPPQLQN---GLNLSAKVVQGSLDSLPQAVREFLENNAELCQPDH 42
RcPEPCK       ---------------MPPQLHN---GLDFSAKVIQGSLDSLPQEVRKFVEGNAQLCQPEY
CmPEPCK       MFWLRGGAQSCRGGETEDRMQRGMWGVGLARRRLSTSLSALPAAARDFVEEAVRLCRPRE
E.Coli PEPCK  -------------------------------MRVNNGLTPQELEAYGISDVHDIVYNPSY
                                              :. .* .    .  : :    : .*
HcPEPCK       IHICDGSEEENGRLLGQMEEEGILRRLKKYDNCWLALTDPRDVARIESKTVIVTQEQRDT 102
RcPEPCK       IHICDGSEEEYGRLLAHMQEEGVIRKLKKYDNCWLALTDPRDVARIESKTVIITQEQRDT
CmPEPCK       VLLCDGSEEEGKELLRGLQDDGVLHPLPKYDNCWLARTDPRDVARVESKTVLVTPEQSDA
E.Coli PEPCK  DLLY---QEELDPSLTGYER-GVLTNLGAVAVDTGIFTG----RSPKDKYIVRDDTTRDT
                :    :**    *   :  *::  *          *.       :.* ::      *:
HcPEPCK       VPIPKT--GLSQLGRWMSEEDFEKAFNARFPGCMKGRTMYVIPFSMGPLGSPLSKIGIEL 160
RcPEPCK       VPIPKS--GQSQLGRWMSEEDFEKAFNARFPGCMKGRTMYVIPFSMGPLGSPLAKIGIEL
CmPEPCK       VPPPPPSGGPPQLGNWMSPNAFQAAVQERFPGCMAGRPLYVIPFSMGPPTSPLAKLGVQV
E.Coli PEPCK  FWWADK--GKGKNDNKPLSPETWQHLKGLVTRQLSGKRLFVVDAFCG--ANPDTRLSVRF
              .  .    *  : ..           .:  ..  : *: ::*:    *   .* :::.:..
HcPEPCK       TDSPYVVASMRIMTRMGTPVLEAVGDGEFVKCLHSVGCPLPLQKPLVNNWPCNPELTLIA 220
RcPEPCK       TDSPYVVASMRIMTRMGTSVLEALGDGEFIKCLHSVGCPLPLKKPLVNNWACNPELTLIA
CmPEPCK       TDSPYVVLSMRIMTRVGPAVLQRLDD-DFVRCLHSVGRPLPLTEPLVSSWPCDRSPVLVA
E.Coli PEPCK  ITEVAWQAHFVKNMFIRPSDEELAGFKPDFIVMNGAKCTNPQWK----EQGLNSENFVAF
                .      :     : ..  :  .    .  ::..  . *  :    .   : .  :
HcPEPCK       HLPDRREIISFGSGYGGNSLLGKKCFALRMASRLAKEEGWLAEHMLILGITNPEGEKKYL 280
RcPEPCK       HLPDRREIISFGSGYGGNSLLGKKCFALRIASRLAKEEGWLAEHMLILGITNPEGKKKYL
CmPEPCK       HIPSERRIVSFGSGYGGNSLLGKKCFALRIASRMAQQQGWLAEHMLILGVTSPSGEKRYM
E.Coli PEPCK  NLTERMQLIG-GTWYGGEMKKG----MFSMMNYLLPLKGIASMHCSAN-----VGEKGDV
              ::... .::. *: ***:   *     : : . :   :*  : *          *:*  :
HcPEPCK       AAAFPSACGKTNLAMMNPSLPGWKVECVGDDIAWMKFDAQGHLRAINPENGFFGVAPGTS 340
RcPEPCK       AAAFPSACGKTNLAMMNPTLPGWKVECVGDDIAWMKFDAQGNLRAINPENGFFGVAPGTS
CmPEPCK       AAAFPSACGKTNLAMMTPSLPGWRIHCVGDDIAWMKFDDEGRLRAINPERGFFGVAPGTS
E.Coli PEPCK  AVFFGLSGTGKTTLSTDP-----KRRLIGDDE--HGWDDDG---VFNFEGGCYAKTIKLS
              *. *  :   ..     *     : . :***     :* :*   .:* * * :. :   *
HcPEPCK       VKTNPNAIKTIQKNTIFTNVAETSDGGVYWEGIDEPLASGVTITSWKNKEWSSEDGEPCA 400
RcPEPCK       VKTNPNAIKTIQKNTIFTNVAETSDGGVYWEGIDEPLAPGVTITSWKNKEWRPQDEEPCA
CmPEPCK       SRTNPNAMATIARNTIFTNVGLRSDGGVYWDGLDEPTEPGVTYTSWLGKPWKHGDPEPCA
E.Coli PEPCK  KEAEPEIYNAIRRDALLENVTVREDGTIDFDDGSKTENTRVSYPIYHIDNIVKP-VSKAG
               .::*:   :* :::::: **   .** : ::. .:.  . *: . :  .       . ..
HcPEPCK       HPNSRFCTPASQCPIIDAAWESPEGVPIEGIIFGGRRPAGVPLVYEALSWQHGVFVGAAM 460
RcPEPCK       HPNSRFCTPASQCPIIDPAWESPEGVPIEGIIFGGRRPAGVPLVYEALSWQHGVFVGAAM
CmPEPCK       HPNSRFCAPADQCPIMDPRWDDPEGVPIDAIIFGGRRPRGVPLVVEAFGWRHGVFMGSAM
E.Coli PEPCK  HATKVIFLTADAFGVLPPVSR----------------------LTADQTQYHFLSGFTA
              *... :  .*.   :: .                          *   :: .: * :
HcPEPCK       RSEATAAAEHKGKIIMHDPFAMRPFFGYNFGKYLAHWLSMAQHPAAKLPKIFHVNWFRKD 520
RcPEPCK       RSEATAAAEHKGKVIMHDPFAMRPFFGYNFGKYLAHWLSMAHRPAAKLPKIFHVNWFRKD
CmPEPCK       RSEATAAAEHKGGRLMHDPFAMRPFFGYNAGRYLEHWLSTGLRSNARLPRLFHVNWFLRD
E.Coli PEPCK  KLAGTERGITEPTPTFSACFGA-AFLSLHPTQYAEVLVKR-MQAAGAQAYLVNTGWNGTG
              :  .*  .  :    :   *.  .*:. :  :*    :.   :. .  . :.:..*   .
```

```
HcPEPCK      KEGKFLWPGFGENSRVLEWMFNRIDGKASTKLTPIGYIPKEDALNLKGLGHINMMELFSI 580
RcPEPCK      KNGKFLWPGFGENSRVLEWMFGRIEGEDSAKLTPIGYVPKEDALNLKGLGDVNVEELFGI
CmPEPCK      NEGRFVWPGFGHNARVLAWIFGRIQGRDTARPTPIGWVPKEGDLDLGGLPGVDYSQLFPM
E.Coli PEPCK KR-----ISIKDTRAIIDAILNGSLDNAETFTLPMFNLAIPTELPGVDTKILDPRNTY-A
             :.      .: ..  ::  ::.   ..  :   *:  :.    *   .   ::  : :
HcPEPCK      SKEFWEKEVEDIEKYLEDQVNADLPCEIEREILALKQRISQM  622
RcPEPCK      SKEFWEKEVEEIDKYLEDQVNADLPYEIERELRALKQRISQM
CmPEPCK      EKGFWEEECRQLREYYGENFGADLPRDVMAELEGLEERVRKM
E.Coli PEPCK SPEQWQEKAETLAKLFIDNFDKYTDTPAGAALVAAGPKL---
             .   *::: . : :   ::..          : .   ::
```

Sequence Alignment percent identity

	HcPEPCK	RcPEPCK	CmPEPCK	E.Coli PEPCK
HcPEPCK	100%	88%	61%	14%
RcPEPCK	88%	100%	62%	14%
CmPEPCK	61%	62%	100%	14%
E.Coli PEPCK	14%	14%	14%	100%

Backbone RMSD

	HcPEPCK	RcPEPCK	CmPEPCK	E.Coli PEPCK
HcPEPCK	0.000	0.576	1.227	2.608
RcPEPCK	0.576	0.000	0.979	2.759
CmPEPCK	1.227	0.979	0.000	2.708
E.Coli PEPCK	2.608	2.759	2.708	0.000

Appendix 2. PEPCK protein data bank entries

Enzyme Complex	PDB ID	Enzyme Complex	PDB ID
PEPCK (e.coli)	1OEN	PEPCK(K213S)-Mn-Mg-ATP (e.coli)	2PY7
PEPCK-ATP-Mg (e.coli)	1AYL	PEPCK-OAA-CO_2-Mn-Mg-ATP (e.coli)	2PXZ
PEPCK-Pyr-Mn-Mg-ATP(e.coli)	1AQ2	PEPCK-OAA-Mn (rat cytosolic)	2QF1
PEPCK (trypansoma cruzi)	1II2	PEPCK-Mn-Mn-GTP (rat cytosolic)	2QEY
PEPCK-AF-Mg-ADP (e.coli)	1K3D	PEPCK-Mn (rat cytosolic)	2QEW
PEPCK-Pyr-AF-Mg-ADP (e.coli)	1K3C	PEPCK-OAA-Mn-Mn-GDP (rat cytosolic)	2QF2
PEPCK-Mn (human cytosolic)	1KHG	PEPCK-PEP-Mn (chicken mitochondrial)	2QZY
PEPCK-Mn-PEP (human cytosolic)	1KHF	PEPCK-SAT-Mn (rat cytosolic)	2RKE
PEPCK-Mn-GCP (human cytosolic)	1KHE 1KHB	PEPCK-3PP-Mn (rat cytosolic)	2RKD
PEPCK (thermophilus HB8)	1J3B	PEPCK-PGA-Mn (rat cytosolic)	2RKA
PEPCK-Pyr-Mg-ATP (e.coli)	1OS1	PEPCK-PPF-Mn (rat cytosolic)	2RK8
PEPCK-PEP-Mn-FTB (human cytosolic)	1NHX	PEPCK-oxalate-Mn (rat cytosolic)	2RK7
PEPCK-PEP-Mn-TSX (human cytosolic)	1M51	PEPCK-PGA-Mn-Mn-GDP (rat cytosolic)	3DTB
PEPCK-Pyr-Mn (actinobaccilus succinogenes)	1YLH	PEPCK-βSP-Mn-Mn-GTP (rat cytosolic)	3DT7
PEPCK (actinobaccilus succinogenes)	1YGG	PEPCK-oxalate-Mn-Mn-GTP (rat cytosolic)	3DT4
PEPCK (Anaerobiospirillum succiniciproducens)	1YVY	PEPCK-oxalate-Mn-Mn-GTP (rat cytosolic)	3DT2
PEPCK-oxalate-Mn-Mg-ATP (Anaerobiospirillum succiniciproducens)	1YTM	PEPCK(A467G)-PGA-Mn-Mn-GDP (rat cytosolic)	3MOH
PEPCK-CO_2-Mg-ATP (e.coli)	2OLR	PEPCK(A467G)-βSP-Mn-Mn-GTP (rat cytosolic)	3MOE
PEPCK-CO_2-Mn-Mg-ATP (e.coli)	2OLQ	PEPCK(A467G)-oxalate-Mn-Mn-GTP (rat cytosolic)	3MOF
PEPCK (cornebacterium glutamicum)	2ZCI		

Appendix 3. All data with curve fits.

WT rcPEPCK from the pGEX expression vector

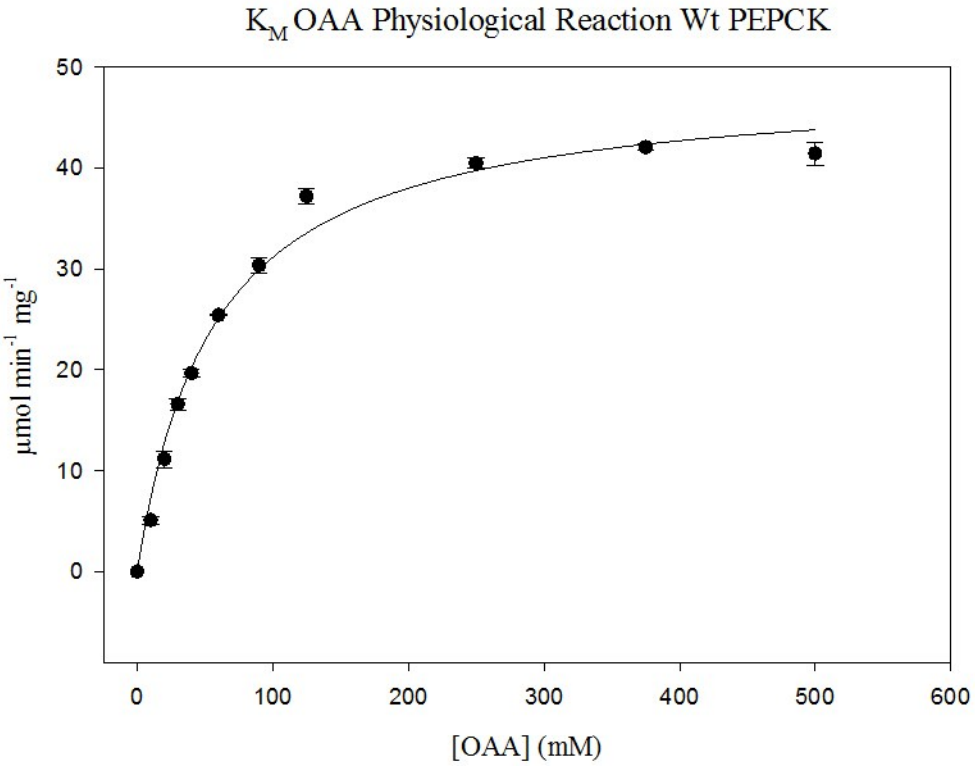

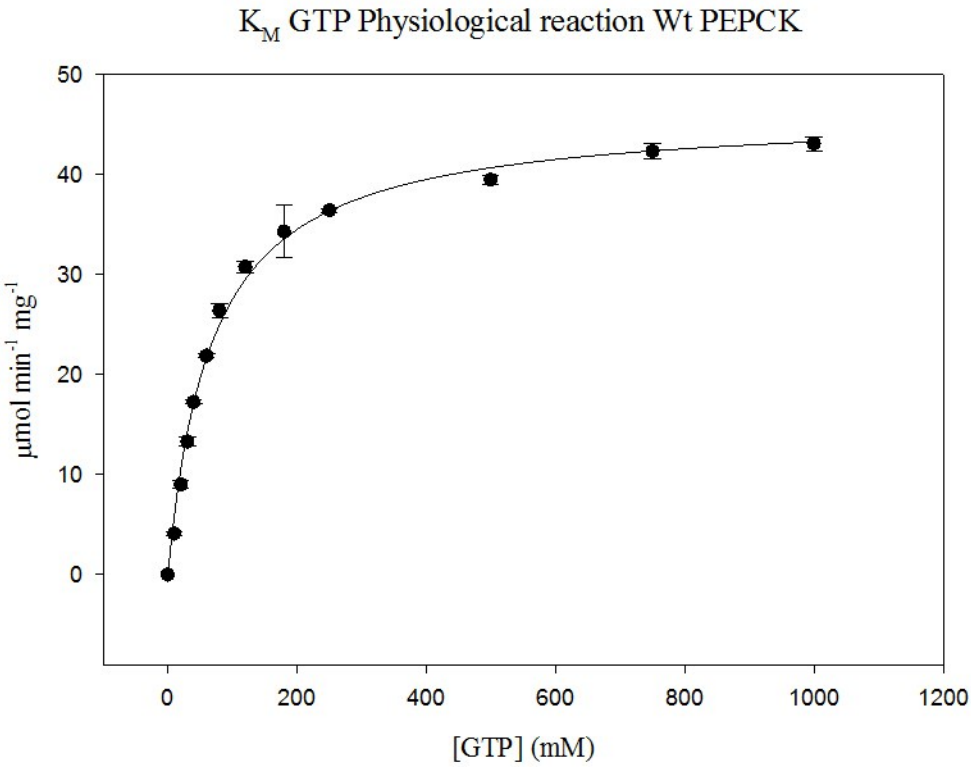

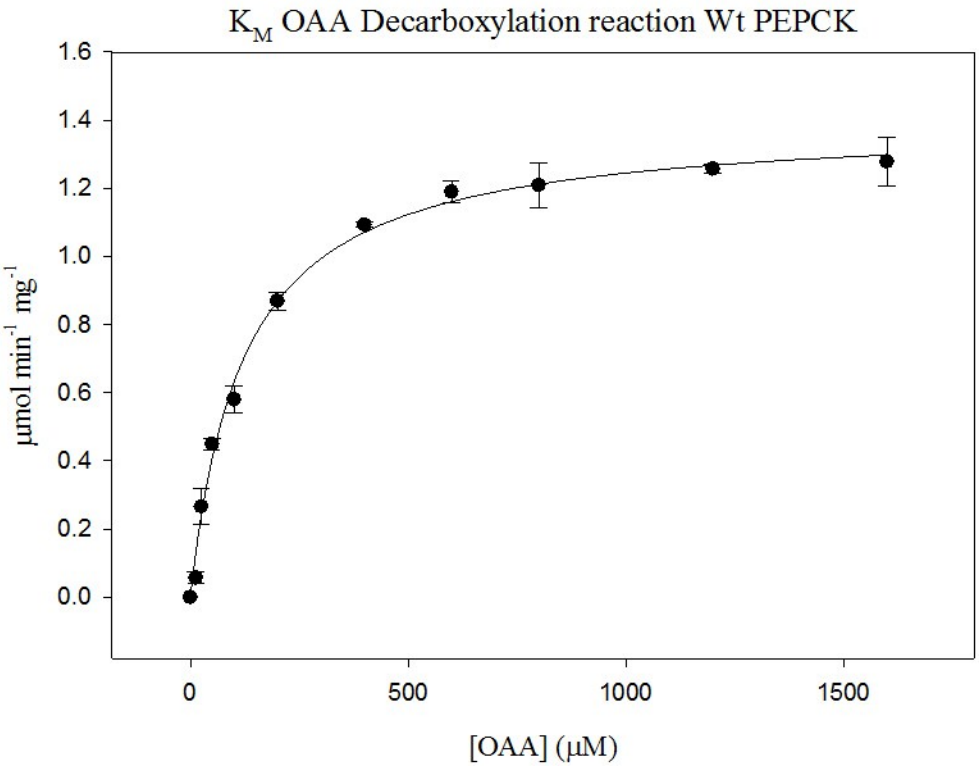
K$_M$ OAA Decarboxylation reaction Wt PEPCK
µmol min^{-1} mg^{-1}
1.6
1.4
1.2
1.0
0.8
0.6
0.4
0.2
0.0
0
500
1000
1500
[OAA] (µM)

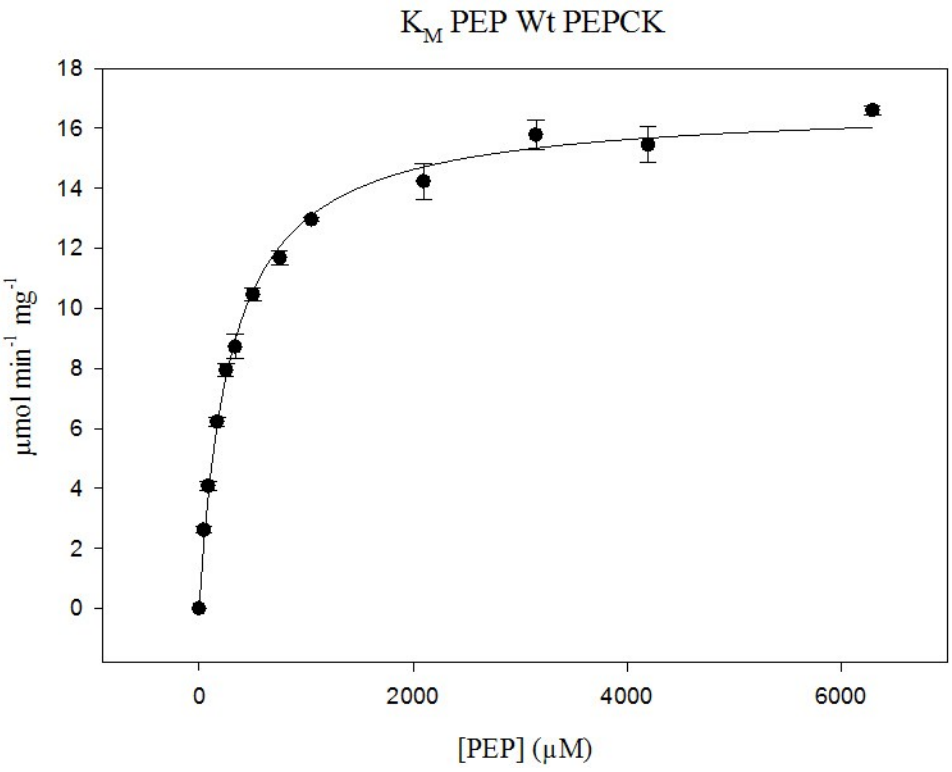
K$_M$ PEP Wt PEPCK
µmol min^{-1} mg^{-1}
18
16
14
12
10
8
6
4
2
0
0
2000
4000
6000
[PEP] (µM)

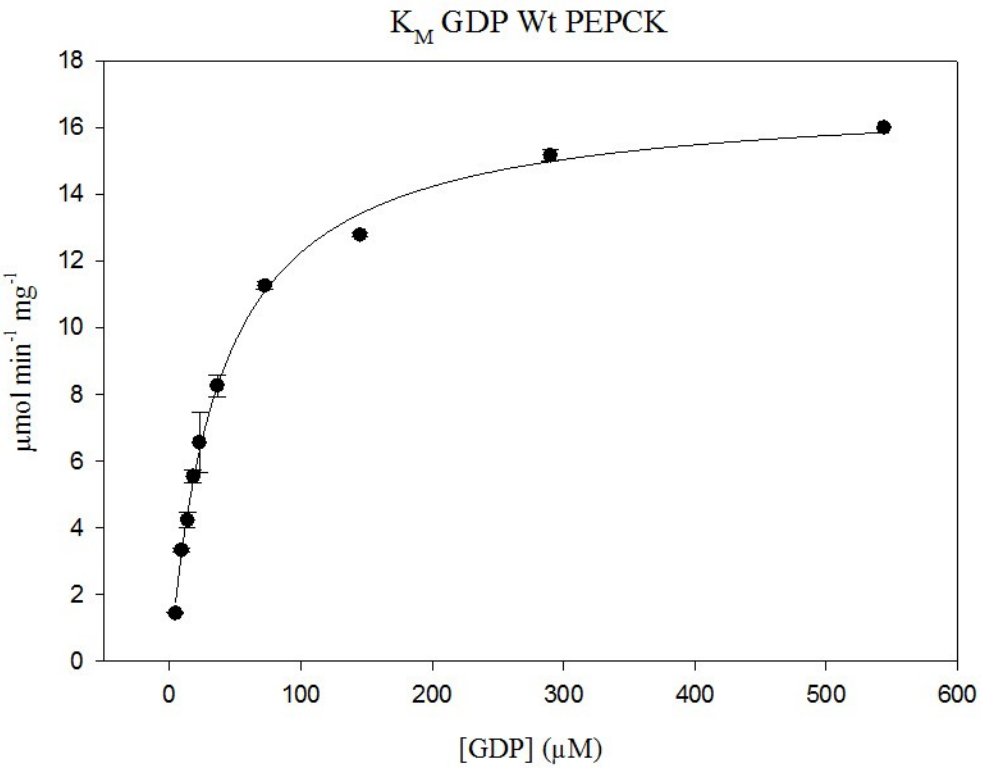
K_M GDP Wt PEPCK
µmol min-1 mg-1
[GDP] (µM)
0
2
4
6
8
10
12
14
16
18
0
100
200
300
400
500
600

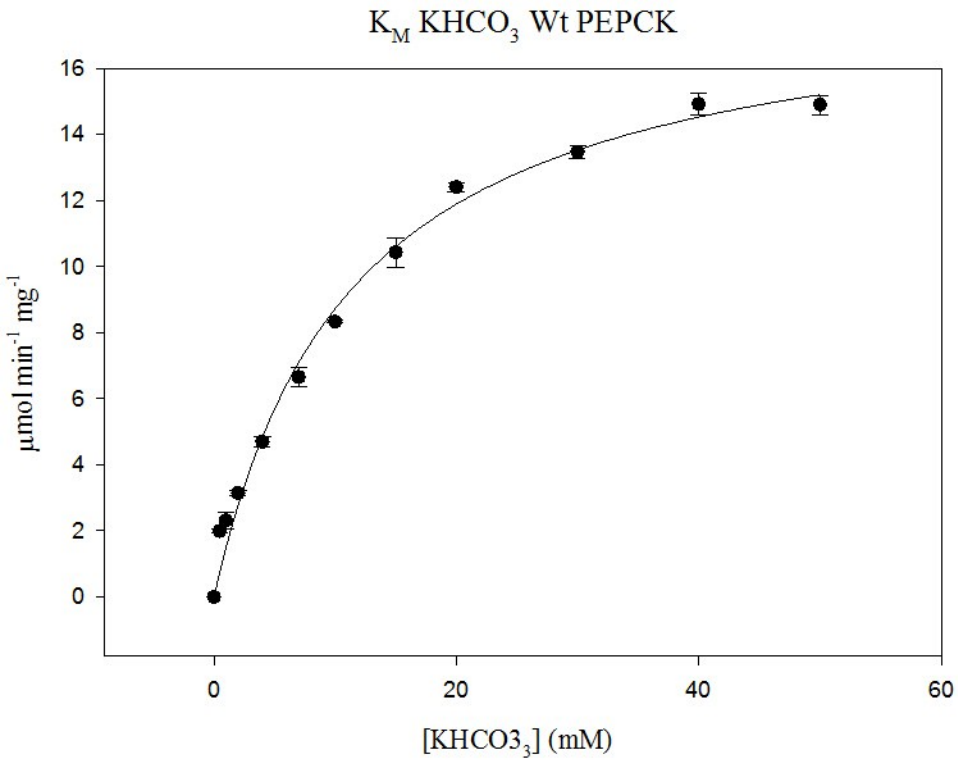
K_M KHCO3 Wt PEPCK
µmol min-1 mg-1
[KHCO3] (mM)
0
2
4
6
8
10
12
14
16
0
20
40
60

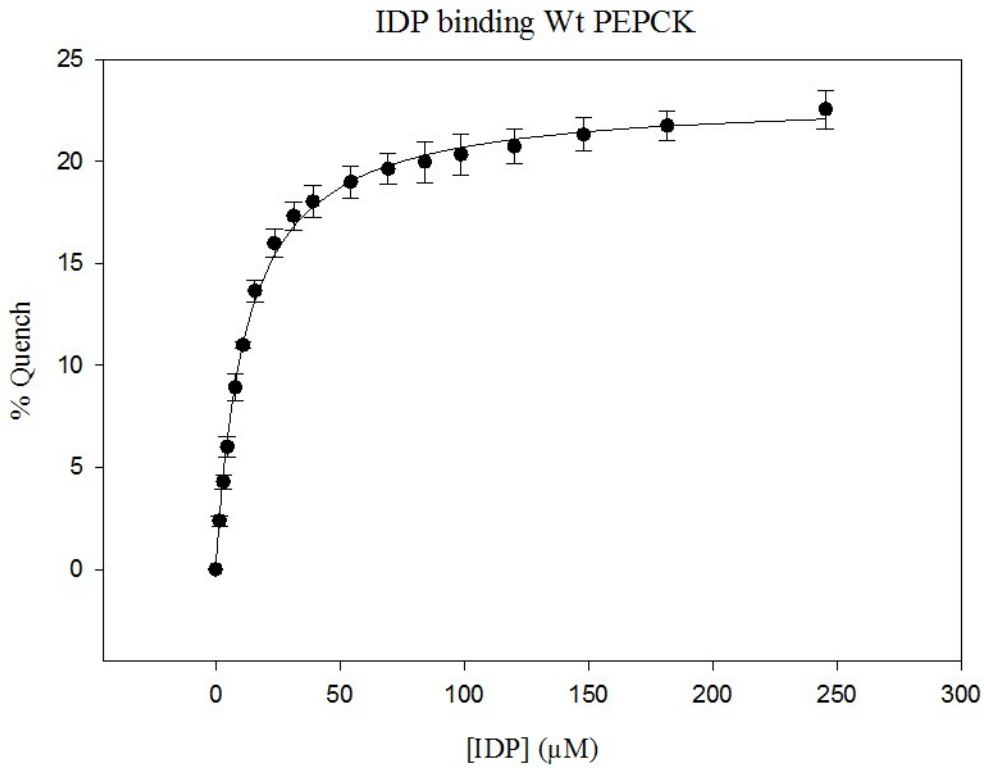
IDP binding Wt PEPCK
% Quench
[IDP] (μM)
0
5
10
15
20
25
0
50
100
150
200
250
300

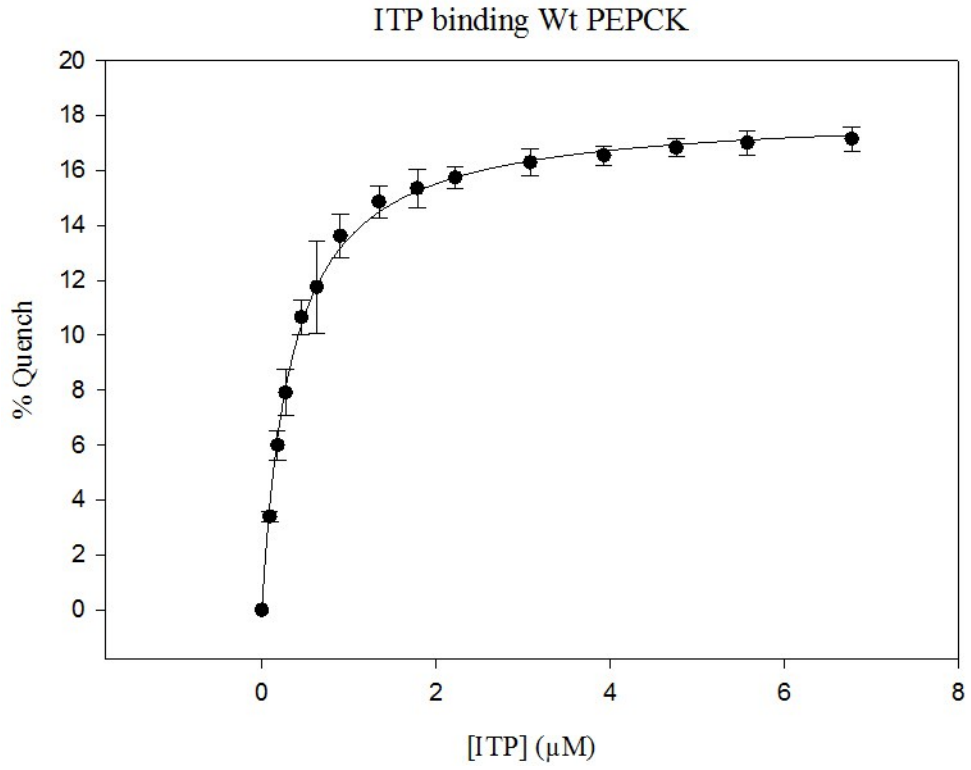
ITP binding Wt PEPCK
% Quench
[ITP] (μM)
0
2
4
6
8
10
12
14
16
18
20

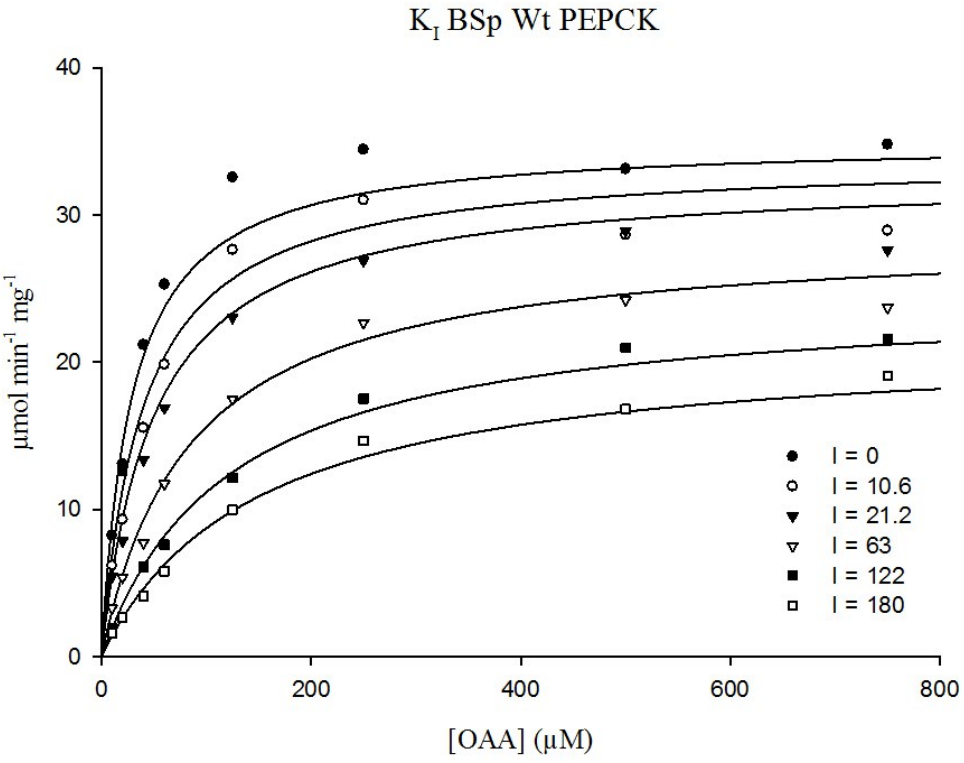
K$_I$ BSp Wt PEPCK
µmol min^{-1} mg^{-1}
[OAA] (µM)
I = 0
I = 10.6
I = 21.2
I = 63
I = 122
I = 180

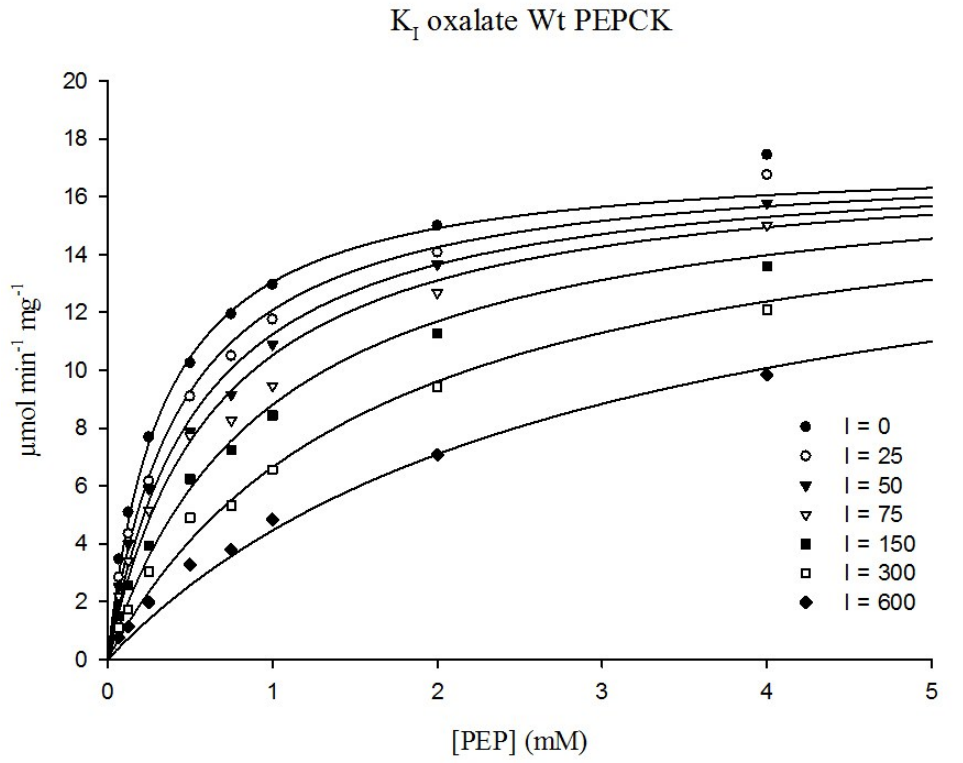
K$_I$ oxalate Wt PEPCK
µmol min^{-1} mg^{-1}
[PEP] (mM)
I = 0
I = 25
I = 50
I = 75
I = 150
I = 300
I = 600

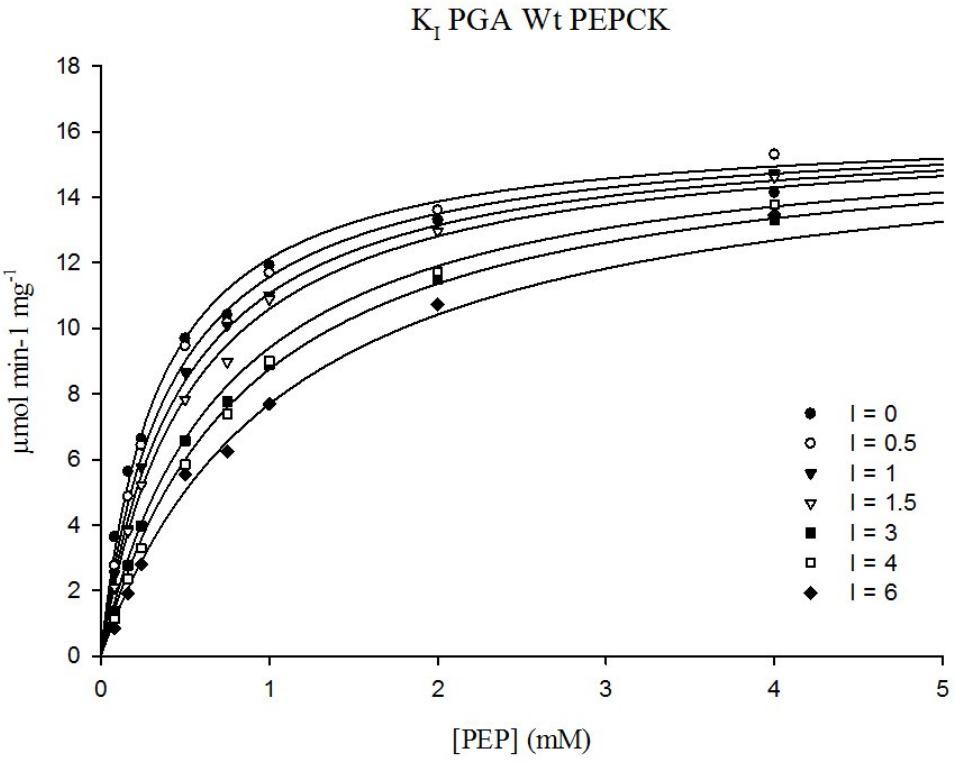
K_I PGA Wt PEPCK
µmol min-1 mg-1
[PEP] (mM)
I = 0
I = 0.5
I = 1
I = 1.5
I = 3
I = 4
I = 6
0
2
4
6
8
10
12
14
16
18
0
1
2
3
4
5

A467G rcPEPCK from the pGEX expression vector

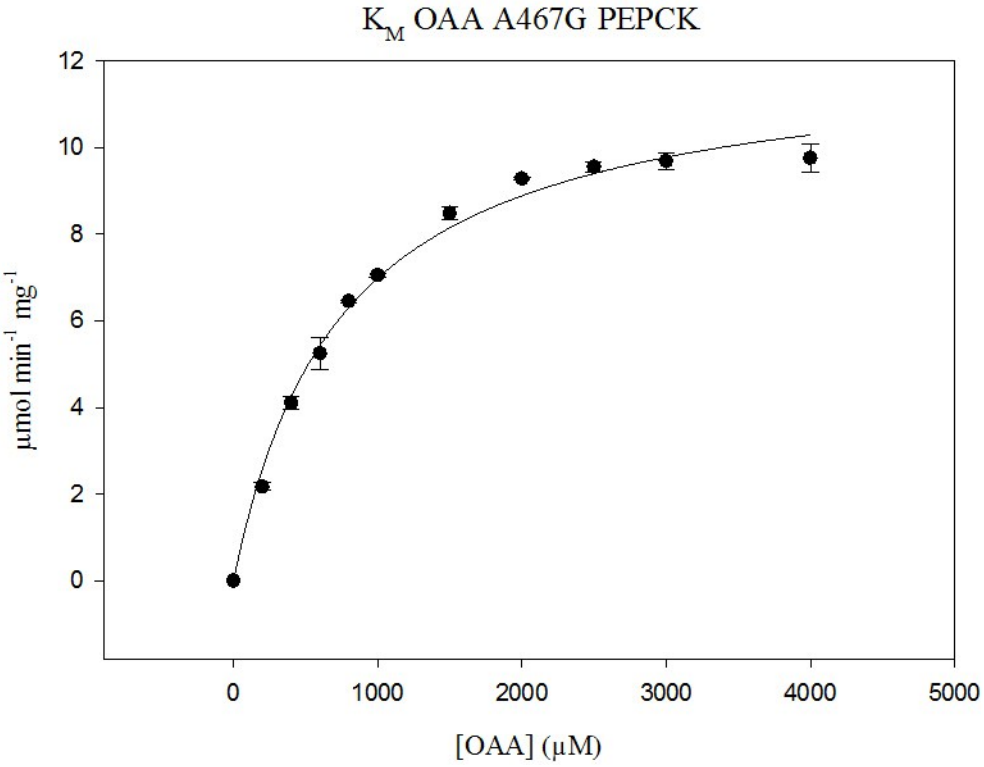

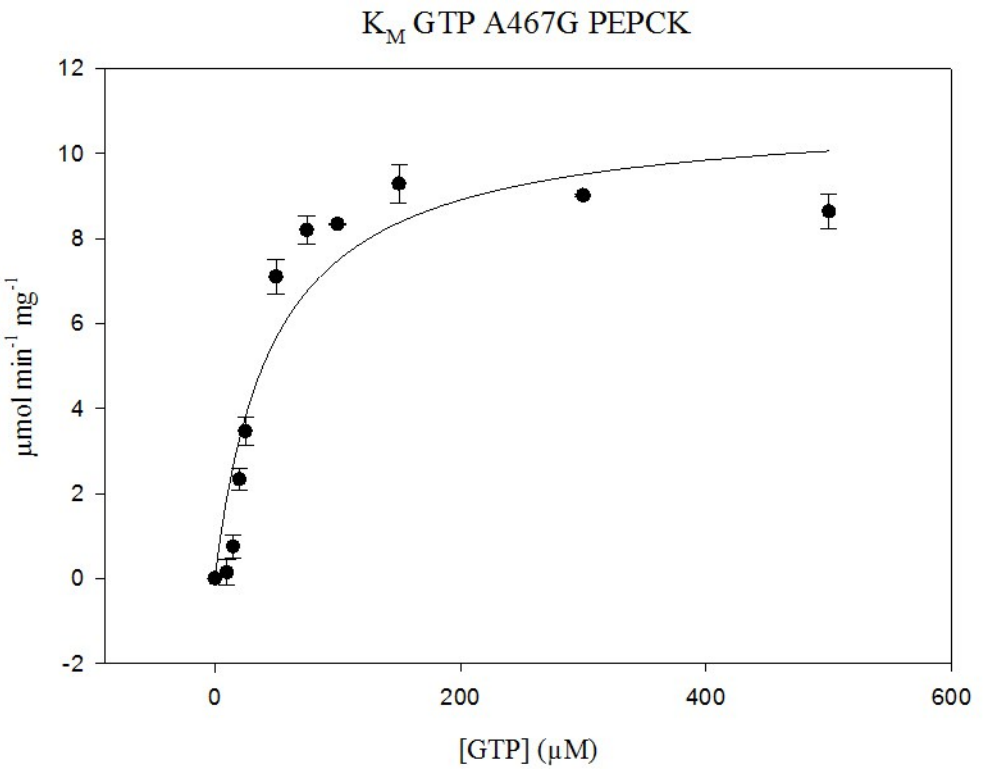

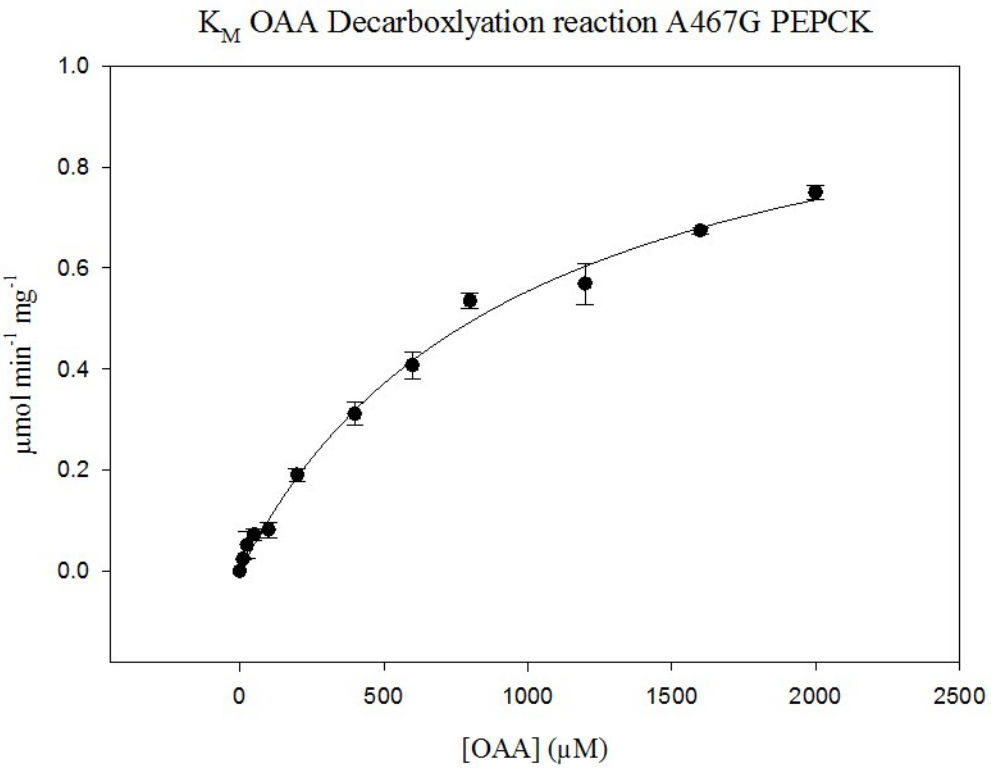
K_M OAA Decarboxlyation reaction A467G PEPCK
1.0
0.8
0.6
0.4
0.2
0.0
µmol min^{-1} mg^{-1}
0
500
1000
1500
2000
2500
[OAA] (µM)

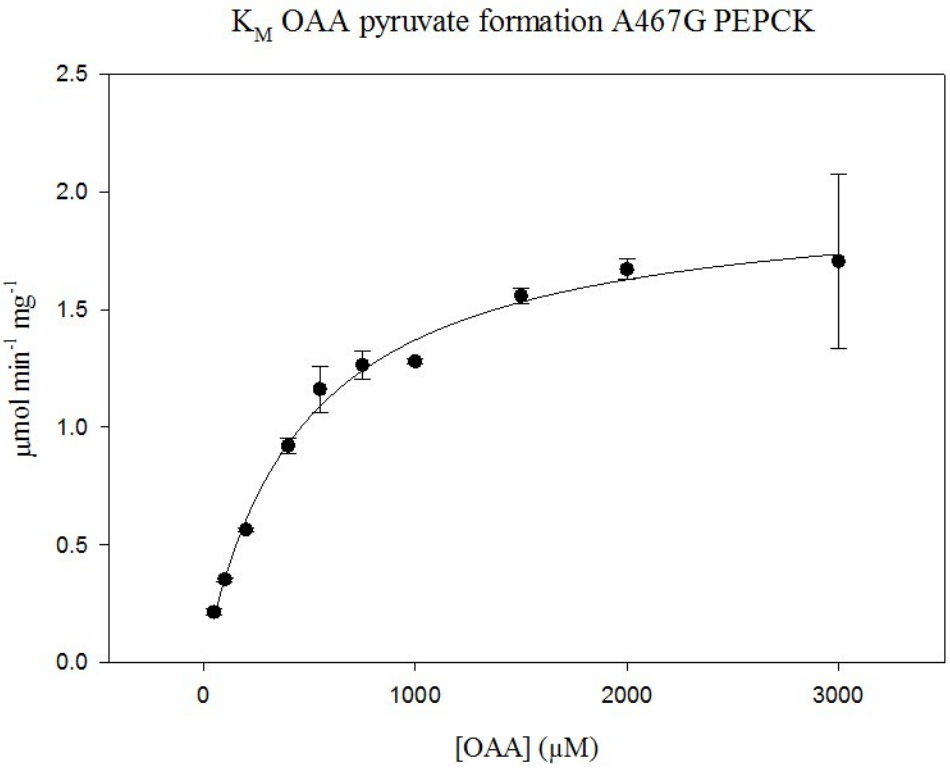
K_M OAA pyruvate formation A467G PEPCK
2.5
2.0
1.5
1.0
0.5
0.0
µmol min^{-1} mg^{-1}
0
1000
2000
3000
[OAA] (µM)

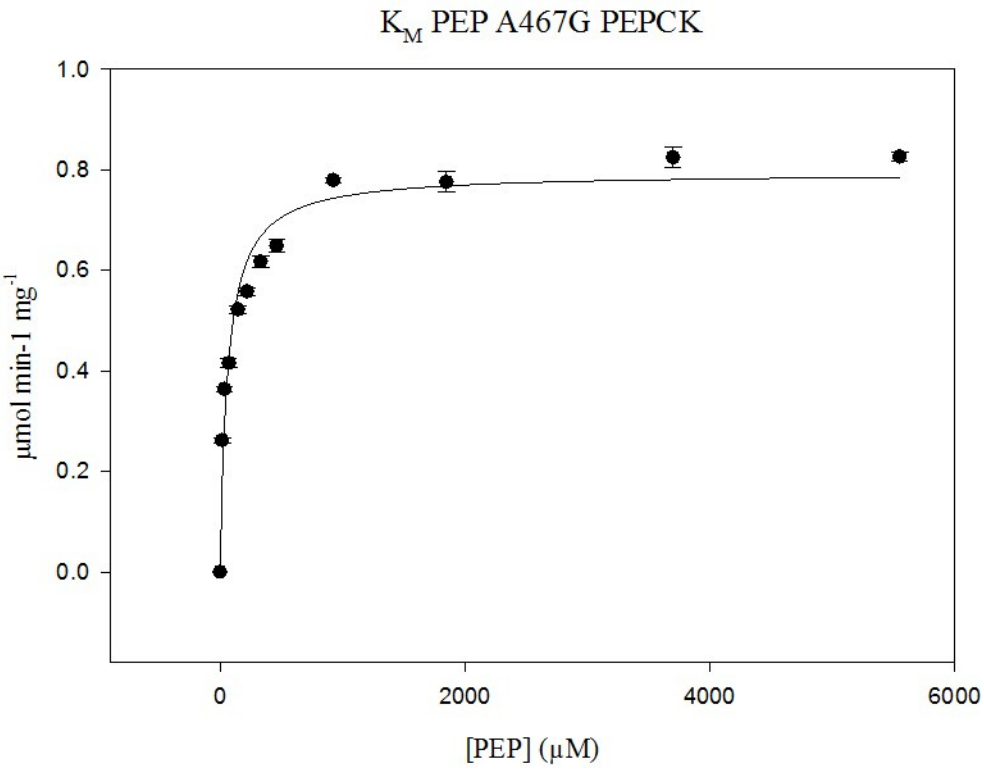
K$_M$ PEP A467G PEPCK
µmol min-1 mg-1
1.0
0.8
0.6
0.4
0.2
0.0
0
2000
4000
6000
[PEP] (µM)

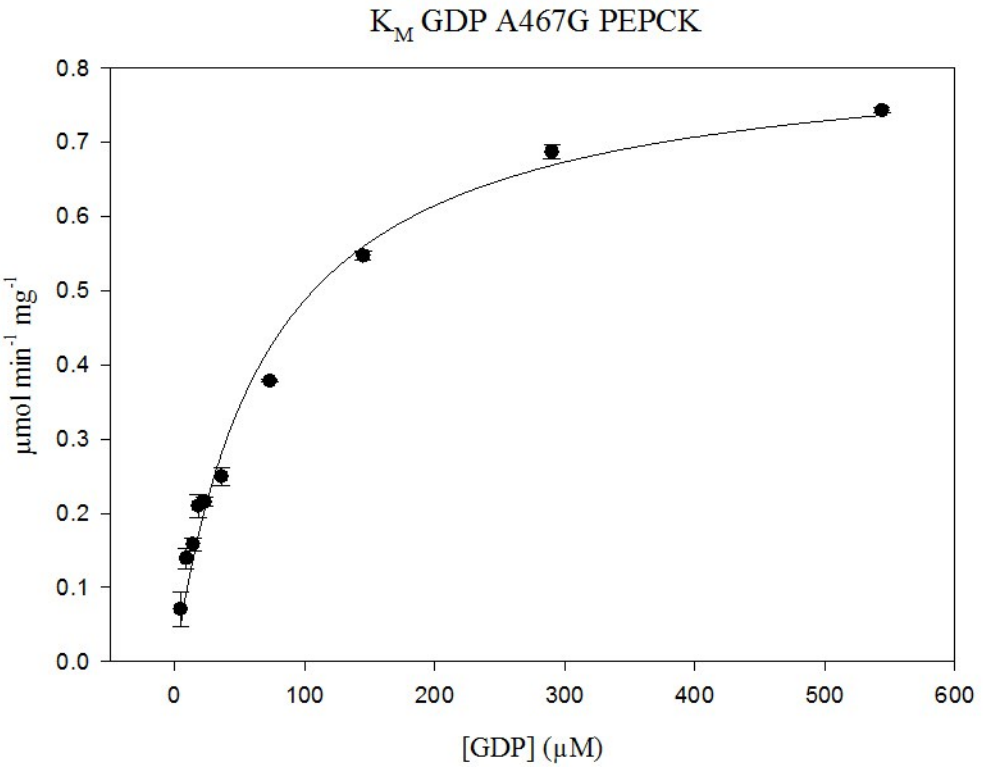
K$_M$ GDP A467G PEPCK
µmol min-1 mg-1
0.8
0.7
0.6
0.5
0.4
0.3
0.2
0.1
0.0
0
100
200
300
400
500
600
[GDP] (µM)

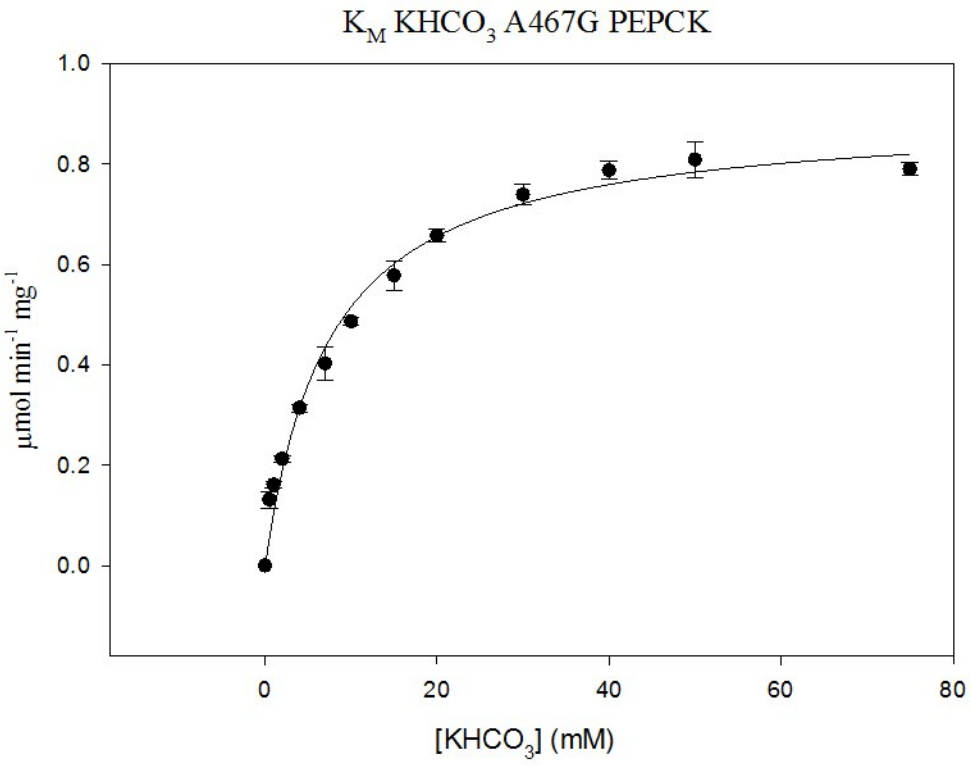
K_M $KHCO_3$ A467G PEPCK
1.0
0.8
0.6
0.4
0.2
0.0
µmol min-1 mg-1
0
20
40
60
80
[KHCO3] (mM)

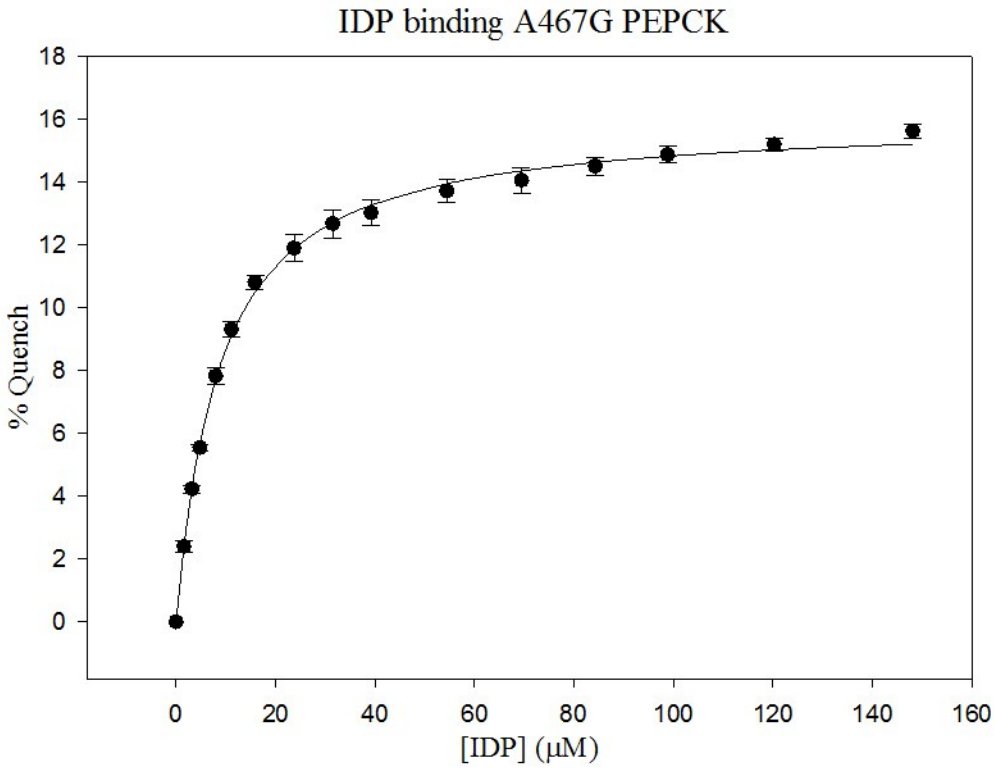
IDP binding A467G PEPCK
18
16
14
12
10
8
6
4
2
0
% Quench
0
20
40
60
80
100
120
140
160
[IDP] (µM)

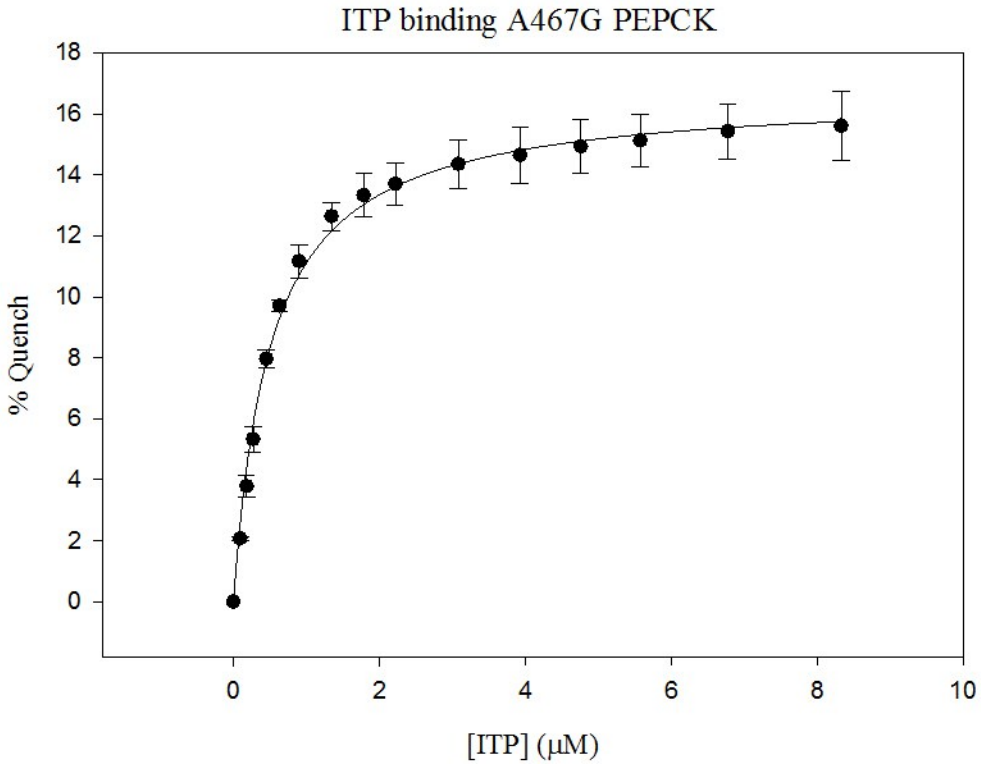
ITP binding A467G PEPCK
% Quench
[ITP] (μM)
0
2
4
6
8
10
12
14
16
18

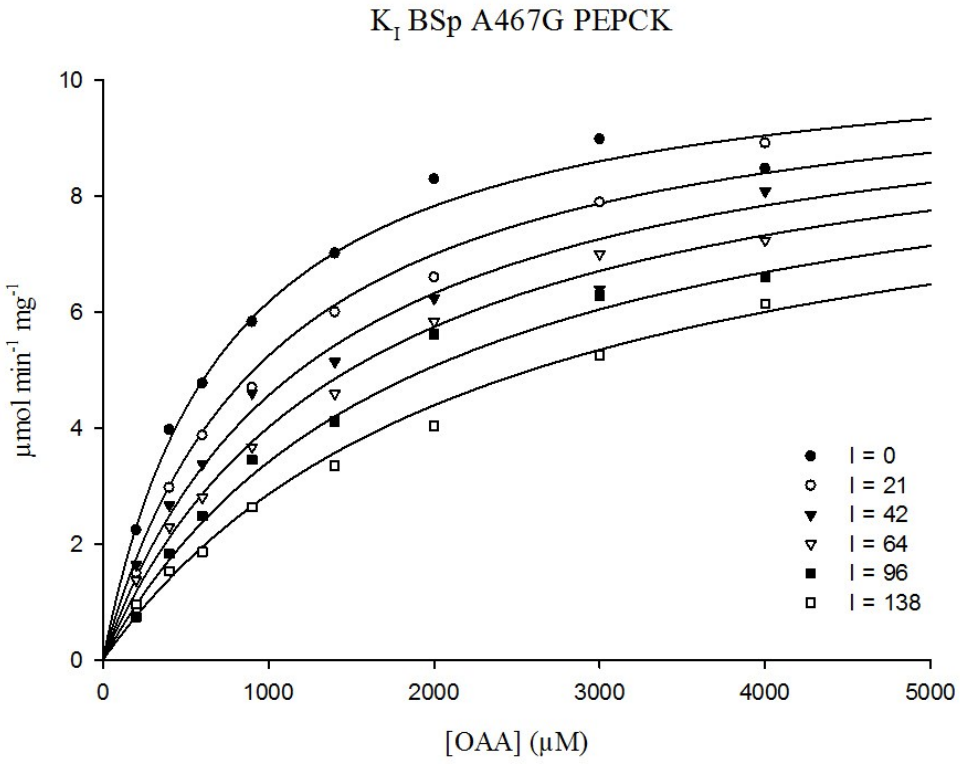
K$_I$ BSp A467G PEPCK
μmol min^{-1} mg^{-1}
[OAA] (μM)
I = 0
I = 21
I = 42
I = 64
I = 96
I = 138
0
1000
2000
3000
4000
5000

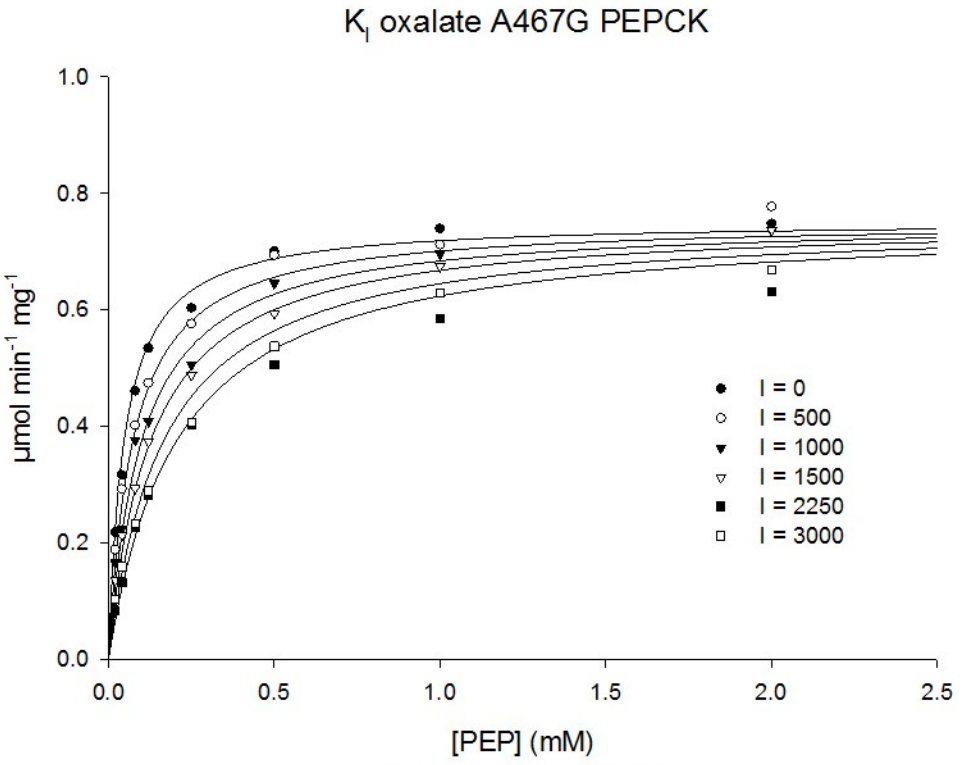
K$_I$ oxalate A467G PEPCK
µmol min^{-1} mg^{-1}
[PEP] (mM)
I = 0
I = 500
I = 1000
I = 1500
I = 2250
I = 3000

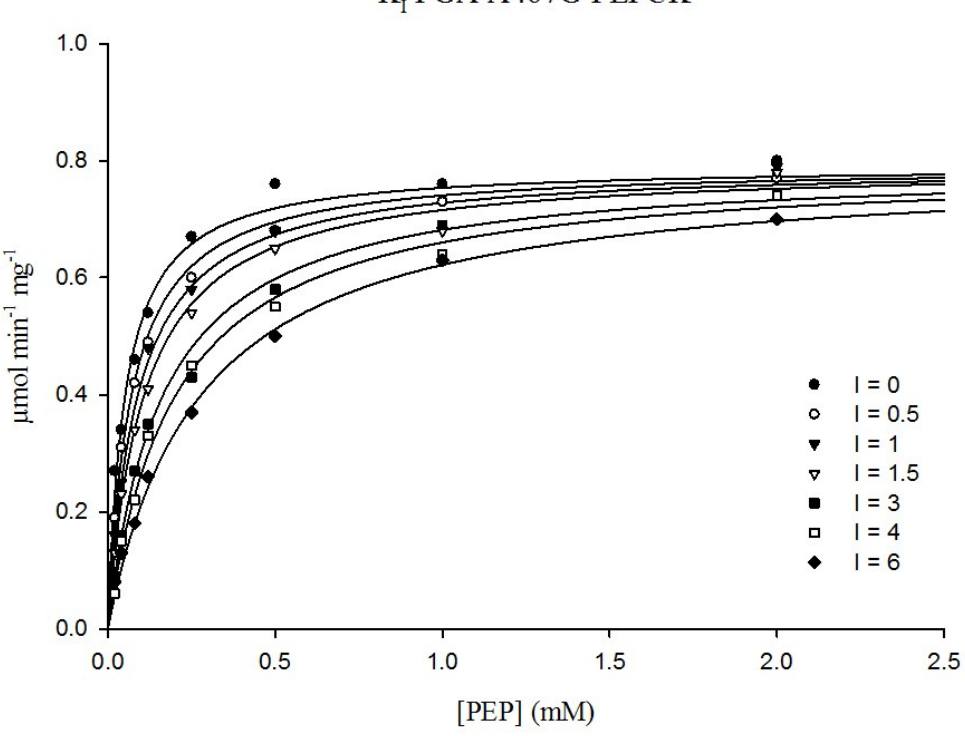
K$_I$ PGA A467G PEPCK
µmol min^{-1} mg^{-1}
[PEP] (mM)
I = 0
I = 0.5
I = 1
I = 1.5
I = 3
I = 4
I = 6

WT rcPEPCK from the pSUMO expression vector

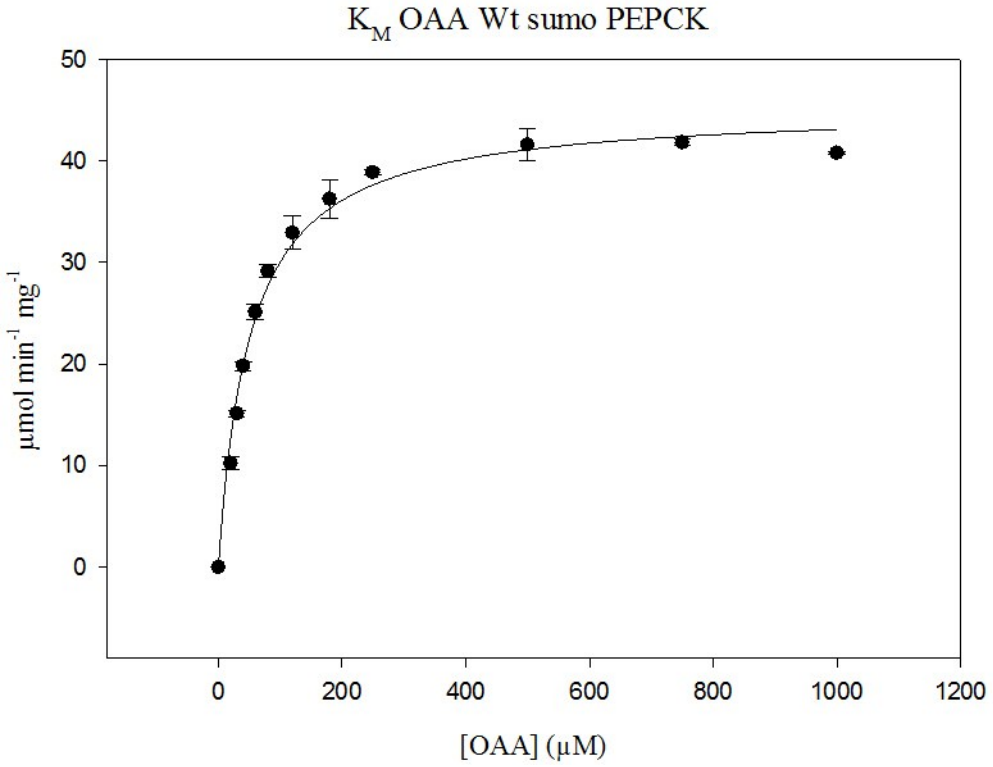

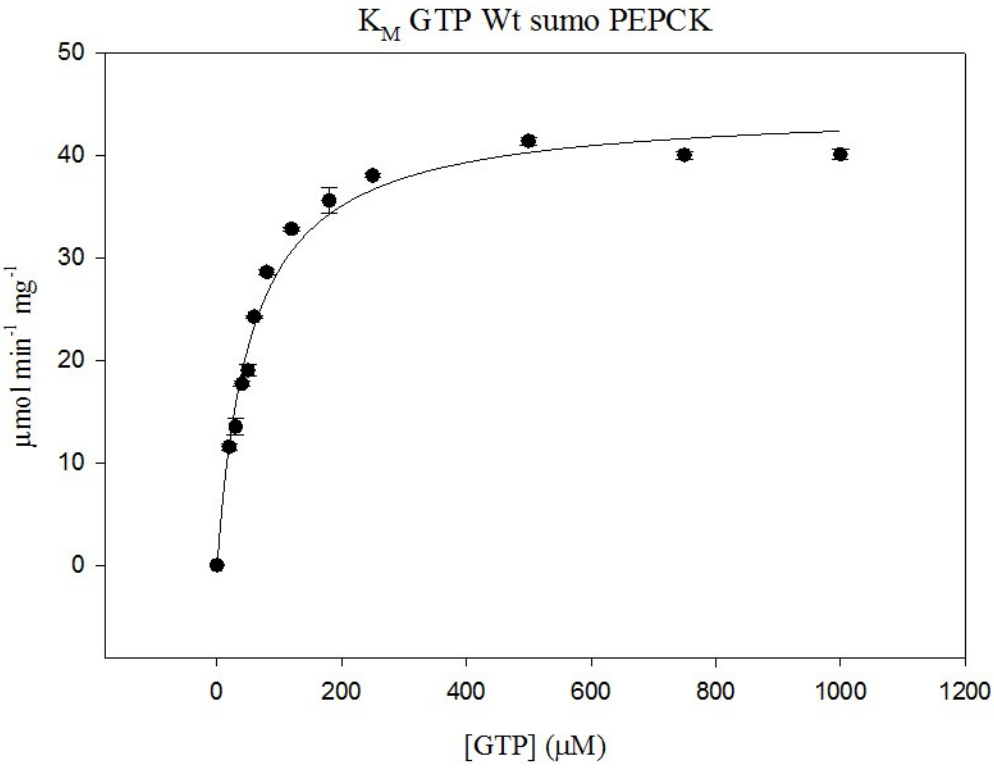

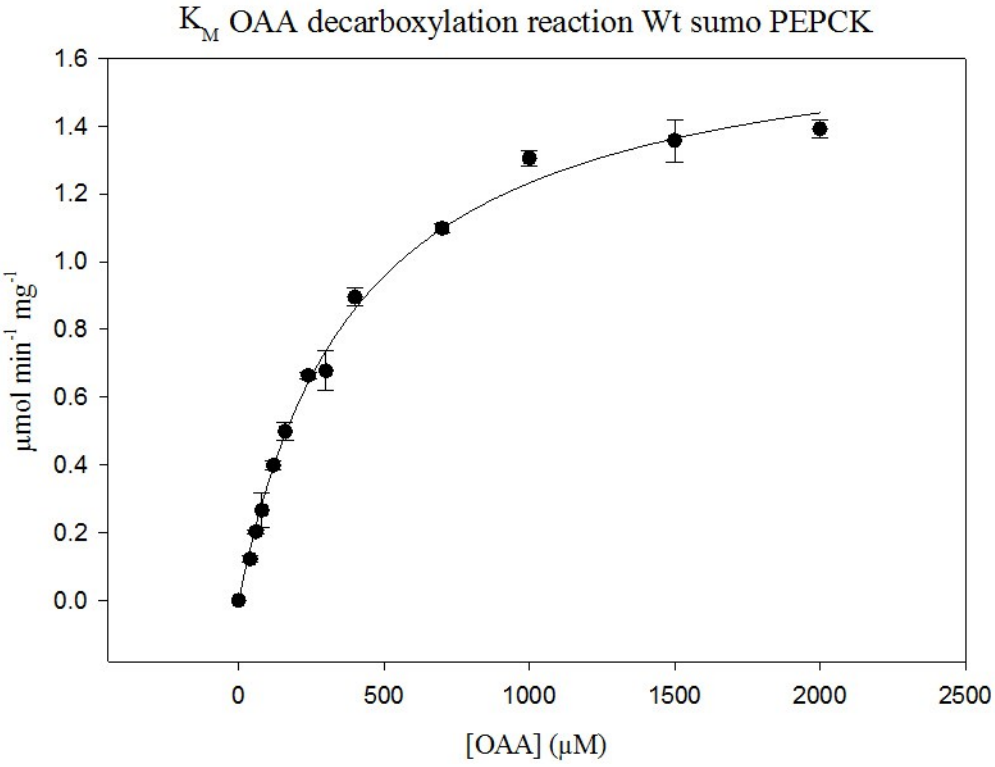
K$_M$ OAA decarboxylation reaction Wt sumo PEPCK
µmol min^{-1} mg^{-1}
[OAA] (µM)
0.0
0.2
0.4
0.6
0.8
1.0
1.2
1.4
1.6
0
500
1000
1500
2000
2500

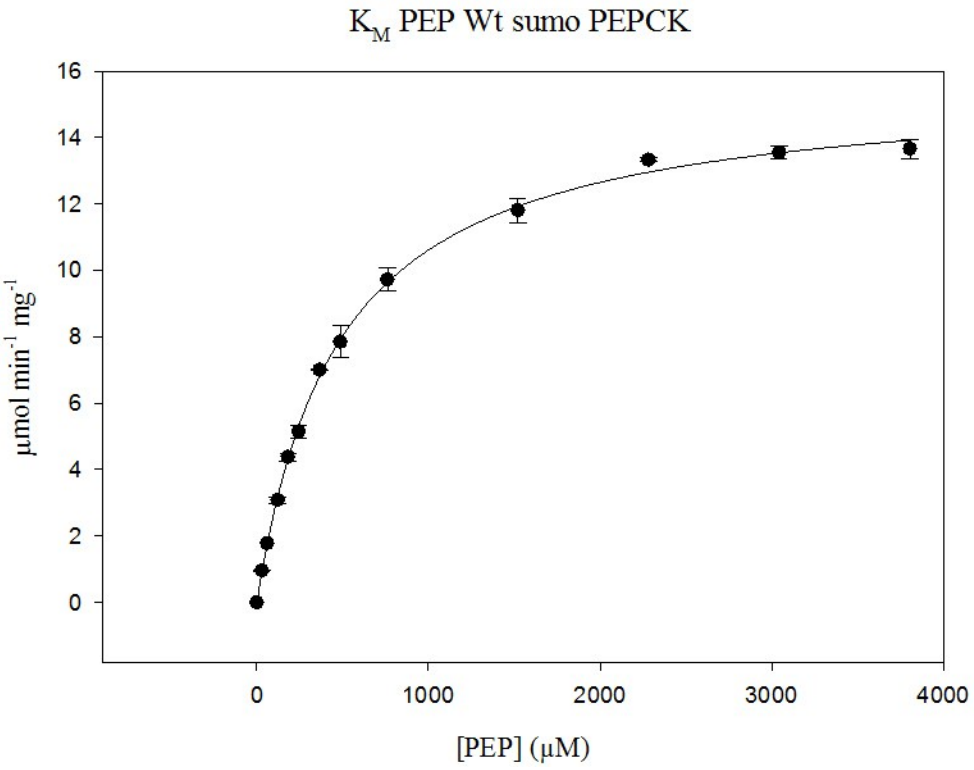
K$_M$ PEP Wt sumo PEPCK
µmol min^{-1} mg^{-1}
[PEP] (µM)
0
2
4
6
8
10
12
14
16
0
1000
2000
3000
4000

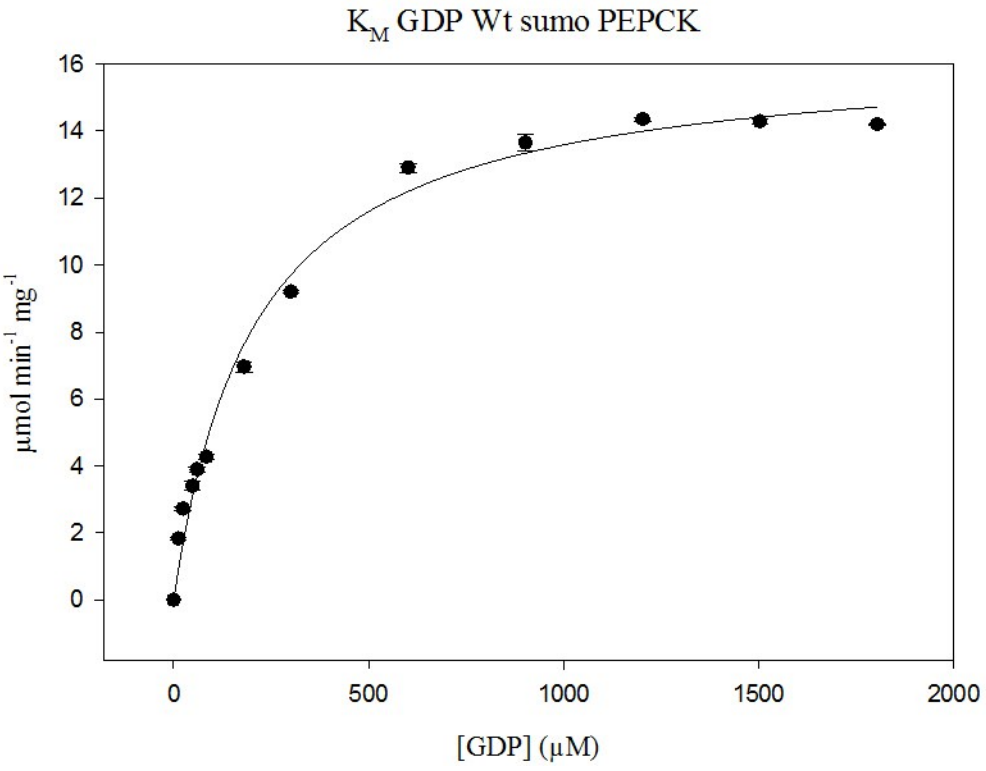
K_M GDP Wt sumo PEPCK
µmol min^{-1} mg^{-1}
[GDP] (µM)
0
2
4
6
8
10
12
14
16
0
500
1000
1500
2000

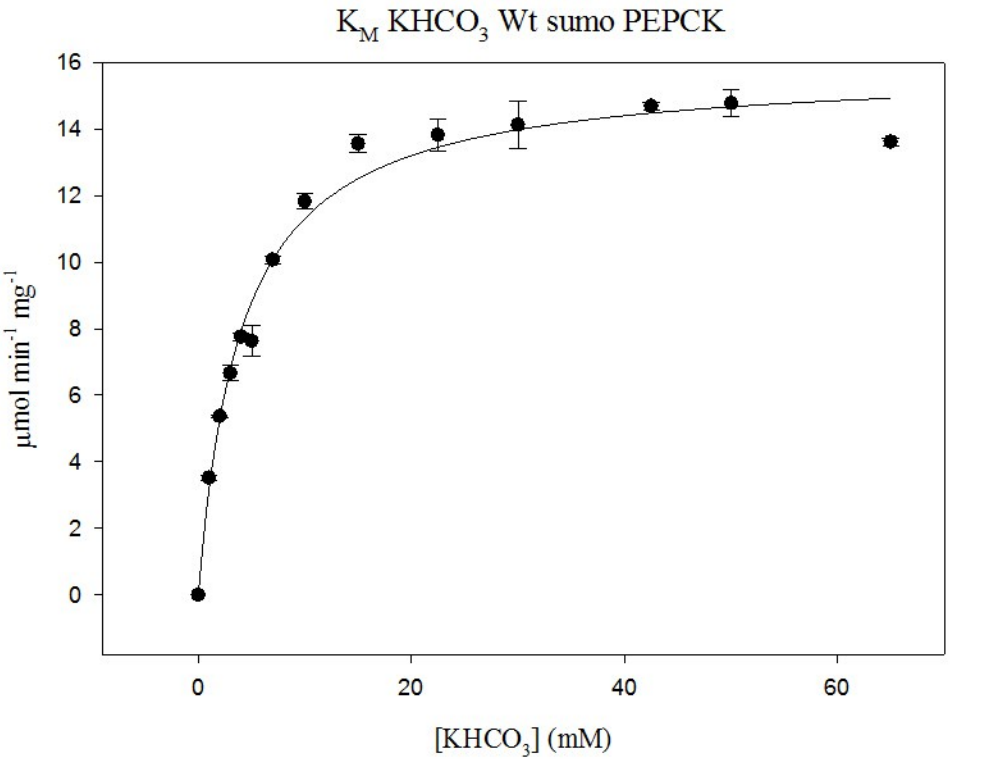
K_M $KHCO_3$ Wt sumo PEPCK
µmol min^{-1} mg^{-1}
[$KHCO_3$] (mM)
0
2
4
6
8
10
12
14
16
0
20
40
60

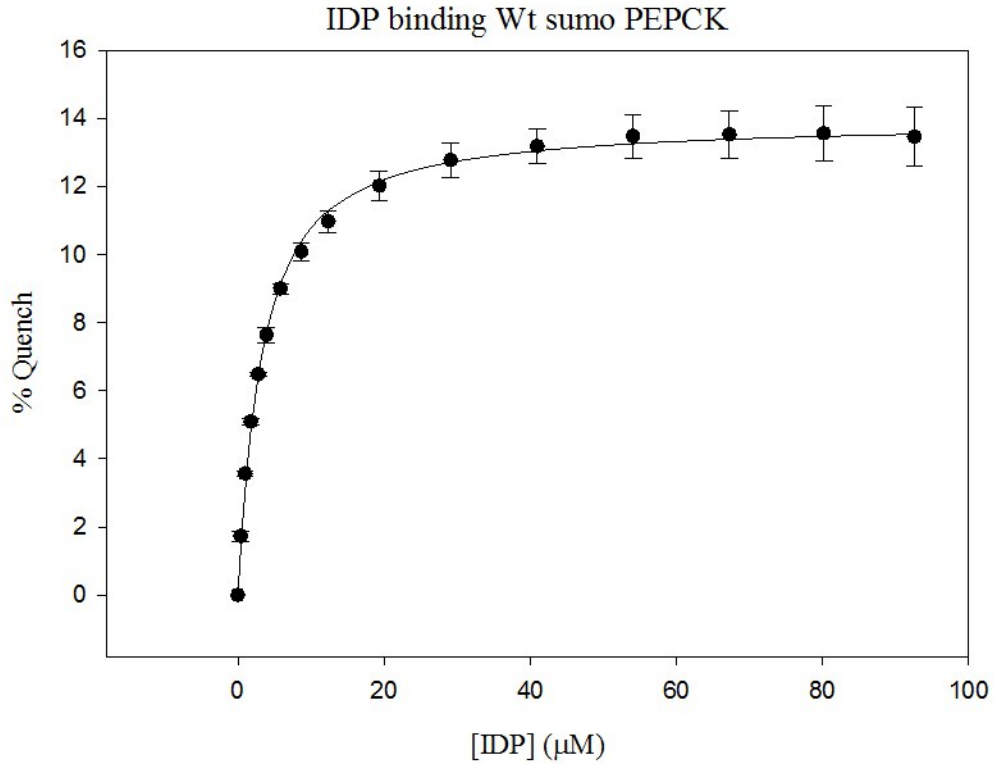
IDP binding Wt sumo PEPCK
% Quench
[IDP] (μM)
0
2
4
6
8
10
12
14
16
0
20
40
60
80
100

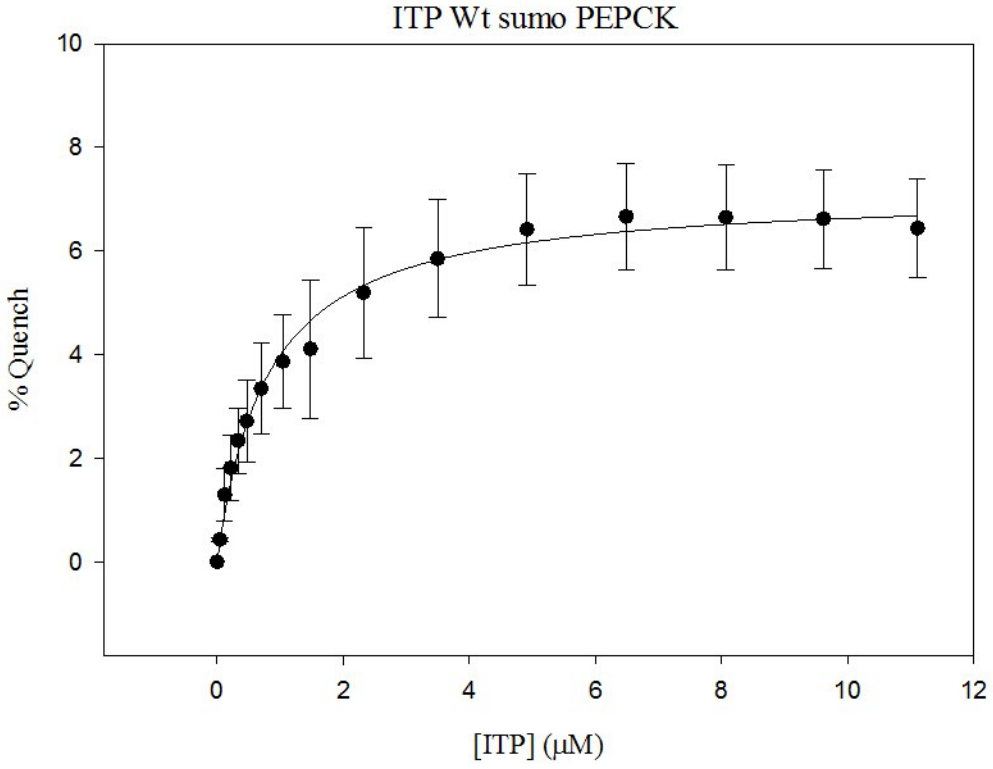
ITP Wt sumo PEPCK
% Quench
[ITP] (μM)
0
2
4
6
8
10
0
2
4
6
8
10
12

E89A rcPEPCK from the pSUMO expression vector

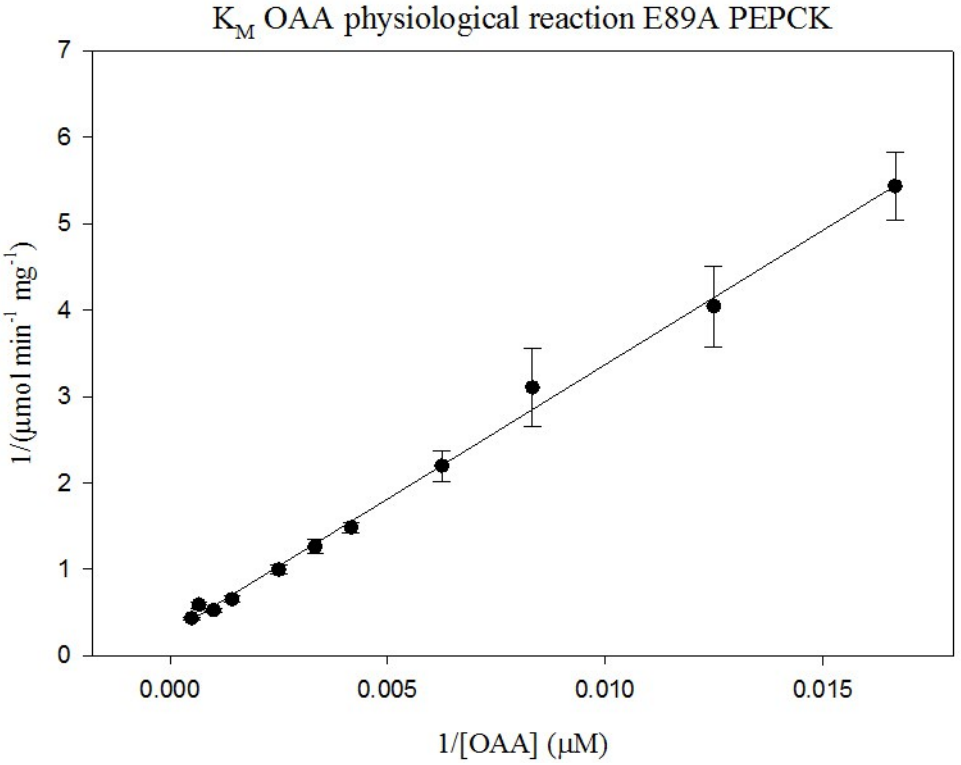

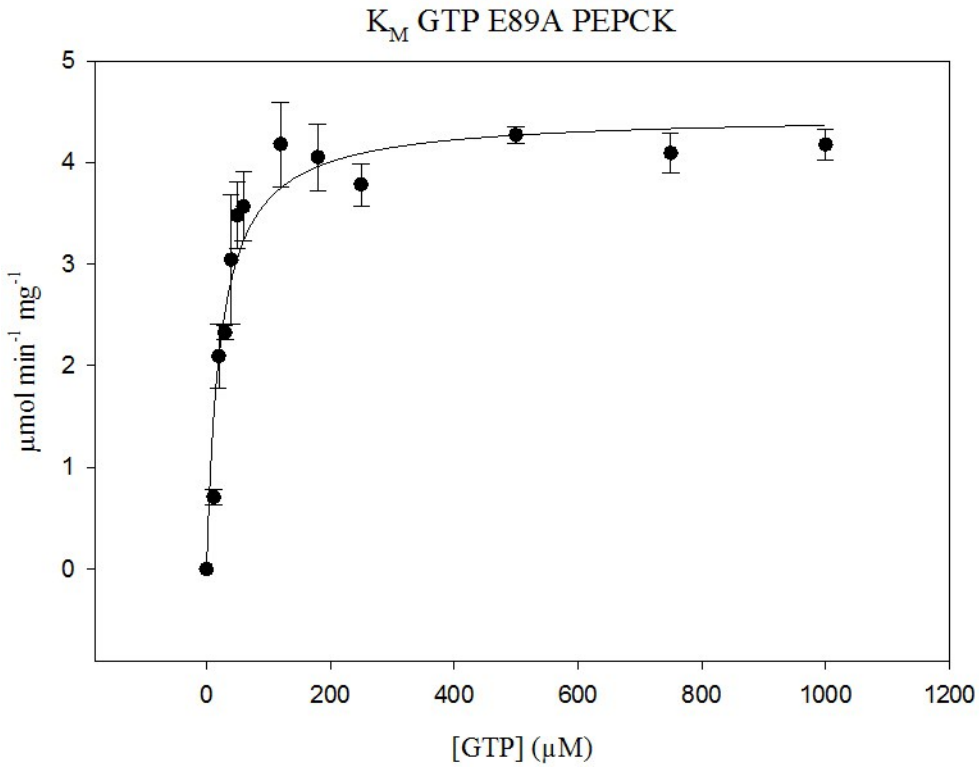

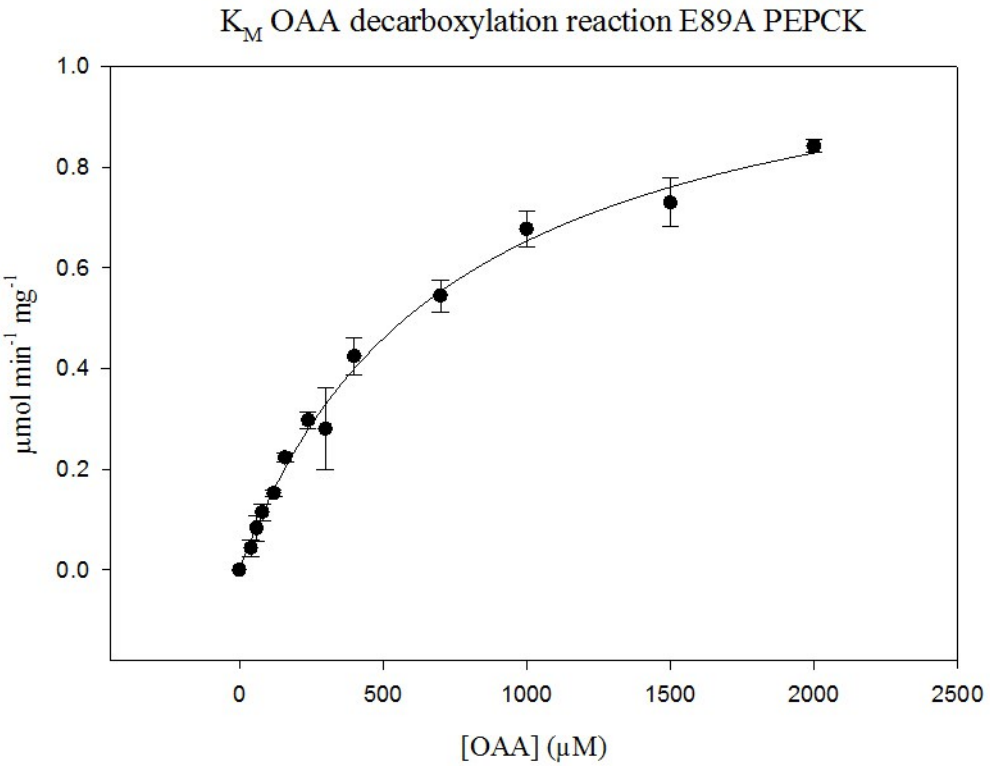
K_M OAA decarboxylation reaction E89A PEPCK
1.0
0.8
0.6
0.4
0.2
0.0
µmol min^{-1} mg^{-1}
0
500
1000
1500
2000
2500
[OAA] (µM)

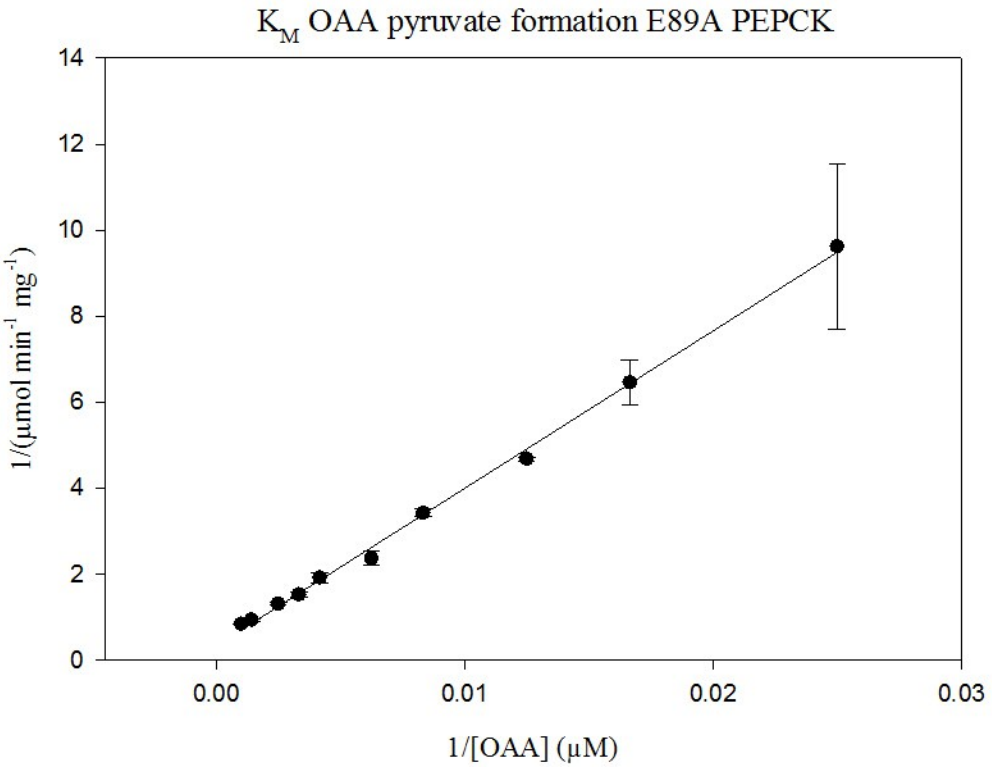
K_M OAA pyruvate formation E89A PEPCK
14
12
10
8
6
4
2
0
1/(µmol min^{-1} mg^{-1})
0.00
0.01
0.02
0.03
1/[OAA] (µM)

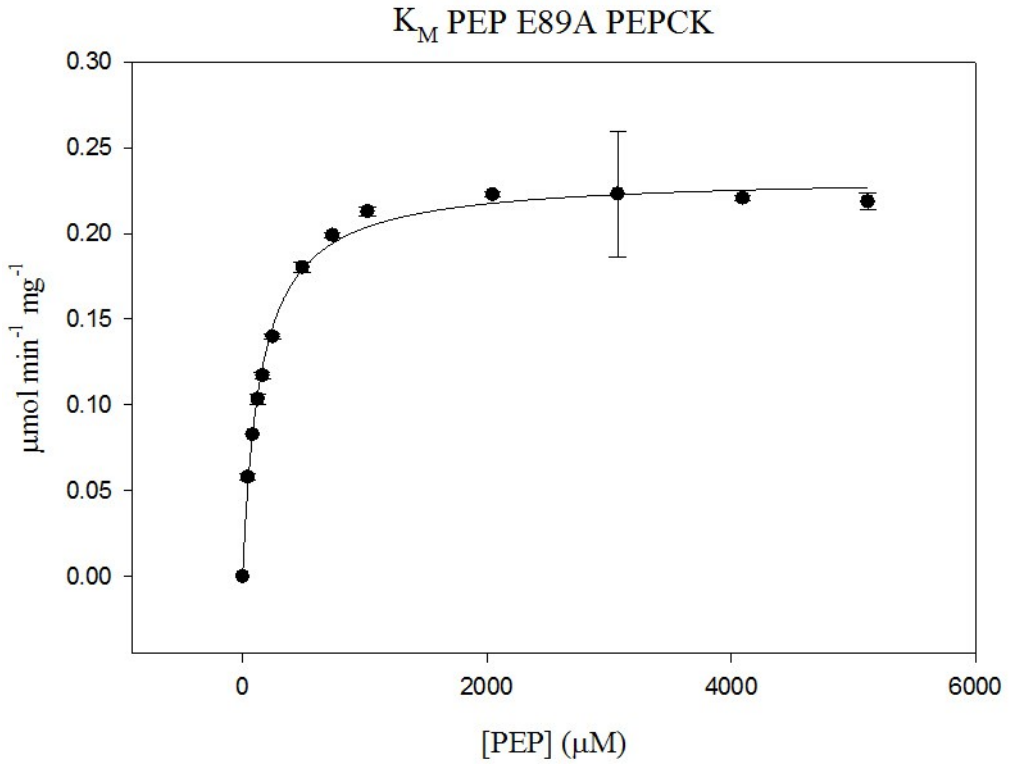
K_M PEP E89A PEPCK
0.30
0.25
0.20
0.15
0.10
0.05
0.00
µmol min-1 mg-1
0
2000
4000
6000
[PEP] (µM)

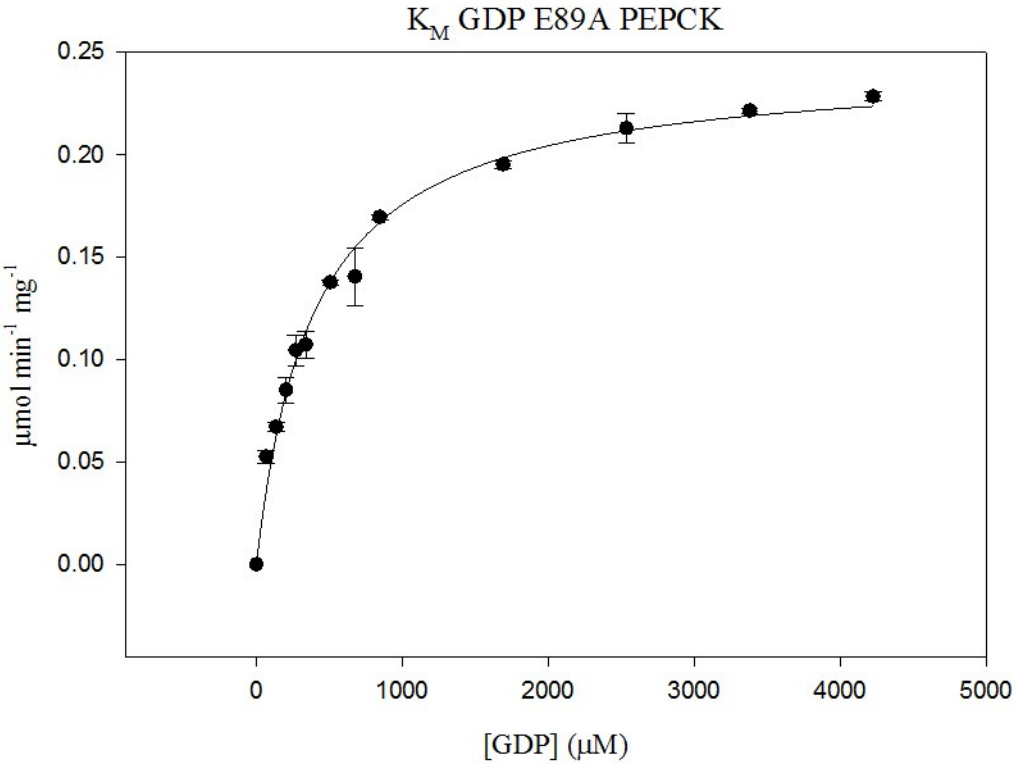
K_M GDP E89A PEPCK
0.25
0.20
0.15
0.10
0.05
0.00
µmol min-1 mg-1
0
1000
2000
3000
4000
5000
[GDP] (µM)

K_M $KHCO_3$ E89A PEPCK

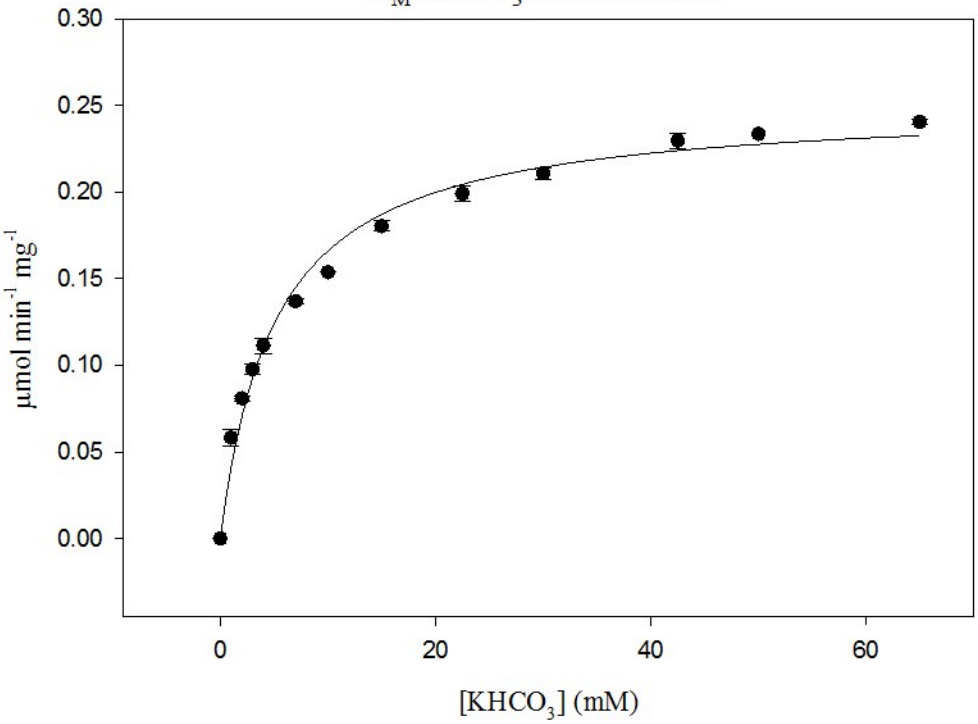

K_I BSp E89A PEPCK

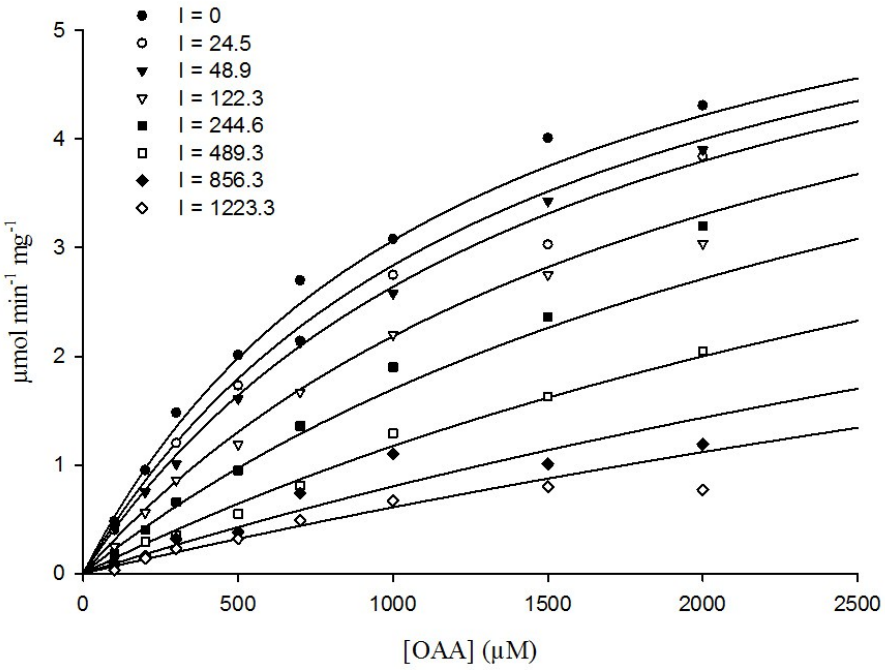

K_I oxalate E89A PEPCK

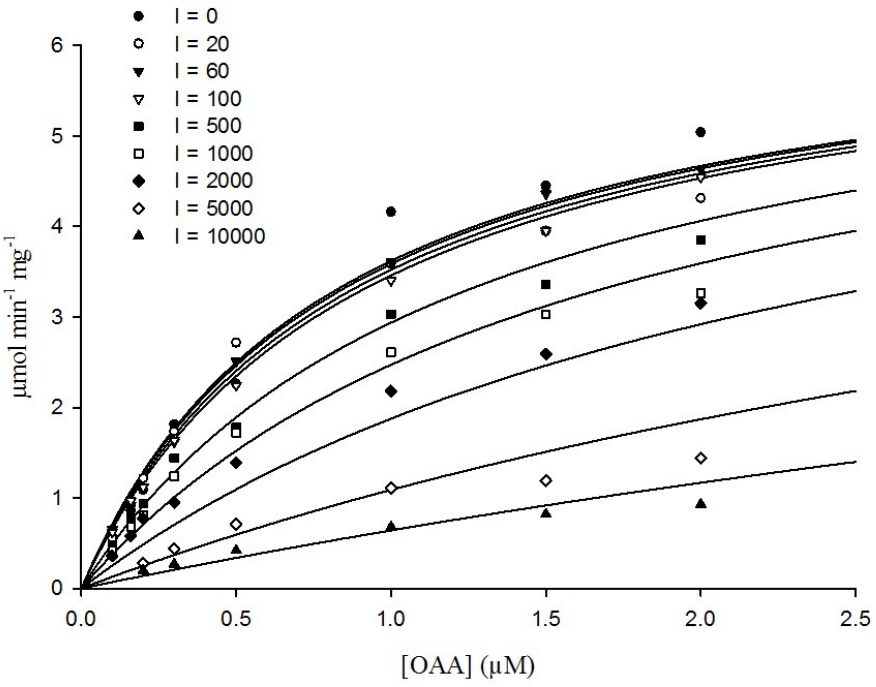

IDP binding E89A PEPCK

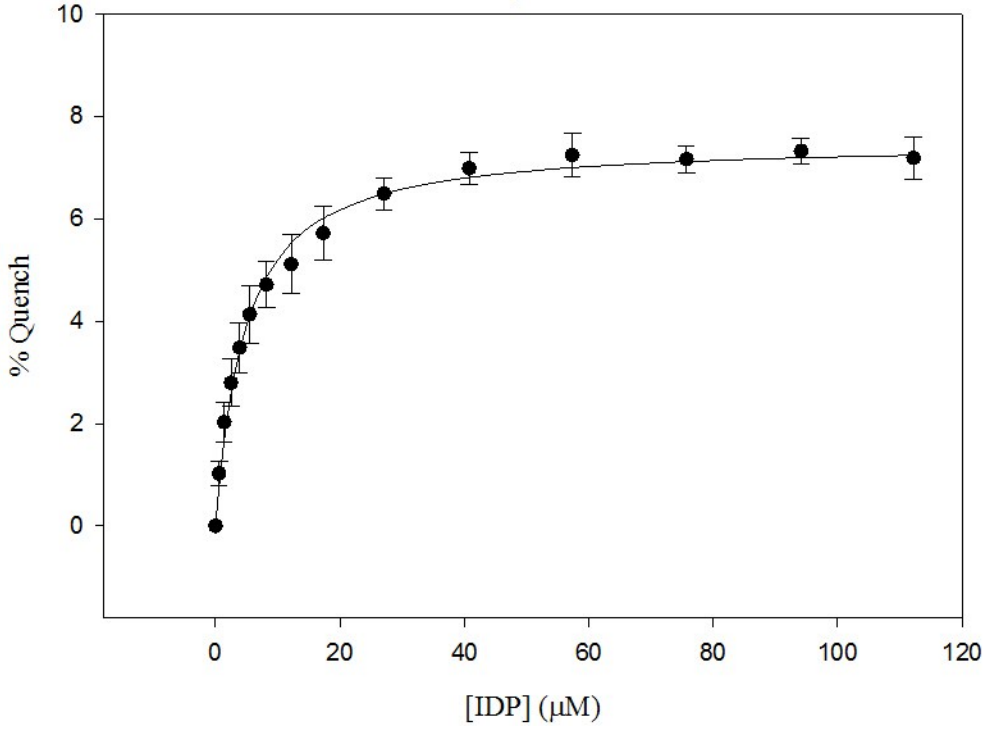

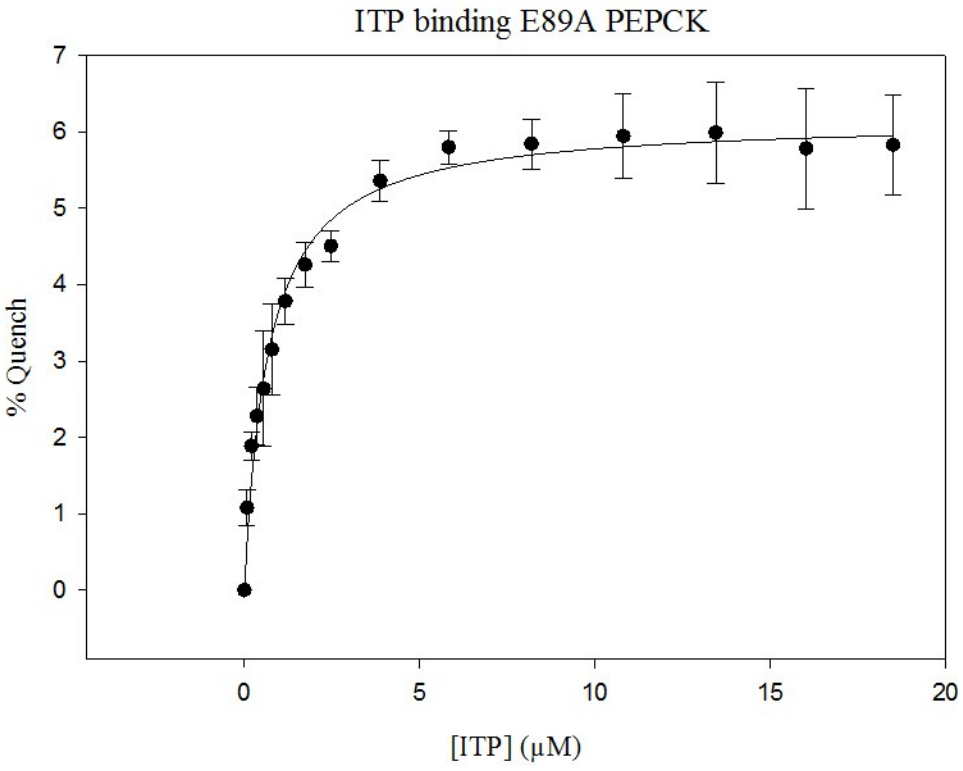
ITP binding E89A PEPCK
% Quench
[ITP] (μM)
0
1
2
3
4
5
6
7
0
5
10
15
20

E89D rcPEPCK from the pSUMO expression vector

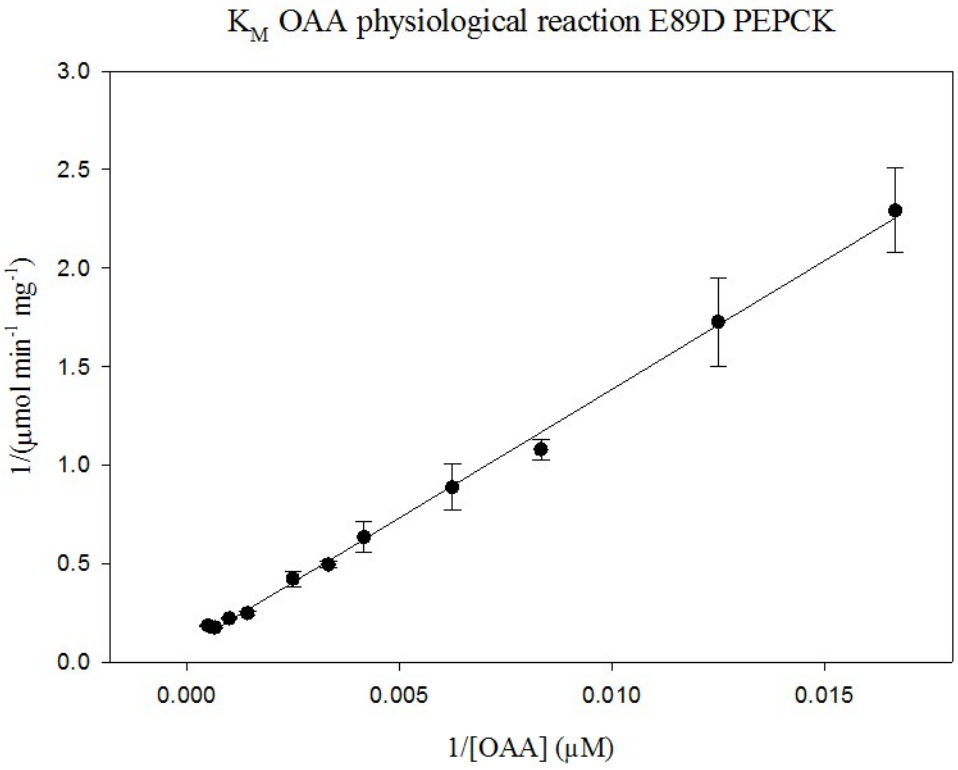

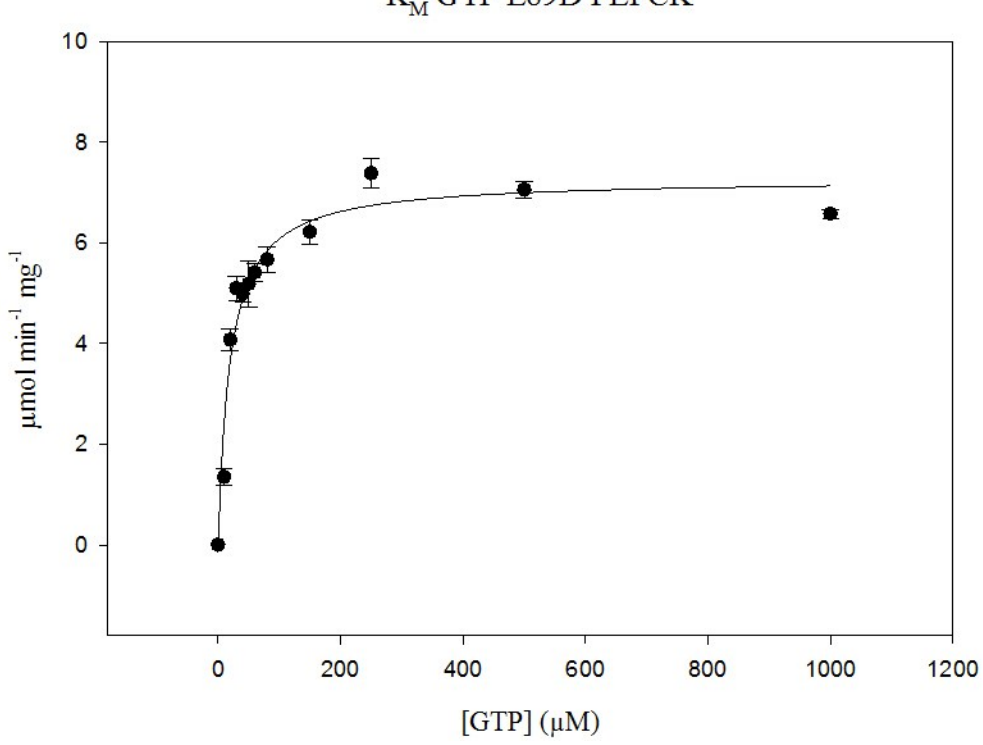

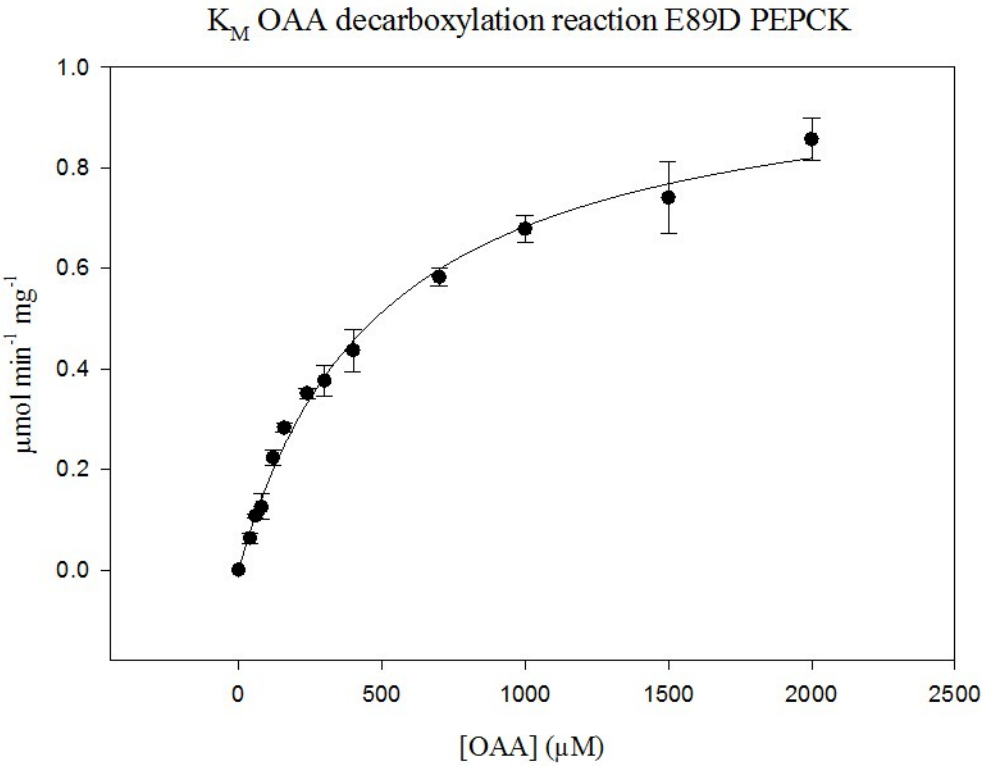
K_M OAA decarboxylation reaction E89D PEPCK
1.0
0.8
0.6
0.4
0.2
0.0
µmol min^{-1} mg^{-1}
0
500
1000
1500
2000
2500
[OAA] (µM)

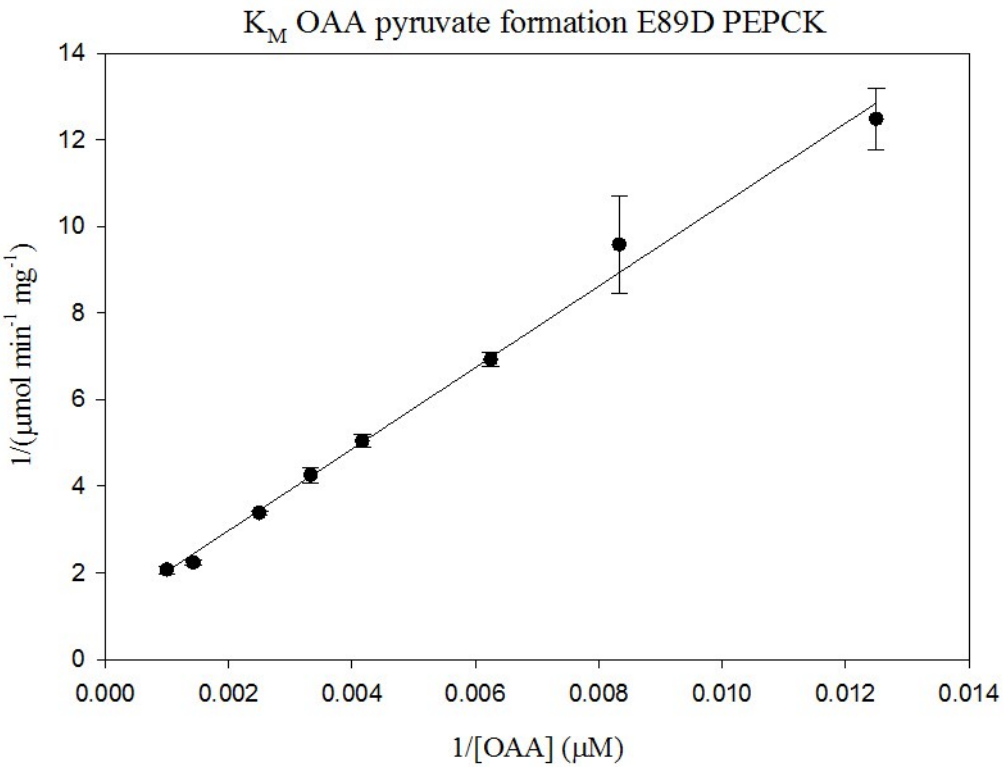
K_M OAA pyruvate formation E89D PEPCK
14
12
10
8
6
4
2
0
1/(µmol min^{-1} mg^{-1})
0.000
0.002
0.004
0.006
0.008
0.010
0.012
0.014
1/[OAA] (µM)

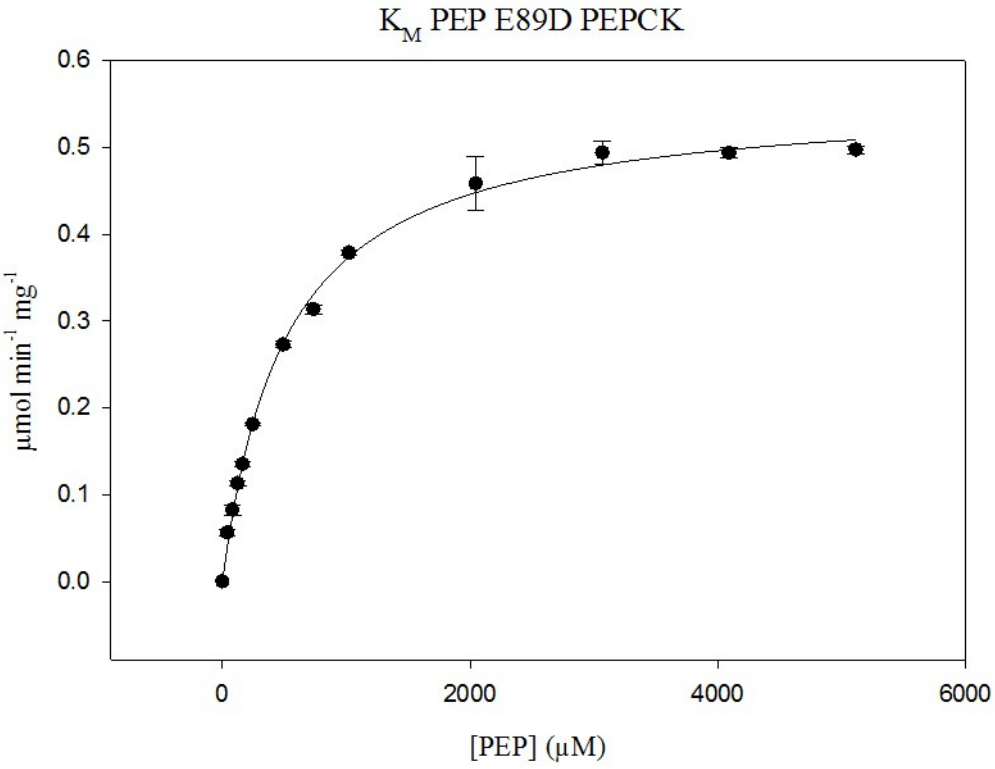
K_M PEP E89D PEPCK
0.6
0.5
0.4
0.3
0.2
0.1
0.0
µmol min-1 mg-1
0
2000
4000
6000
[PEP] (µM)

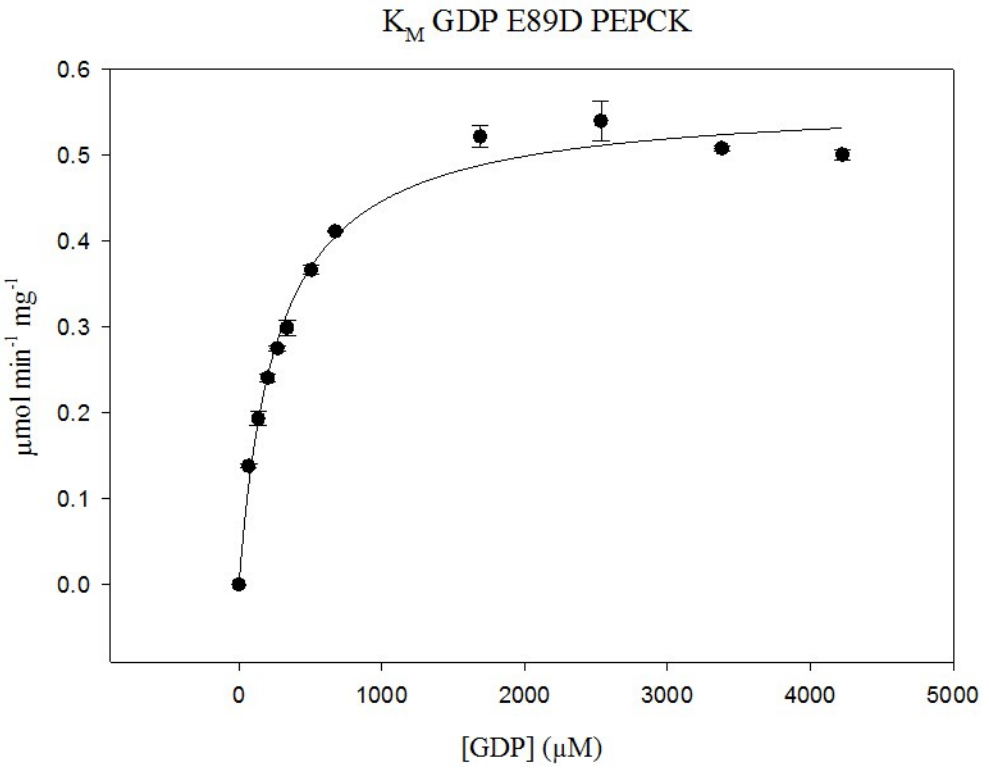
K_M GDP E89D PEPCK
0.6
0.5
0.4
0.3
0.2
0.1
0.0
µmol min-1 mg-1
0
1000
2000
3000
4000
5000
[GDP] (µM)

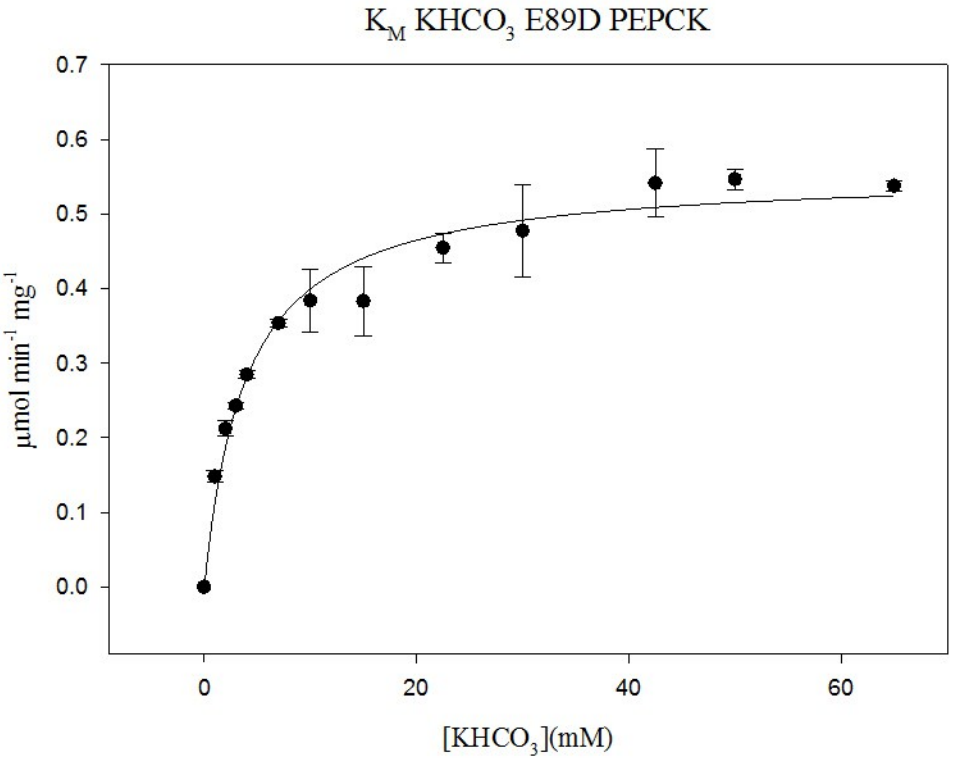
K_M $KHCO_3$ E89D PEPCK
0.7
0.6
0.5
0.4
0.3
0.2
0.1
0.0
µmol min^{-1} mg^{-1}
0
20
40
60
[$KHCO_3$](mM)

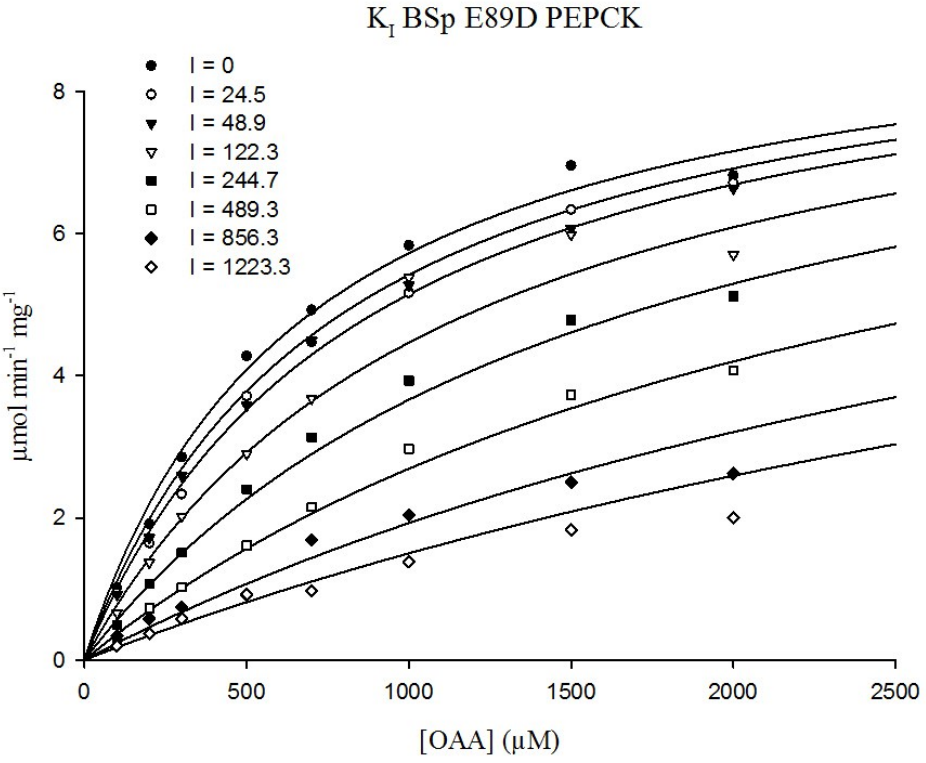
K_I BSp E89D PEPCK
I = 0
I = 24.5
I = 48.9
I = 122.3
I = 244.7
I = 489.3
I = 856.3
I = 1223.3
8
6
4
2
0
µmol min^{-1} mg^{-1}
0
500
1000
1500
2000
2500
[OAA] (µM)

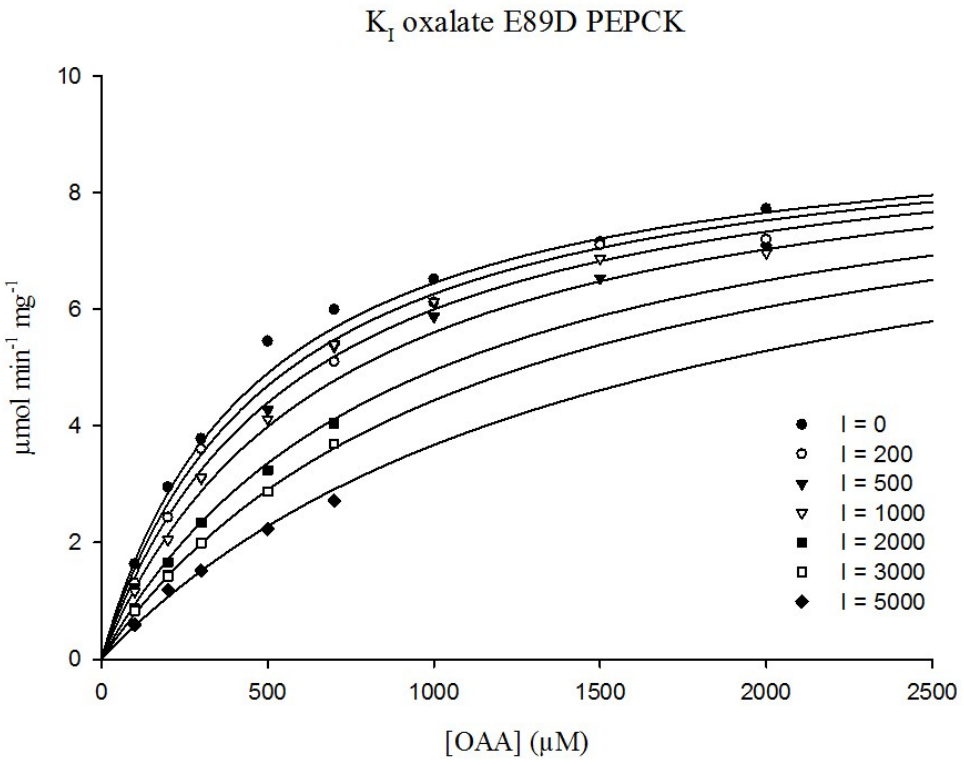
K_I oxalate E89D PEPCK
µmol min^{-1} mg^{-1}
[OAA] (µM)
I = 0
I = 200
I = 500
I = 1000
I = 2000
I = 3000
I = 5000
0
2
4
6
8
10
0
500
1000
1500
2000
2500

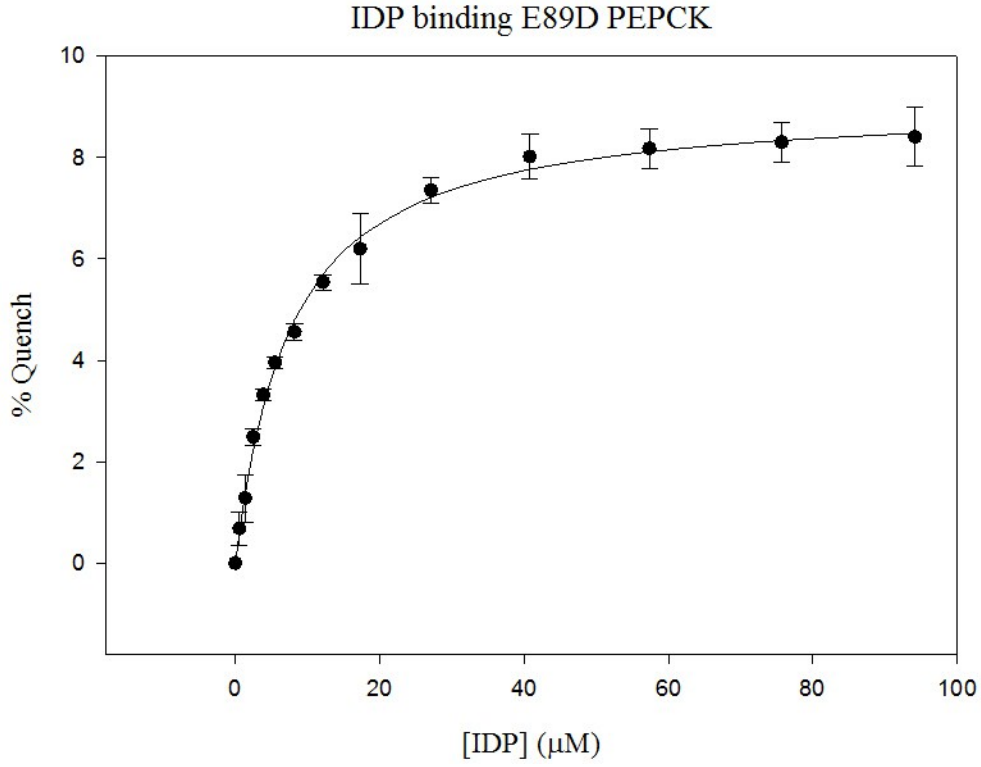
IDP binding E89D PEPCK
% Quench
[IDP] (µM)
0
2
4
6
8
10
0
20
40
60
80
100

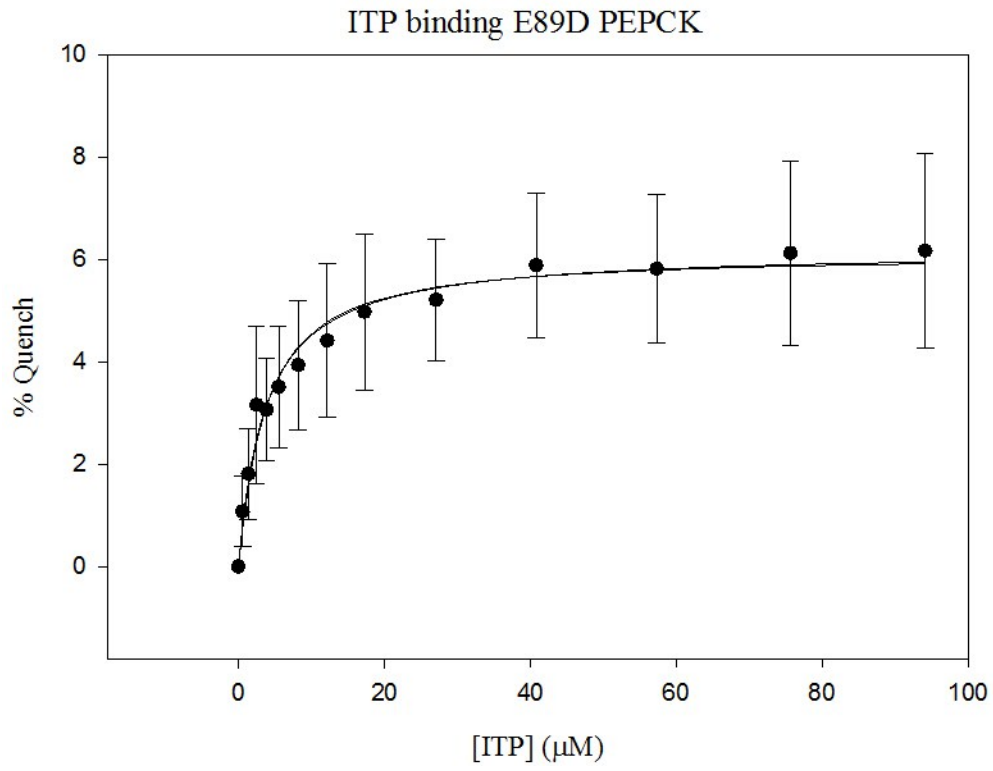
ITP binding E89D PEPCK
% Quench
[ITP] (μM)
0
2
4
6
8
10
0
20
40
60
80
100

E89Q rcPEPCK from the pSUMO expression vector

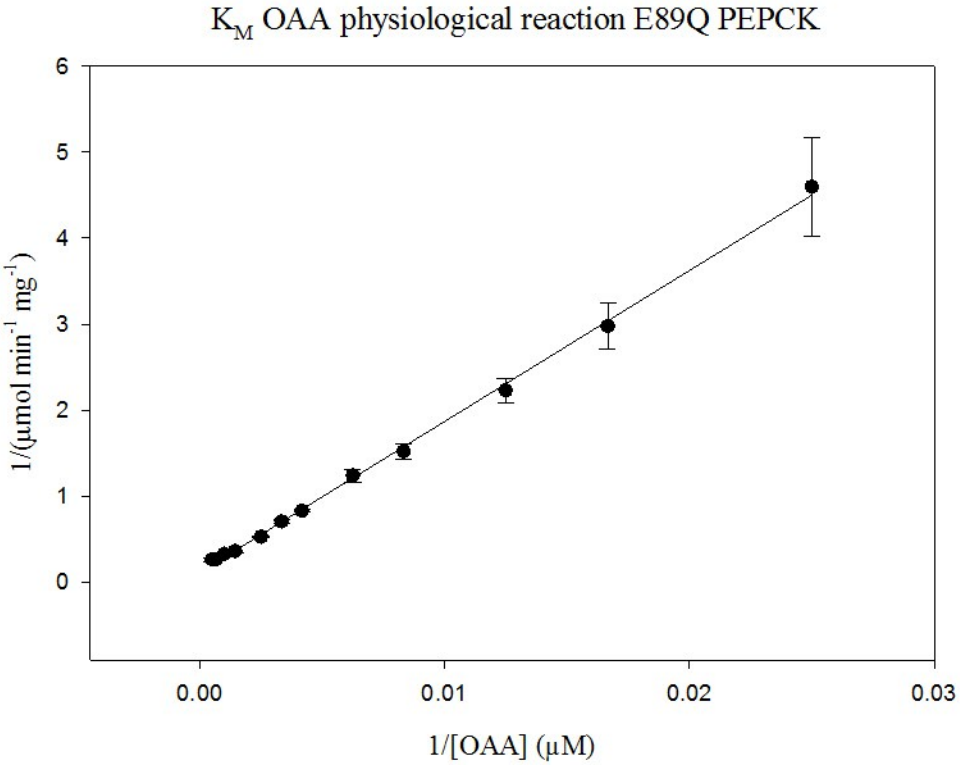

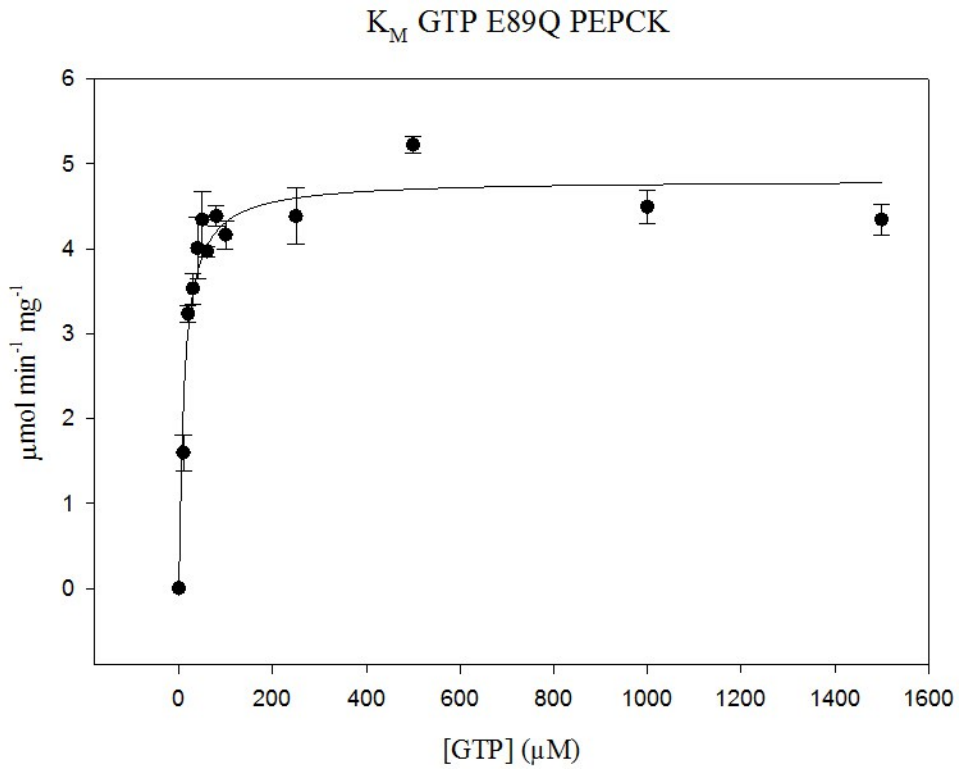

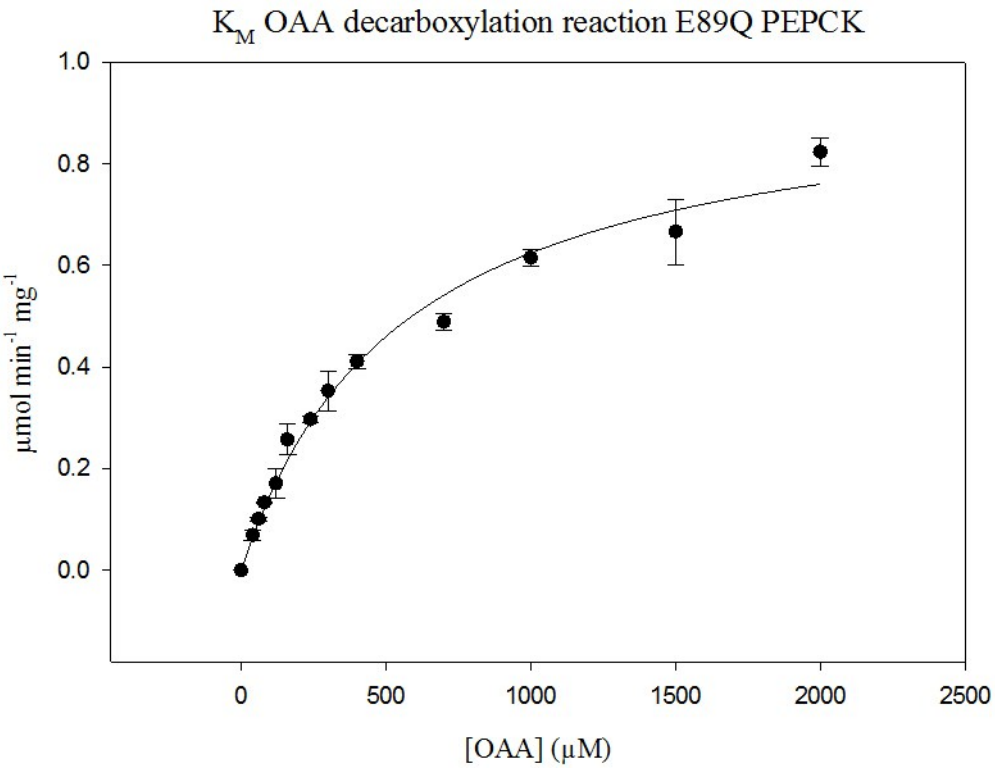
K$_M$ OAA decarboxylation reaction E89Q PEPCK
1.0
0.8
0.6
0.4
0.2
0.0
µmol min^{-1} mg^{-1}
0
500
1000
1500
2000
2500
[OAA] (µM)

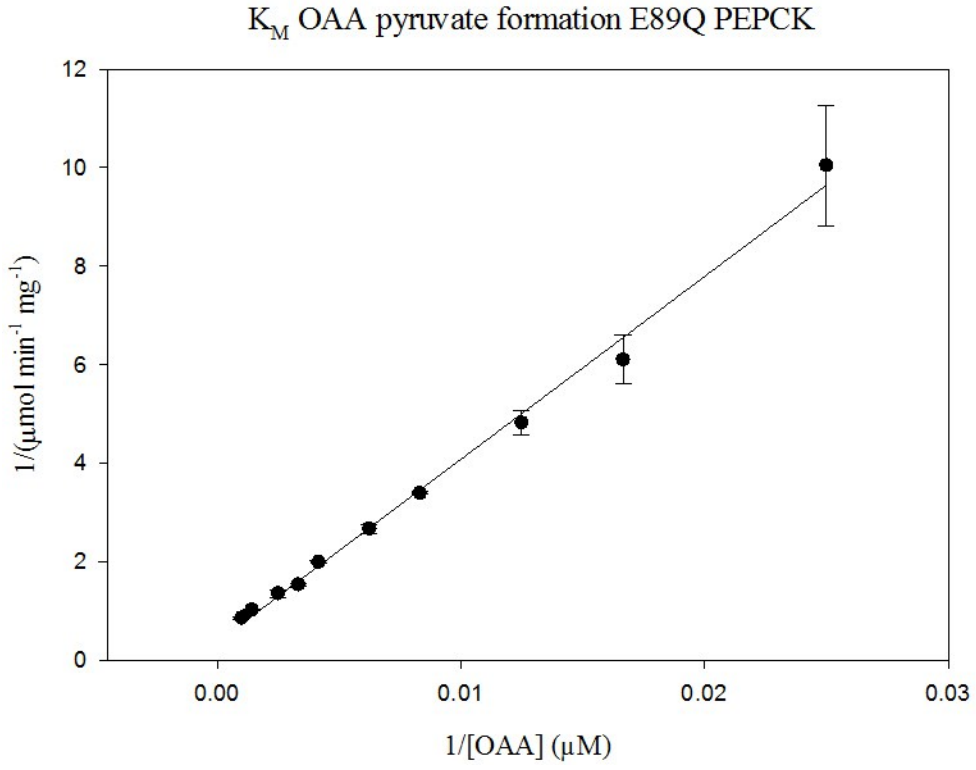
K$_M$ OAA pyruvate formation E89Q PEPCK
12
10
8
6
4
2
0
1/(µmol min^{-1} mg^{-1})
0.00
0.01
0.02
0.03
1/[OAA] (µM)

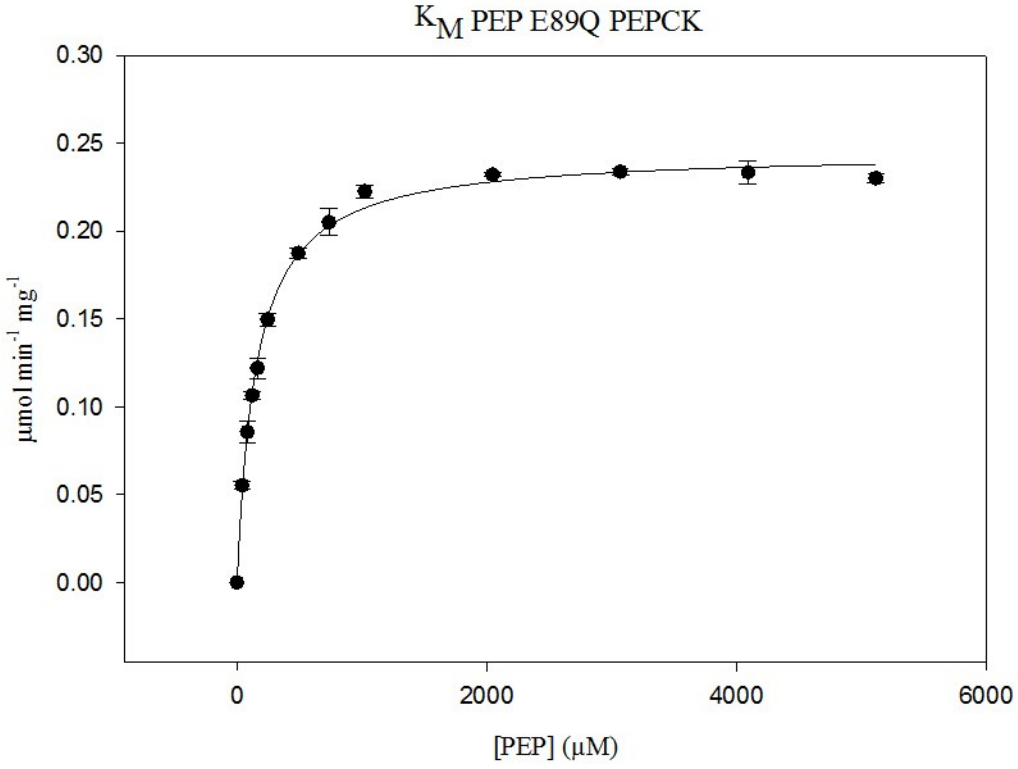
K_M PEP E89Q PEPCK
0.30
0.25
0.20
0.15
0.10
0.05
0.00
µmol min-1 mg-1
0
2000
4000
6000
[PEP] (µM)

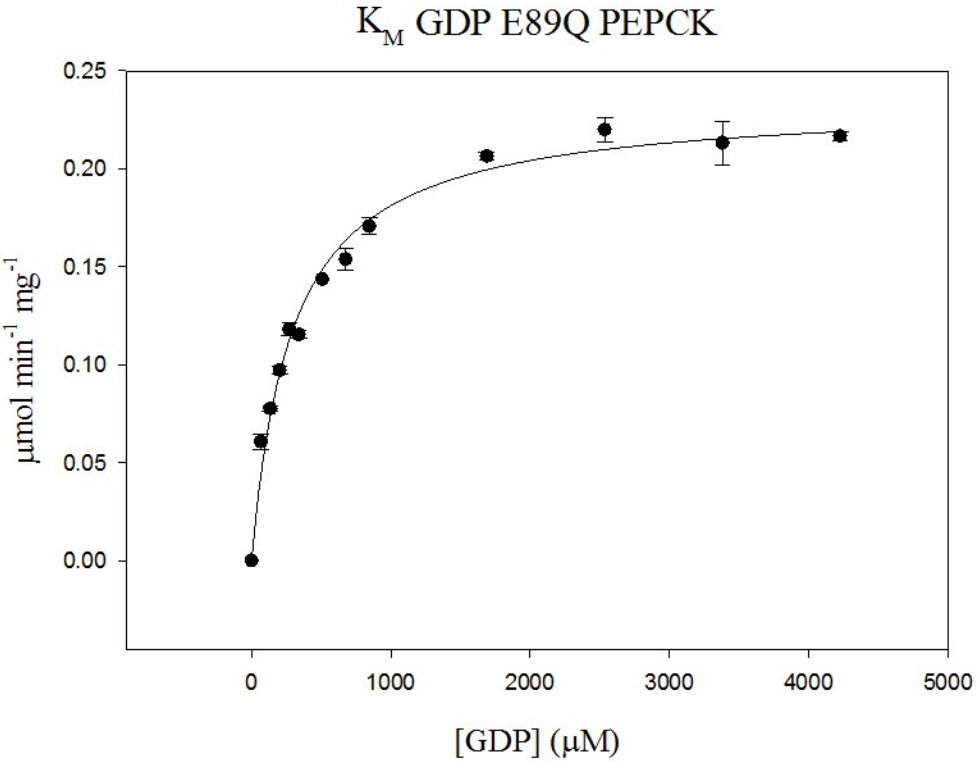
K_M GDP E89Q PEPCK
0.25
0.20
0.15
0.10
0.05
0.00
µmol min-1 mg-1
0
1000
2000
3000
4000
5000
[GDP] (µM)

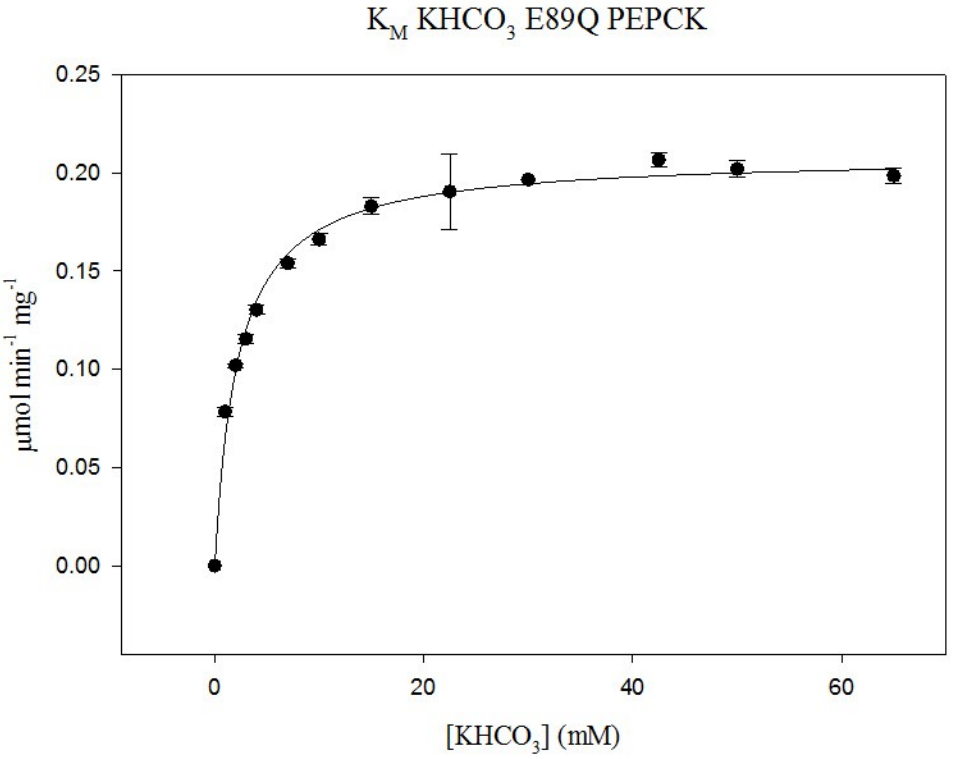
K_M $KHCO_3$ E89Q PEPCK
0.25
0.20
0.15
0.10
0.05
0.00
µmol min^{-1} mg^{-1}
0
20
40
60
[$KHCO_3$] (mM)

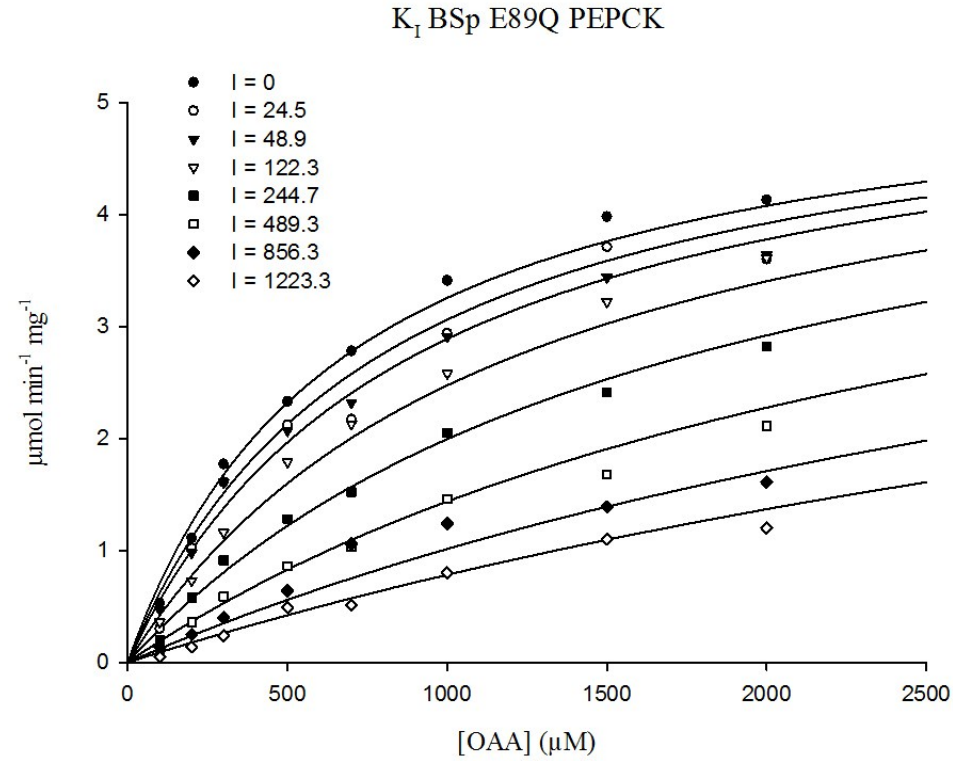
K_I BSp E89Q PEPCK
I = 0
I = 24.5
I = 48.9
I = 122.3
I = 244.7
I = 489.3
I = 856.3
I = 1223.3
5
4
3
2
1
0
µmol min^{-1} mg^{-1}
0
500
1000
1500
2000
2500
[OAA] (µM)

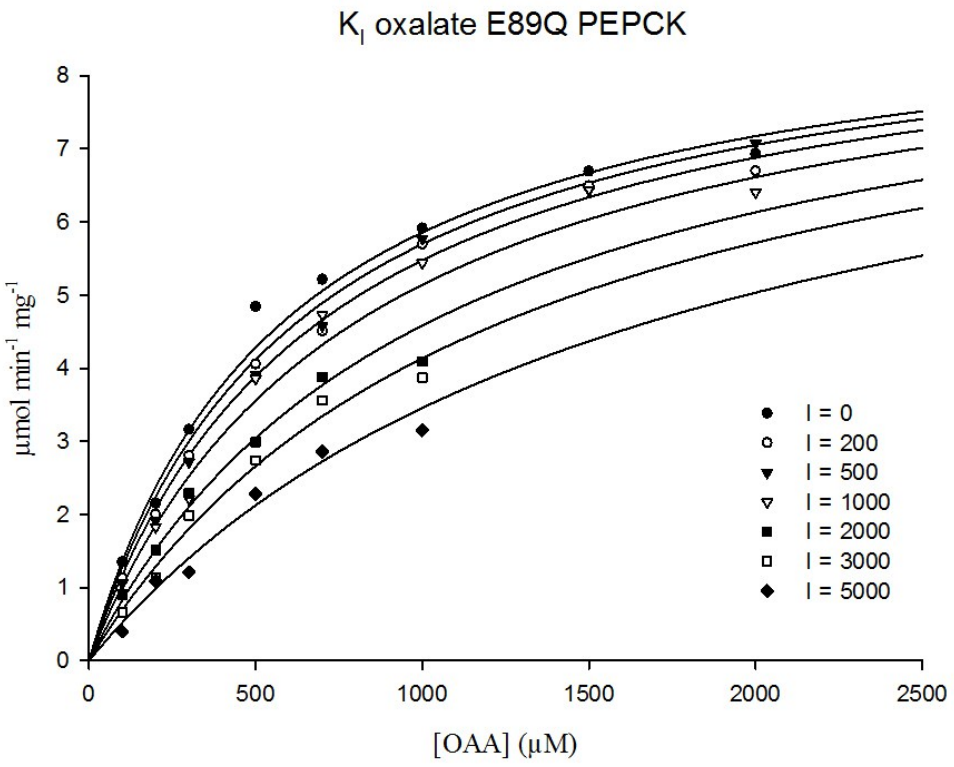
K$_I$ oxalate E89Q PEPCK
µmol min^{-1} mg^{-1}
[OAA] (µM)
I = 0
I = 200
I = 500
I = 1000
I = 2000
I = 3000
I = 5000

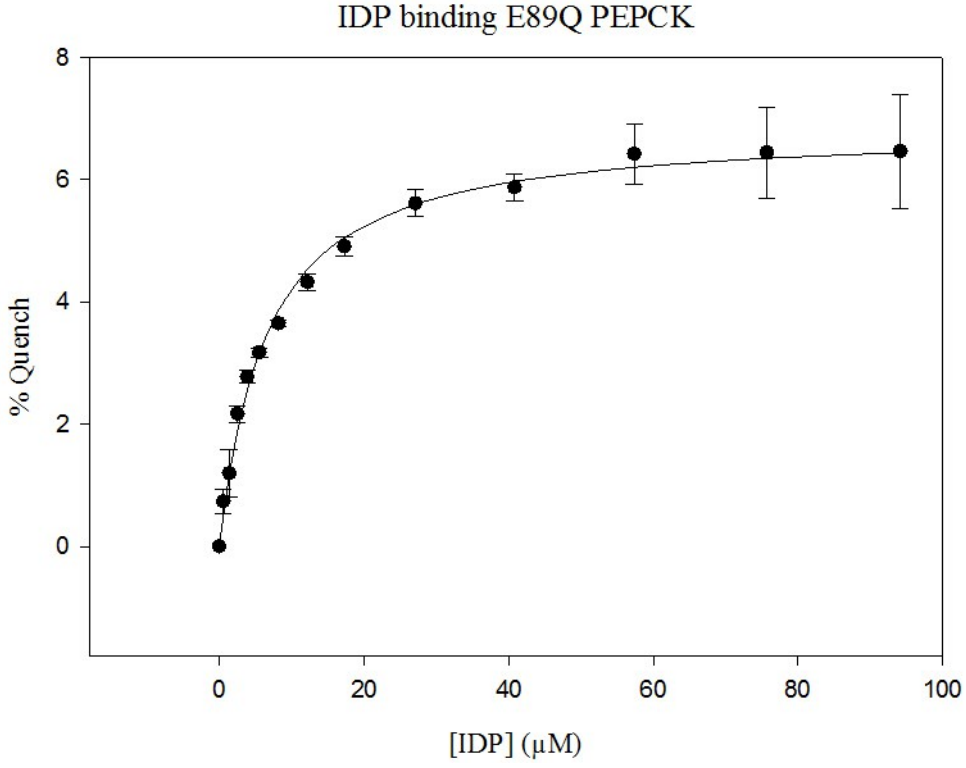
IDP binding E89Q PEPCK
% Quench
[IDP] (µM)

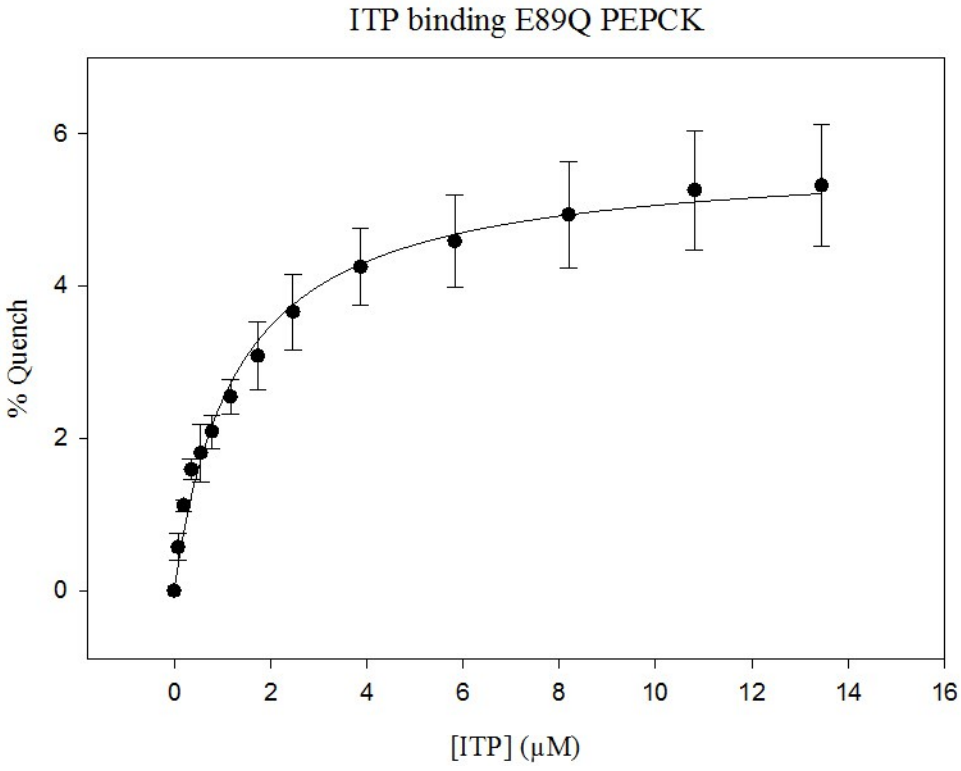
ITP binding E89Q PEPCK
% Quench
0
2
4
6
0
2
4
6
8
10
12
14
16
[ITP] (μM)

Appendix 4. Crystallographic data and model statistics

	Ld_1g-Mn^{2+}-βSP-Mn^{2+}GTP	Ld_1g-Mn^{2+}-PEP-Mn^{2+}GDP	Ld_1g-Mn^{2+}-oxalate-Mn^{2+}GTP
Wavelength (Å)	0.9	0.9	0.9
Space group	$P2_12_12_1$	$P2_12_12_1$	$P2_12_12_1$
Unit cell	a = 60.5Å b = 84.8 Å c = 119.1 Å α =β= γ = 90.0°	a = 60.7Å b = 85.3 Å c = 118.9 Å α =β= γ = 90.0°	a = 60.5Å b = 85.5 Å c = 118.8 Å α =β= γ = 90.0°
Resolution Limits, Å	33.2-1.74	69.3-1.6	27.8-1.2
No. of unique reflections	62571	82498	188021
Completeness, % (all data)	98.6 (96.0)	99.9 (99.9)	97.9 (94.0)
Redundancy	3.8 (3.7)	5.6 (5.3)	3.9 (3.2)
$I/\sigma_{(I)}$	14.1 (1.9)	20.2 (3.5)	25 (2.7)
R_{merge}	0.07 (0.56)	0.06 (0.4)	0.03 (0.3)
No. of ASU molecules	1	1	1

	Ld_2g-Mn^{2+}-βSP-Mn^{2+}GTP	Ld_2g-Mn^{2+}-PEP-Mn^{2+}GDP	Ld_2g-Mn^{2+}-oxalate-Mn^{2+}GTP
Wavelength (Å)	0.9		0.9
Space group	$P2_12_12_1$		$P2_12_12_1$
Unit cell	a = 60.7Å b = 84.3 Å c = 118.8 Å α =β= γ = 90.0°		a = 60.6Å b = 84.7 Å c = 118.8 Å α =β= γ = 90.0°
Resolution Limits, Å	34.6-1.5		37.9-1.4
No. of unique reflections	98001		120488
Completeness, % (all data)	99.9 (100)		99.9 (99.9)
Redundancy	12.2 (11.8)		12.1 (10.8)
$I/\sigma_{(I)}$	30.2 (2.4)		34.2 (2.2)
R_{merge}	0.05 (0.5)		0.04 (0.7)
No. of ASU molecules	1		1

	Ld_3g-Mn^{2+}-βSP-Mn^{2+}GTP	Ld_3g-Mn^{2+}-PEP-Mn^{2+}GDP	Ld_3g-Mn^{2+}-oxalate-Mn^{2+}GTP
Wavelength (Å)	0.9	0.9	0.9
Space group	$P2_12_12_1$	$P2_12_12_1$	$P2_12_12_1$
Unit cell	a = 60.8Å b = 84.1 Å c = 118.6 Å α =β= γ = 90.0°	a = 60.7Å b = 84.9 Å c = 119.1 Å α =β= γ = 90.0°	a = 60.5Å b = 84.3 Å c = 119.0 Å α =β= γ = 90.0°
Resolution Limits, Å	34.6-1.5	40.0-1.7	27.4-1.4
No. of unique reflections	91864	67674	119287
Completeness, % (all data)	93.8 (86.4)	99.3 (98.7)	98.6 (90.2)
Redundancy	4.5 (4.4)	5.6 (5.4)	8.4 (5.3)
$I/\sigma_{(I)}$	19.4 (2.5)	11.9 (2.8)	28.6 (1.5)
R_{merge}	0.04 (0.4)	0.13 (0.6)	0.05 (0.6)
No. of ASU molecules	1	1	1

	A467G-Mn^{2+}-βSP-Mn^{2+}GTP	A467G-Mn^{2+}-PGA-Mn^{2+}GDP	A467G-Mn^{2+}-oxalate-Mn^{2+}GTP
Wavelength (Å)	0.9	1.54	0.9
Space group	$P2_1$	$P2_1$	$P2_1$
Unit cell	a = 44.3Å b = 119.1 Å c = 60.1 Å α = γ = 90.0° b = 111.2°	a = 62.1 Å b =119.5 Å c = 87.0 Å α = γ = 90.0° b = 107.2°	a = 62.0 Å b = 119.6 Å c = 87.1 Å α = γ = 90.0° b = 106.9°
Resolution Limits, Å	20.6-1.25	35.93-2.10	33.24-1.75
No. of unique reflections	152044	68697	118295
Completeness, % (all data)	95.0 (67.2)	97.2 (80.3)	96.7 (94.9)
Redundancy	6.9 (3.5)	7.0 (4.9)	7.1 (6.9)
$I/\sigma_{(I)}$	28.2 (2.1)	10.0 (1.6)	18.0 (2.3)
R_{merge}	0.04 (0.46)	0.1(0.59)	0.06 (0.55)
No. of ASU molecules	1	2	2
R_{free}	17.3(34.2)	24.6(34.3)	22.7(32.8)
R_{work}	14.7(32.8)	18.7(27.7)	17.9(29.2)
Estimated coordinate error based on maximum likelihood, Å	0.03	0.15	0.10
Bond length rmsd, Å	0.03	0.01	0.02
Bond angle rmsd,	2.6	1.5	1.5
Ramachandran Statistics (preferred, allowed, outliers), %	96.9, 2.4, 0.7	96.4, 3.0, 0.6	96.5, 2.8, 0.7
State of Active Site Lid	Molecule A: Open	Molecule A: Open Molecule B: Open	Molecule A: 70% closed Molecule B: Open

	E89A-Mn^{2+}-βSP-Mn^{2+}GTP	E89A-Mn^{2+}-PGA-Mn^{2+}GDP	E89A-Mn^{2+}-oxalate-Mn^{2+}GTP
Wavelength (Å)	0.9	0.9	0.9
Space group	$P2_1$	$P2_1$	$P2_1$
Unit cell	a = 45.6Å	a = 45.0 Å	a = 45.7 Å
	b = 119.3 Å	b =119.2 Å	b = 119.3 Å
	c = 60.18Å	c = 60.6 Å	c = 60.8 Å
	α = γ = 90.0°	α = γ = 90.0°	α = γ = 90.0°
	b = 109.1°	b = 108.9°	b = 108.0°
Resolution Limits, Å	35.0-1.45	59.6-1.7	59.7-1.6
No. of unique reflections	106270	63855	80122
Completeness, % (all data)	97.5 (81.0)	95.2 (67.7)	98.7 (5.2)
Redundancy	4.2 (3.2)	4.8 (4.3)	5.9 (5.2
$I/\sigma_{(I)}$	17.5 (2.8)	12.6 (2.6)	20.8 (4.8)
R_{merge}	0.05 (0.3)	0.08 (0.5)	0.06 (0.3)
No. of ASU molecules	1	1	1

	E89D-Mn^{2+}-βSP-Mn^{2+}GTP	E89D-Mn^{2+}-PGA-Mn^{2+}GDP	E89D-Mn^{2+}-oxalate-Mn^{2+}GTP
Wavelength (Å)	0.9	0.9	0.9
Space group	$P2_1$	$P2_1$	$P2_1$
Unit cell	a = 44.6Å	a = 45.7 Å	a = 63.8 Å
	b = 118.8 Å	b =119.7 Å	b =119.164 Å
	c = 60.5Å	c = 60.9 Å	c = 86.6 Å
	α = γ = 90.0°	α = γ = 90.0°	α = γ = 90.0°
	b = 109.3°	b = 109.0°	b = 106.8°
Resolution Limits, Å	34.3-1.5	35.0-1.6	82.9-1.55
No. of unique reflections	95906	81458	178391
Completeness, % (all data)	99.9 (99.9)	99.7 (99.0)	99.7 (97.8)
Redundancy	6.1 (5.9)	5.9 (5.4)	6.1 (5.5)
$I/\sigma_{(I)}$	13.9 (2.9)	14.2 (3.2)	17.4 (3.4)
R_{merge}	0.07 (0.4)	0.09 (0.4)	0.06 (0.3)
No. of ASU molecules	1	1	2

	E89Q-Mn^{2+}-βSP-Mn^{2+}GTP	E89Q-Mn^{2+}-PGA-Mn^{2+}GDP	E89Q-Mn^{2+}-oxalate-Mn^{2+}GTP
Wavelength (Å)	0.9	0.9	0.9
Space group	$P2_1$	$P2_1$	$P2_1$
Unit cell	a = 44.6Å	a = 46.2Å	a = 45.7 Å
	b = 119.1 Å	b =119.7 Å	b = 119.3 Å
	c = 60.5Å	c = 60.69Å	c = 60.9 Å
	α = γ = 90.0°	α = γ = 90.0°	α = γ = 90.0°
	b = 109.9°	b = 107.3°	b = 107.6°
Resolution Limits, Å	33.8-1.54	59.9-1.55	39.1-1.55
No. of unique reflections	86115	90078	88932
Completeness, % (all data)	99.7 (99.8)	98.3 (96.4)	98.5 (95.8)
Redundancy	4.1 (4.0)	5.8 (5.0)	6.9 (6.2)
$I/\sigma_{(I)}$	16.8 (2.5)	22.4 (4.6)	13.4 (4.6)
R_{merge}	0.06 (0.4)	0.05 (0.3)	0.1 (0.3)
No. of ASU molecules	1	1	1